THESIS REPORT
Ph.D.

S Y S T E M S
R E S E A R C H
C E N T E R

Redundant-Drive Backlash-Free
Robotic Mechanisms:
Mechanisms Creation, Analysis, and Control

by S.-L. Chang
Advisor: L.-W. Tsai

Redundant-Drive Backlash-Free
Robotic Mechanisms:
Mechanisms Creation, Analysis, and Control

by
Sun-Lai Chang

Advisory Committee:

Professor Lung-Wen Tsai, chairman/advisor
Assistant Professor Muniswamappa Anjanappa
Associate Professor Shapour Azarm
Assistant Professor W.P. Dayawansa
Professor Jackson Yang

ABSTRACT

Title of Dissertation: Redundant-drive Backlash-free
                         Robotic Mechanisms: mechanisms
                         Creation, Analysis, and Control

Name of degree candidate: Sun-Lai Chang, Doctor of Philosophy, 1991

Dissertation directed by: Professor Lung-Wen Tsai
                            Department of Mechanical Engineering
                                        and
                            Systems Research Center

In this dissertation, the concept of transmission lines for topological synthesis of articulated gear mechanisms is introduced. It is shown that the structure matrix, which relates input displacements to the joint angles of a multi-degree-of-freedom articulated gear mechanism, can be derived using the concept of transmission lines. Applying the characteristics of the structure matrix, a new methodology for the topological synthesis of articulated gear mechanisms has been established. All the basic admissible structure matrices of conventional, three-DOF (degree-of-freedom), geared robotic mechanisms have been enumerated.

Furthermore, an innovative concept for the control of gear backlash in robotic mechanisms has been conceived. The concept utilizes redundant unidirectional drives to assure positive coupling of gear meshes at all times. It is shown that, through proper arrangement of gear trains, backlash of an N-DOF robotic mechanism can be completely eliminated by a minimum of (N+1) unidirectional drives. A methodology for the enumeration of admissible RBR (Redundant-drive Backlash-free Robotic) mechanisms has been established. This class of mechanisms also has the fail-safe advantage in

that, unless there is loss of backlash control, the mechanisms can continue to function whenever any one of its actuators fails.

The actuator sizing has been studied for a general class of N-DOF RBR mechanisms. The actuator torques are given in term of either the joint torques or the end-effector dynamical performance requirement. The methodology for the determination of actuator size can also be applied to tendon-driven robotic mechanisms.

Frictional forces in gear-coupled robotic mechanisms can have significant effects on the manipulator dynamics and control and are therefore also included in this study. Gearing efficiency for various gear drives, e.g., two mating gears, N mating gears with a common carrier, and gear trains, has been investigated. As an example, the frictional effect has been demonstrated where it involves the dynamics of a two-DOF RBR arm.

In order to demonstrate this concept, a two-DOF experimental RBR arm has been constructed. A computed torque with PD control scheme is implemented in the experimental RBR robot. An experiment using a laser tracking system to verify the improvement of repeatability was conducted. In order to compare the performance difference, two control algorithms, one with redundant drives and the other without, were used in this experiment. The result of this experiment has shown that use of redundant drives greatly improves the repeatability.

Redundant-Drive Backlash-Free
Robotic Mechanisms:
Mechanisms Creation, Analysis, and Control

by
Sun-Lai Chang

Dissertation submitted to the Faculty of the Graduate School
of The University of Maryland in partial fulfillment
of the requirements for the degree of
Doctor of Philosophy
1991

Advisory Committee:

Professor Lung-Wen Tsai,   chairman/advisor
Assistant Professor Muniswamappa Anjanappa
Associate Professor Shapour Azarm
Assistant Professor W.P. Dayawansa
Professor Jackson Yang

ACKNOWLEDGEMENT

Nomenclature

A: structure matrix which relates joint torques and input torques

A^+: pseudo inverse of matrix A

A_{ij}: sub-matrix of A with the ith and j^{th} column omitted

A_{ij}^l: sub-matrix of A_{ij} with the lth row omitted

$\hat{A}_i$: sub-matrix of A with the ith column omitted

A_j: the jth column of matrix A

a_{ij}: the (i,j) element of matrix A

a_s: specification on acceleration

B: A^T

E_j: power consumption of motor j

$\underline{e}$: position error vector

$\underline{e}_i$: a positive unit vector along the axis of relative rotation

F_n: normal contact force between two meshing gears

f_i: resultant joint torque i contributed from conservative force

$\underline{f}_r$: joint torques contributed from velocity and coriolis force

$\underline{G}$: inertia matrix of a robotic system

g_i: $= \frac{X_i}{\mu_i}$

h_i: $= \frac{\hat{\xi}_j - X_j}{\mu_j}$

I_i: moment of inertia of gear i about its axis of rotation

i_j: armature current of motor j

J_i: moment of inertia of a carried link i about its joint axis

K: kinetic energy of a system

K_m: kinetic energy contributed from major links

$(K_\xi)_j$: torque constant of motor j

K': kinetic energy contributed from carried links

$K'_{i,j}$: the kinetic energy contributed from the rotation of link i with respect to link j

$\underline{k}_i$: feedback gain of the position integration

$\underline{k}_p$: position feedback gain

$\underline{k}_v$: velocity feedback gain

L: $= K - V$

l: link length

N_i: number of teeth on gear i

N_{ij}: $= \frac{N_i}{N_j}$

P_e: rate of change of internal energy

P_i: input power

$\underline{P}_i$: position vector of a point in the end-effector and expressed in the ith coordinate system

P_o: output power

p: coefficient of power loss

Q_i: generalized active force

q_i: generalized coordinate

R_i: radius of the base circle of gear i

T: matrix of transformation

$\underline{U}_i$: a unit vector attached to the end-effector and expressed in the ith coordinate system

V: potential energy

v_s: specification on velocity

W_v: velocity weighting matrix

W_α: acceleration weighting matrix

$\underline{w}_j$: angular velocity of link j with respect to inertia frame

$\hat{\xi}_i$: available torque from the ith actuator

X_j: particular solution of ξ_j

Z_j: $= \frac{z_j}{(K_\xi)_j^2}$

z_j: internal impendence of motor j

Γ_i: amplitude of τ_i

Θ_i: amplitude of joint i

η: gearing efficiency

λ: free parameter in the homogenous solution of $\underline{\xi}$

$\underline{\mu}$: null vector of matrix A

μ: friction coefficient

ω: frequency of a sinusoidal input

$\underline{\phi}$: column matrix denoting input displacements

$\underline{\tau}$: column matrix denoting joint torques

$\underline{\theta}$: column matrix denoting joint displacements

$\underline{\theta}_d$: desired joint angles

θ_{ij}: relative angular displacement of link i with respect to link j

$\underline{\xi}$: column matrix denoting input torques

$\underline{\xi}_{ij}$: column matrix of $\underline{\xi}$ with the ith and j^{th} elements omitted

Contents

List of Tables

List of Figures

Chapter 1

Introduction

1.1 Robots

Under the description of science fiction writers and moviemakers, super-human seems to fit the description of a robot. A robot is imagined to have all the capabilities of a human being. In reality, nowadays robots are far from the expectation. Presently, not even one robot can drive safely around New York city. Comparing with the popular concept, current robotic technology is still in its infancy. Probably, a dream robot will be built some day. But in the near future, research and technology development will be still emphasized on *computer controlled mechanical devices* performing useful work in a factory environment. That is moving an object from one position to another quickly and accurately, such as parts transfer, material handling, and mechanical assembly.

1

However, in the pursuit of high technology, today's robots need to perform tasks far beyond the coarsely controlled welder/assembler. They must be designed to perform more accurate assembling, welding, as well as other sophisticated jobs. To satisfy these requirements, a robot with repeatability better than one half of a minimeter is usually required. Various drive configurations such as direct drive manipulators, tendon-drive manipulators, and closed-loop manipulators have been suggested to improve the performance. However, each configuration has its own inherited drawbacks. Engineers are still eagerly studying the configuration and structure of manipulators. In this research, a novel class of robotic configurations has been introduced to improve the repeatability of a manipulator. Associated with a control algorithm, backlash in the robotic structure can be eliminated completely. This has been verified via a prototype design.

1.2 Motivation of This Study

Various robotic mechanisms have been constructed to achieve certain desired functions and performance. The kinematic structure of a robot often takes the form of an open-loop chain. An open-loop manipulator is mechanically simple and easy to construct. However, it does require its actuators to be located along the joint axes which, in turn, increases the inertia of the manipulator. Moreover, torque ripples from the actuators will directly impose on its joints. These are considered as major disadvantages which can affect stability and accuracy of a manipulator. For these reasons, cable and push/pull elements are commonly used to permit the actuators to be

2

located at the base or as close to the base as possible. However, cable-driven robot manipulators have limited load handling capability and suffer from large vibration.

To overcome this difficulty, most of the industrial robots use gear trains for power transmission to reduce compliance. Gear trains are also used for torque amplification which, in turn, permits the use of smaller actuators. Theoretically, gear backlash should be zero. But in practice, some backlash must be included to prevent jamming of teeth due to manufacturing errors and thermal expansions. However, gear backlash introduces discontinuity, uncertainty and impact on mechanical systems. These undersirable properties also cause the response of a robot to deviate from the input command. Up to date, backlash cannot be successfully controlled with existing techniques. It is usually minimized by the use of precision gears, spring-loaded split gear assemblies, and precise mechanical adjustments. Although these techniques can reduce the effect of backlash, the production cost is relatively high and the accuracy is also inadequate. This can be illustrated by the uncertainty estimation of the PUMA 560 robot. Fig. 1.1 shows the transmission system in the first joint of the PUMA 560. According to the AGMA handbook, the tooth clearance of precision gears ranges from -0.025 mm to -0.050 mm. Hence, the angular uncertainty due to the pinion and bull gear in this transmission system is approximately given by

$$\delta\theta = \frac{2 \times 0.0375 \ mm}{110 \ mm} = 0.000682 \ rad \tag{1.1}$$

And when the arm is fully extended, the position uncertainty at the end-effector is

3

JT1 SERVOMOTOR

SPUR PINION

SPUR GEAR

IDLER CARTRIDGE

PINION

BULL GEAR

JT1 AXIS
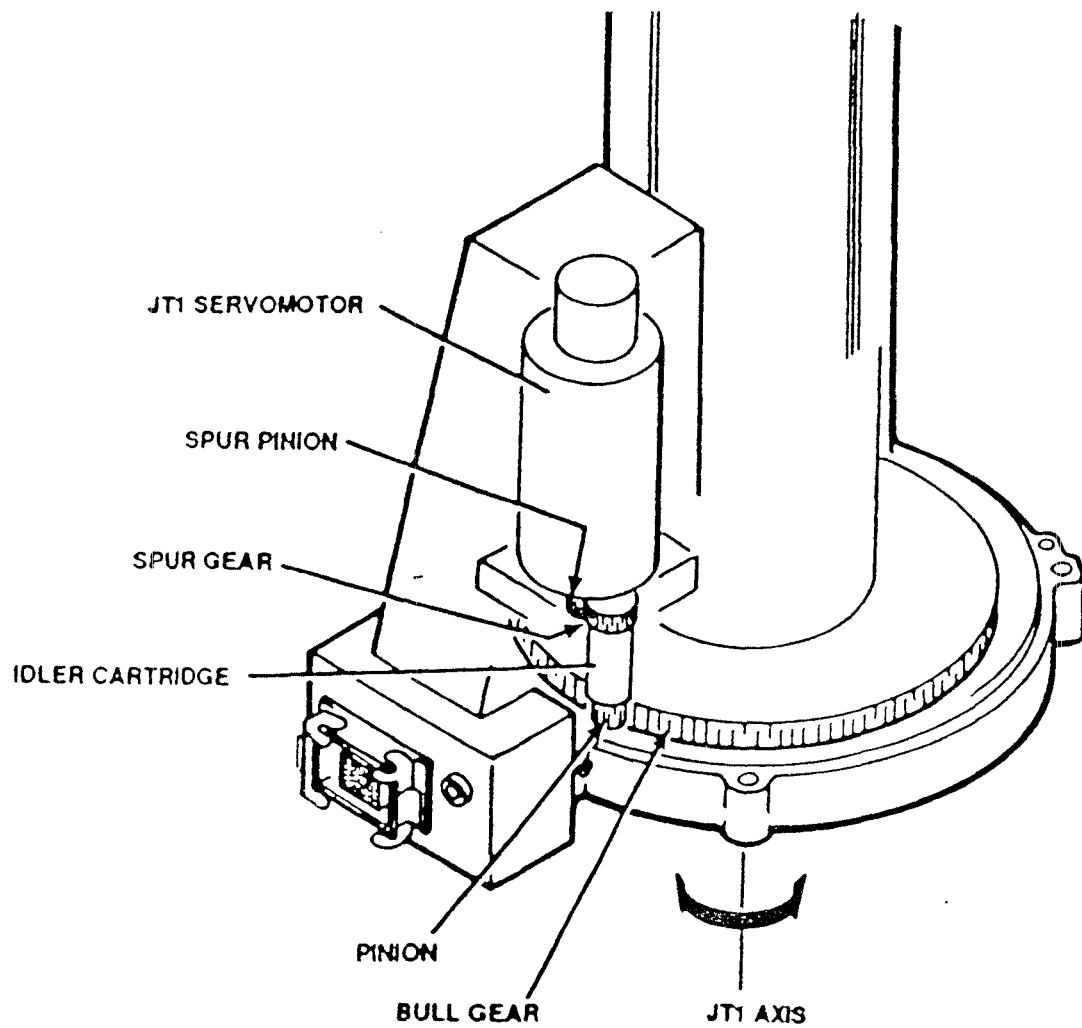
Figure 1.1: Transmission System Used in the First Joint of PUMA 560 (reproduced from the mannual of the Unimate PUMA Robot Operating Systems)

4

$$914 \ mm \times 0.000682 = 0.62 \ mm \qquad (1.2)$$

This position uncertainty is caused by the pinion and bull gear in the first joint only. From this example, it can be realized that backlash plays an important role in repeatability and accuracy of a robot manipulator and further studies on reducing or eliminating its effects are urgently needed.

1.3   Prior Work

Many methods such as backlash compensation (Veitschegger and Wu, 1986), antibacklash gears (Michalec, 1966), adjustable tooth thickness gears (Michalec, 1966), adjustable center distance (Dagalakis and Myers, 1985), and harmonic drives (Calson, 1985) have been proposed for the elimination of gear backlash. Improvement on problems caused from gear backlash has been made by using these methods, e.g., backlash compensation used in machine tools. However, these methods become inadequate in for robotic systems. Presently, none of those methods can eliminate backlash in robotic system completely. Disadvantages often arise from these methods. For example, the method of adjustable center distance has been used for the assembly of PUMA 560 robot. The backlash control mechanism supplied by the manufacturer for the PUMA robot is an eccentric cartridge-bearing arrangement, as shown in Fig. 1.2. A small adjustable screw is mounted on the side of cartridge. Rotating the cartridge counter-clockwise reduces the center distance between the two mating gears and, therefore, decreases the gear backlash. Increasing the center distance has the opposite effect. However, this method requires a skillful assembler to do the adjustments, and can further increase

5
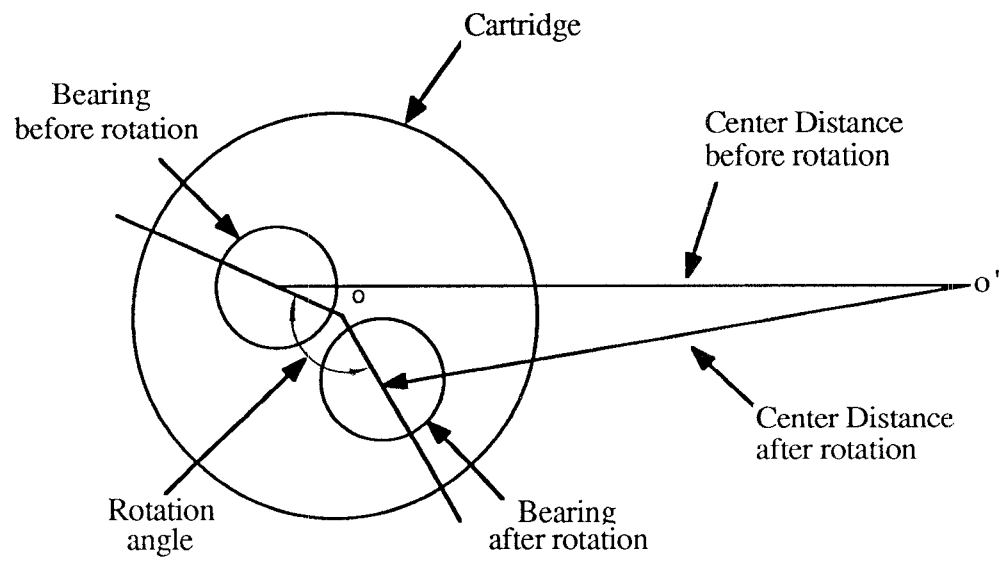
Figure 1.2: Backlash Control Mechanism Using Adjustable Center Distance

the cost of assembling. Furthermore, adjustable centers are subject to mal-adjustments, and in the field there is no assurance that the quality of a readjustment will be comparable to the original.

1.4　Outline of the Research

This research consists of three major parts, which are described as follows:

(a) A new methodology for the creation of geared robotic mechanisms

The concept of mechanism enumeration using graph representation has been studied by Freudenstein (1971), Freudenstein and Maki (1979), Buchsbaum and Freudenstein (1970), and Tsai (1987), etc. This method requires the enumeration of all admissible graphs of kinematic chain. Then graphs satisfying desired mechanism specifications are selected. And, finally, edges of candidate graphs are labeled and their corresponding mechanisms are sketched. This procedure is considered to be very thorough and systematic. However, when the number of links increases, it becomes very complicated and difficult to deal with.

A new methodology for the creation of mechanism based on the concept of transmission lines has been developed during the course of this research. Using this methodology, mechanisms can be enumerated directly from a set of predetermined mechanical characteristics, such as the number of DOF (Degrees-of-Freedom), and the form of the structure matrix which relates the input displacements and joint angles. This method is considered to be

7

more direct and purpose-oriented. It also leads to the creation of backlash-free robotic mechanisms.

(b) The creation of redundant-drive backlash-free robotic (RBR) mechanisms

An innovative concept for the control of gear backlash in robotic mechanisms has been conceived. This concept utilizes redundant unidirectional drives to assure positive coupling of gear meshes at all times. Through proper arrangement of gear trains, it has been shown that the backlash of an N-DOF robotic mechanism can be completely eliminated by a minimum of (N+1) unidirectional drives. A methodology for the enumeration of admissible RBR mechanisms has been established. It is worthy to note that this class of mechanisms also has the fail-safe advantage in that, except for the loss of backlash control, it can continue to function when anyone of its actuators fails. In this research, a two-DOF experimental RBR arm has been constructed to establish the proof of this concept.

(c) Analysis and control of RBR mechanisms

Since the concept of RBR mechanisms created in this research is totally new, the analysis and control of this class of mechanisms has also been explored, which includes actuator sizing, gear friction, dynamical equations of motion, system parameter estimation, control algorithm, and experimental verification.

1.5 Contributions

The major concern of this dissertation is to completely eliminate backlash in the transmission system of a robotic mechanism. However, methodology for mechanisms creation, analysis and control of geared coupled mechanisms have also been studied. The major contributions of this research can be summarized as follows:

1. Creation of an innovative concept for elimination of gear backlash in robotic mechanisms.

2. Development of a methodology for systematic creation of geared robotic mechanisms.

3. Development of an atlas of structure matrices for the design of backlash-free robotic mechanisms.

4. Improved repeatability and stability of a robot manipulator.

5. Friction and efficiency modeling.

6. Derivation of a general theory governing the manipulation and design of RBR mechanisms.

7. Prototype demonstration of a two-DOF RBR manipulator.

Chapter 2

Topological Synthesis of Articulated Gear Mechanisms Having N-DOF and N Articulation Joints

2.1   Introduction

In recent years, topological synthesis of geared mechanisms has been accomplished by the use of graph theory and combinatory analysis. Using graph representation, the function of a desired mechanism is separated from structural consideration during the conceptual design stage. First, kinematic structures of the same type, i.e., the number of links, degrees of freedom, etc., are enumerated systematically. Then potentially useful mechanism structures are selected for the purpose of functional evaluation. The method of graph representation is very thorough and systematic. However, when the number

10

of links increases, it becomes very complicated and difficult to deal with.

To overcome this difficulty, a new methodology for topological synthesis of geared robotic mechanism is introduced in this chapter. This new method allows us to perform topological synthesis for a class of geared robotic mechanisms from its mechanical coupling point of view, i.e. mechanism synthesis can be performed to satisfy a desired relationship between input actuator torques and joint torques. This methodology is considered to be more direct and efficient. Moreover, one of the major objectives of this research is to create a class of gear mechanisms for which backlash can be completely controlled.

2.2   Structural Representations

Various methods have been used to represent the topological structure of a mechanism. In what follows, two such representations that are pertinent to the development of this work will be reviewed.

(1) Functional Representation:

This refers to the conventional drawing of a mechanism. Shafts, gears, and other elements are identified as such. For the reason of clarity and simplicity, only functional elements essential to the kinematic structure are shown. Different functional representations may represent different designs of the same topological structure (e.g., planar versus spatial mechanisms, internal gear mesh versus external gear mesh).

For example, the functional representation of Cincinnati Milacron T^3 wrist (Stachhouse, 1979) is shown in Fig. 2.1(a), where three bevel gear pairs, 6-2, 3-5, and 4-5, transmit power to the end-effector through three articulated joint axes, Z_1, Z_2, and Z_3. We note that, in addition to the gear dimensions, the geometry of this mechanism can be defined by the Hartenberg and Denavit parameters, i.e., the offset distance, twist angle, and translational distance between two adjacent axes (Hartenberg and Denavit, 1964).

(2) Planar Representation:

In this representation, a positive direction of rotation is assigned to each joint axis in the mechanism of interest. Then, starting from the second joint axis, every axis is twisted about the common normal defined by the axis itself and its preceding joint axis until all the joint axes are parallel to each other and are pointed toward the same positive Z direction. Finally, all the bevel gears are replaced by spur gears and, if two adjacent axes intersect at a point, then an offset distance is added to permit the spatial bevel gear pair to be replaced by an equivalent planar spur gear pair. The gear mesh, internal or external, depends on whether a positive rotation of one gear with respect to its positive joint axis results in a positive or negative rotation of the mating gear. Fig. 2.1(b) shows the planar representation of the mechanism shown in Fig. 2.1(a). For the reason of simplicity, sometimes all the gear meshes will be represented by external gear meshes only. The simplified planar representation of the Cincinnati Milacron T^3 wrist is shown in Fig. 2.1(c).
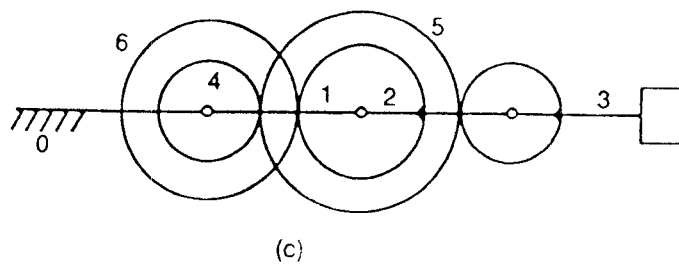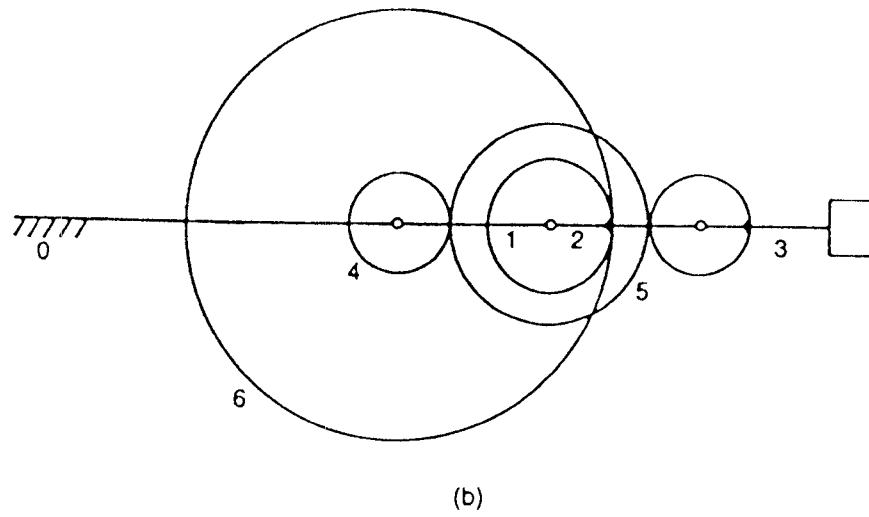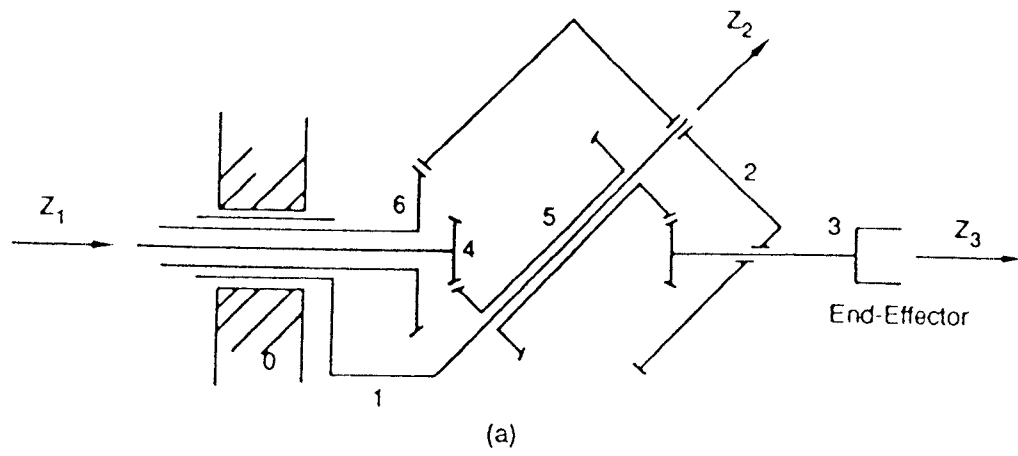
Figure 2.1: Kinematic Representations of the Cincinnati Milacron T^3 Wrist

2.3 The Kinematics of Robotic Mechanisms

The kinematic analysis of geared robotic mechanisms can be accomplished by applying the concept of equivalent open-loop chain and the theory of fundamental circuits (Tsai, 1988). Generally, the number of articulation points in a robotic mechanism is equal to the number of degrees of freedom and this will be assumed to be the case for the study to follow.

According to Tsai's approach, the analysis of spatial robotic mechanisms can be performed in two steps. The first step is to derive the relationship between the position and/or orientation of the end-effector and the joint angles in the equivalent open-loop chain. The second step is to derive the relationship between the joint angles and the input actuator displacements. The first step can be accomplished by the matrix method or vector approach while the second step can be accomplished by applying the fundamental circuit equations and coaxiality conditions.

For example, the Cincinnati Milacron T^3 wrist shown in Fig. 2.1(a) has an equivalent open-loop chain shown in Fig. 2.2, where a_k, α_k, and d_k ($k = 1, 2, 3$) are the Hartenberg and Denavit parameters. The relation between the joint angles and the end-effector position and orientation can be written as

$$\bar{P}_0 = T\bar{P}_3 \tag{2.1}$$

and

$$\bar{U}_0 = T\bar{U}_3, \tag{2.2}$$

14
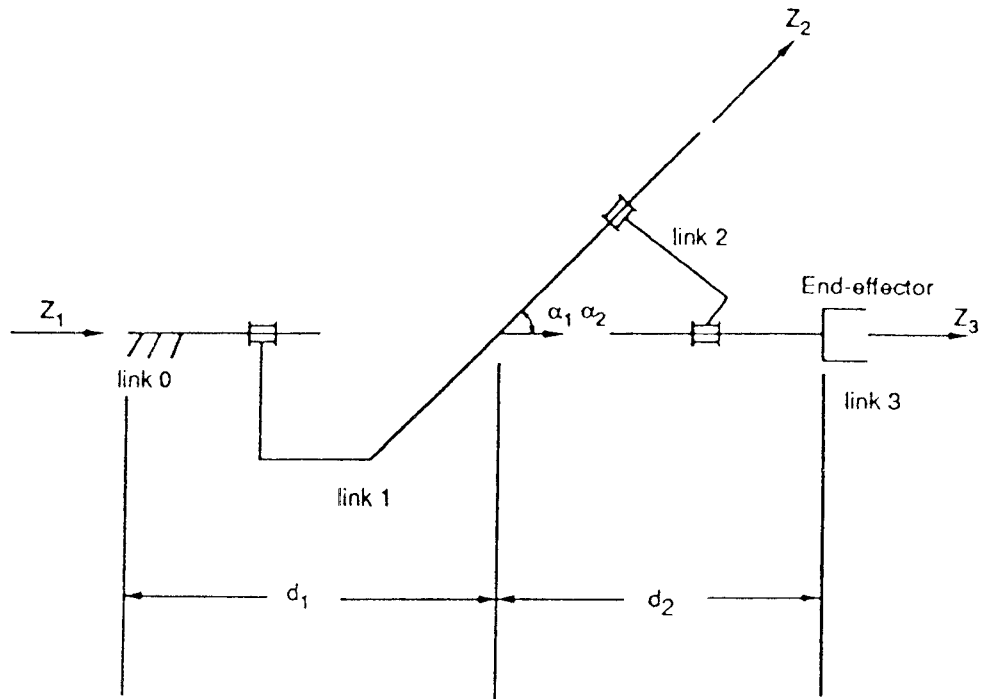
Figure 2.2: The Equivalent Open-loop Chain of the Cincinnati Milacron T^3 Wrist

where T is the transformation matrix relating the coordinate in the third coordinate system to that in the 0th coordinate system and is a function of the Hartenberg and Denavit parameters, $\bar{P}_i$ is the position vector of a point in the end-effector and expressed in the ith coordinate system, and $\bar{U}_i$ is a unit vector attached to the end-effector and expressed in the ith coordinate system.

In the Cincinnati-Milacron T^3 wrist, there are three fundamental circuits, (3, 5, 2), (4, 5, 1), and (6, 2, 1), where the first two numbers represent the gear pair and the third the carrier. The fundamental circuit equations are given by

$$\theta_{32} = -N_{53}\theta_{52}, \tag{2.3}$$

$$\theta_{41} = -N_{54}\theta_{51}, \tag{2.4}$$

and

$$\theta_{61} = N_{26}\theta_{21}. \tag{2.5}$$

Links 1, 2 and 5 share a common joint axis, Z_2. Similarly, links 0, 1, 4 and 6 share a common joint axis, Z_1. The coaxiality conditions can be written as:

$$\theta_{52} = \theta_{51} - \theta_{21}, \tag{2.6}$$

$$\theta_{41} = \theta_{40} - \theta_{10}, \tag{2.7}$$

and

$$\theta_{61} = \theta_{60} - \theta_{10}, \tag{2.8}$$

where θ_{ij} denotes the relative angular displacement of link i with respect to link j, $N_{jk} = N_j/N_k$ is the gear ratio for the gear pair attached on links j and k, and where N_j and N_k are number of teeth on gears j and k, respectively.

Solving Eqs. (2.3) through (2.8), yields

$$\bar{\phi} = B\bar{\theta} \tag{2.9}$$

where

$$B = \begin{bmatrix} 1 & -N_{54} & N_{35}N_{54} \\ 1 & N_{26} & 0 \\ 1 & 0 & 0 \end{bmatrix}$$

$$\bar{\phi} = [\phi_1, \phi_2, \phi_3]^T = [\theta_{40}, \theta_{60}, \theta_{10}]^T$$
$$= \text{input displacements}$$

and

$$\bar{\theta} = [\theta_{10}, \theta_{21}, \theta_{32}]^T = \text{joint angles}$$

and where $[\ ]^T$ denotes the transpose of $[\ ]$.

It can be shown that the equation relating the joint torques to the input torques is given by

$$\bar{\tau} = B^T\bar{\xi} = A\bar{\xi} \tag{2.10}$$

17

where $\bar{\tau} = [\tau_1, \tau_2, \tau_3]^T$ denotes the resultant torques about joint axes 1, 2, and 3, and $\bar{\xi} = [\xi_1, \xi_2, \xi_3]^T$ denotes the input torques applied at links 4, 6, and 1, respectively. The matrix A, the transpose of B, is determined by the structural topology of the mechanism and the gear ratios. The matrix A is called the structure matrix of the mechanism.

2.4 Transmission Lines

Taking the derivative of Eq. (2.10), yields

$$d\bar{\tau} = A(d\bar{\xi}). \tag{2.11}$$

The (i, j) element of matrix A can be interpreted as the partial rate of change of the joint torque τ_i with respect to the input torque ξ_j, i.e.,

$$a_{ij} = \partial\tau_i/\partial\xi_j. \tag{2.12}$$

Hence, $a_{ij} \neq 0$ implies that torque ξ_j will be transmitted to joint i and amplified by a_{ij} times, and $a_{ij} = 0$ implies that input torque ξ_j does not have any influence on the resultant torque at joint i. Therefore, the ith row of the structure matrix A describes how the resultant torque about joint i is affected by the input actuators and, on the other hand, the jth column of matrix A describes how the torque of an input actuators j is transmitted to various joints of the mechanism. For the type of mechanisms considered, removal of all the gears from the mechanism results in an open-loop chain. Except for the case of a direct drive or an individual joint drive, torques

18

are transmitted by gear train, and the joint torques affected by an actuator must be consecutive. The gear train which results in a series of non-zero elements in the kth column is, therefore, called the transmission line for the input actuator k.

Fig. 2.3 shows a typical transmission line in planar representation where a series of links, numbered i, $i+1$, $\cdots$, $i+j$, are connected together by revolute joints to form an open-loop chain, and where gears k, $k+1$, $\cdots$, $k+j-1$ are pivoted about the ith, $(i+1)^{th}$, $\cdots$, and $(i+j-1)^{th}$ joint axes, respectively. The last gear, $(k+j-1)$, is attached to link $(i+j)$, and the rotation of gear k with respect to link i is considered as the input.

For such a transmission line, the fundamental circuit equations can be written as follows:

$$\theta_{(m-1)n} = \pm N_{m(m-1)}\theta_{mn} \tag{2.13}$$

where

$$m = (k+1),\ (k+2),\cdots,\ (k+j-1)$$

$$n = m - k + i$$

and where the sign of Eq. (2.13) depends on whether the gear mesh is internal or external.

The coaxiality conditions can be written as

$$\theta_{mn} = \theta_{m(n+1)} + \theta_{(n+1)n} \tag{2.14}$$

19
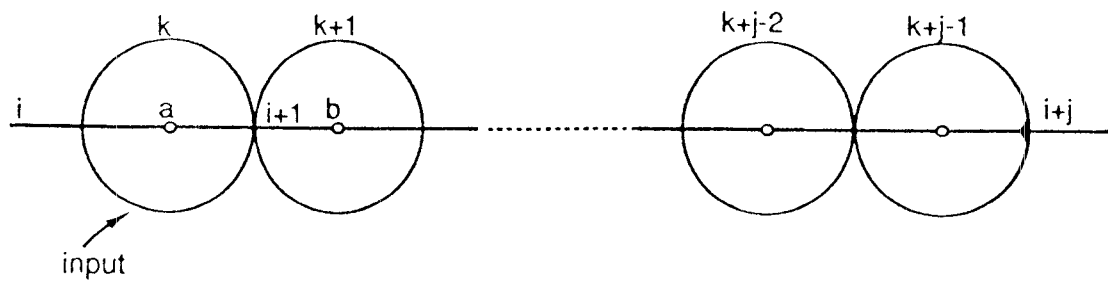
Figure 2.3: A Typical Transmission Line

where

$$m = k, \ k+1, \cdots, \ k+j-2$$

$$n = m - k + i.$$

We note that $\theta_{k+j-1} = \theta_{i+j}$, since the last gear, $(k+j-1)$, is attached to link $(i+j)$. Using (2.13) and (2.14), it can be shown that

$$\theta_{ki} = \sum_{n=1}^{j} b_{kn} \theta_{(i+n)(i+n-1)}, \tag{2.15}$$

where

$$b_{k1} = 1,$$

$$b_{kn} = \pm b_{k(n-1)} N_{(k+n-1)(k+n-2)}, \qquad n = 2, \ 3, \ \cdots, \ j$$

and where the sign depends on the gear mesh between links $(k+n-1)$ and $(k+n-2)$. The angle θ_{ki} denotes the displacement of the input link k with respect to its reference link i, and the angle $\theta_{(i+n)(i+n-1)}$, $n = 2, \ 3, \cdots, \ j$, denote the joint angles of the open-loop chain in a transmission line.

Following Eq. (2.15), it can be concluded that the coefficient b_{kn} is equal to the *train value* defined from the gear pivoted about the nth joint axis to the input gear k. For example, b_{13} for the Cincinnati Milacron T^3 wrist is equal to the train value defined from gear 3 pivoted about the third joint axis to the input gear 4, and is equal to $(+N_{35}N_{54})$, where the positive sign comes from the fact that when the input link makes a positive rotation with respect to the Z_1-axis, gear 3 will also make a positive rotation with respect

21

to the Z_3-axis. Hence, the coefficient of the structure matrix $a_{nk} = b_{kn}$ can be determined by writing Eq. (2.15) as many times as the number of inputs. Note that if the stator of a motor is mounted on the ith link and the rotor is connected to the $(i+1)^{th}$ link, and there are no other gears connected to the motor, then we have a direct drive. The coefficient of a matrix for a direct drive is equal to one, i.e., $\theta_{ki} = \theta_{(i+1)i}$.

2.5 Methodology of Synthesis

As discussed in the previous section, the joint torques of a geared robotic mechanism are related to the input torques by a linear transformation called the structure matrix. There exists a unique structure matrix corresponding to a given mechanism. On the other hand, given a structure matrix, we can construct either planar spur-gear, or spatial bevel-gear mechanisms. The creation of mechanisms can, therefore, be accomplished by the enumeration of structure matrices followed by the construction of mechanisms.

2.5.1 Enumeration of structure matrices

For convenience of enumeration, the non-zero elements of a structure matrix shall be denoted by the "#" sign and the gear ratio and type of gear mesh shall be neglected temporarily. Only those n-DOF geared mechanisms with n articulation points will be considered. From the previous discussions, it can be concluded that the structure matrix A obeys the following rules:

(1) The matrix is an $n \times n$ square matrix. Its determinant shall not be zero, otherwise the mechanism is uncontrollable.

(2) The matrix can always be arranged in a sequence such that the elements in the ith row represent the influence coefficients for the ith joint. The joints shall be renumbered in sequence and the one fixed to the reference frame shall be defined as the first joint.

(3) Since the joints influenced by an actuator are consecutive, non-zero elements in a column of the structure matrix must also be consecutive, i.e., there cannot exist one or more zero elements between any two non-zero elements in a column.

(4) Switching any two columns of the matrix results in renumbering of the two corresponding actuators. Hence, two kinematic structures are said to be isomorphic if their corresponding structure matrices become identical after one or repeated operations of column exchange.

Applying the above rules, the structure matrices can be synthesized in a systematic manner. For example, all the structure matrices for 3-DOF geared mechanisms with three articulation points have been enumerated and listed in Table 2.1. In this table, the matices are arranged according to the distribution of the actuators. It is assumed that each actuator is to be located on the joint axis nearest to the ground of the corresponding transmission line. The letters "g", "s", and "e" denote the location of the actuators are located on the first, second, and third joint axes, respectively, which correspond to the ground, shoulder, and elbow joints of a robot arm, and the power stands for the number of actuators to be installed on that joint axis.

$$
\begin{bmatrix} \# & \# & \# \\ \# & \# & \# \\ \# & \# & \# \end{bmatrix}
\quad
\begin{bmatrix} \# & \# & \# \\ \# & \# & \# \\ \# & \# & 0 \end{bmatrix}
\quad
\begin{bmatrix} \# & \# & \# \\ \# & \# & 0 \\ \# & \# & 0 \end{bmatrix}
\quad
\begin{bmatrix} \# & \# & \# \\ \# & \# & \# \\ \# & 0 & 0 \end{bmatrix}
\quad
\begin{bmatrix} \# & \# & \# \\ \# & \# & 0 \\ \# & 0 & 0 \end{bmatrix}
$$

g^3-1 $\qquad$ g^3-2 $\qquad$ g^3-3 $\qquad$ g^3-4 $\qquad$ g^3-5

$$
\begin{bmatrix} \# & \# & 0 \\ \# & \# & \# \\ \# & \# & \# \end{bmatrix}
\quad
\begin{bmatrix} \# & \# & 0 \\ \# & \# & \# \\ \# & \# & 0 \end{bmatrix}
\quad
\begin{bmatrix} \# & \# & 0 \\ \# & \# & \# \\ \# & 0 & \# \end{bmatrix}
\quad
\begin{bmatrix} \# & \# & 0 \\ \# & \# & \# \\ \# & 0 & 0 \end{bmatrix}
\quad
\begin{bmatrix} \# & \# & 0 \\ \# & 0 & \# \\ \# & 0 & \# \end{bmatrix}
\quad
\begin{bmatrix} \# & \# & 0 \\ \# & \# & \# \\ 0 & 0 & \# \end{bmatrix}
$$

g^2s-1 $\qquad$ g^2s-2 $\qquad$ $g^2$2-3 $\qquad$ g^2s-4 $\qquad$ g^2s-5 $\qquad$ g^2s-6

$$
\begin{bmatrix} \# & \# & 0 \\ \# & 0 & \# \\ \# & 0 & 0 \end{bmatrix}
\quad
\begin{bmatrix} \# & \# & 0 \\ \# & 0 & \# \\ 0 & 0 & \# \end{bmatrix}
$$

g^2s-7 $\qquad$ g^2s-8

$$
\begin{bmatrix} \# & \# & 0 \\ \# & \# & 0 \\ \# & \# & \# \end{bmatrix}
\quad
\begin{bmatrix} \# & \# & 0 \\ \# & \# & 0 \\ \# & 0 & \# \end{bmatrix}
\quad
\begin{bmatrix} \# & \# & 0 \\ \# & 0 & 0 \\ \# & 0 & \# \end{bmatrix}
\quad
\begin{bmatrix} \# & \# & 0 \\ \# & \# & 0 \\ 0 & 0 & \# \end{bmatrix}
\quad
\begin{bmatrix} \# & \# & 0 \\ \# & 0 & 0 \\ 0 & 0 & \# \end{bmatrix}
$$

g^2e-1 $\qquad$ g^2e-2 $\qquad$ g^2e-3 $\qquad$ g^2e-4 $\qquad$ g^2e-5

$$
\begin{bmatrix} \# & 0 & 0 \\ \# & \# & \# \\ \# & \# & \# \end{bmatrix}
\quad
\begin{bmatrix} \# & 0 & 0 \\ \# & \# & \# \\ \# & \# & 0 \end{bmatrix}
\quad
\begin{bmatrix} \# & 0 & 0 \\ \# & \# & \# \\ 0 & \# & \# \end{bmatrix}
\quad
\begin{bmatrix} \# & 0 & 0 \\ \# & \# & \# \\ 0 & 0 & \# \end{bmatrix}
\quad
\begin{bmatrix} \# & 0 & 0 \\ 0 & \# & \# \\ 0 & \# & \# \end{bmatrix}
\quad
\begin{bmatrix} \# & 0 & 0 \\ 0 & \# & \# \\ 0 & 0 & \# \end{bmatrix}
$$

gs^2-1 $\qquad$ gs^2-2 $\qquad$ gs^2-3 $\qquad$ gs^2-4 $\qquad$ gs^2-5 $\qquad$ gs^2-6

$$
\begin{bmatrix} \# & 0 & 0 \\ \# & \# & 0 \\ \# & \# & \# \end{bmatrix}
\quad
\begin{bmatrix} \# & 0 & 0 \\ \# & \# & 0 \\ \# & 0 & \# \end{bmatrix}
\quad
\begin{bmatrix} \# & 0 & 0 \\ \# & \# & 0 \\ 0 & \# & \# \end{bmatrix}
\quad
\begin{bmatrix} \# & 0 & 0 \\ \# & \# & 0 \\ 0 & 0 & \# \end{bmatrix}
\quad
\begin{bmatrix} \# & 0 & 0 \\ 0 & \# & 0 \\ 0 & \# & \# \end{bmatrix}
\quad
\begin{bmatrix} \# & 0 & 0 \\ 0 & \# & 0 \\ 0 & 0 & \# \end{bmatrix}
$$

gse-1 $\qquad$ gse-2 $\qquad$ gse-3 $\qquad$ gse-4 $\qquad$ gse-5 $\qquad$ gse-6

Table 2.1: A List of Admissible 3R Structure Matrices

2.5.2 Construction of mechanisms

Once the structure matrix has been enumerated, the corresponding mechanisms can be constructed as follows:

(1) Construction of transmission lines:

A transmission line can be constructed for each column of a structure matrix. For example, the transmission lines corresponding to the structure matrix $g^2s - 8$ are sketched in Fig. 2.4(a). Note that there are n transmission lines corresponding to an $n \times n$ structure matrix. All of these transmission lines share a common open-loop chain. The common open-loop chain always starts from the base link and ends at the end-effector link. Spur gears are then added on to the open-loop chain according to the existence of non-zero elements in the corresponding column of the structure matrix. The first gear of the kth transmission line is to be pivoted about the joint axis corresponding to the row number of the first non-zero element in the kth column and is considered as the input link. The last gear of the kth transmission line is to be pivoted about the joint axis corresponding to the row number of the last non-zero element in the kth column, and is to be attached to the link which pivotes about the same joint axis and belongs to the far end of the open-loop chain. In the $g^2s - 8$ example, the first column is $(\#\ \#\ 0)^T$. Hence, the open-loop chain consists of links 0, 1, 2, and 3, where link 0 is the base link and link 3 is the end-effector link. The first gear is pivoted about the first joint axis and is considered to be the input link. The second, which is also the last gear, is pivoted about the second joint axis and is attached to link 2. For the purpose of convenience only external gear meshes are used.
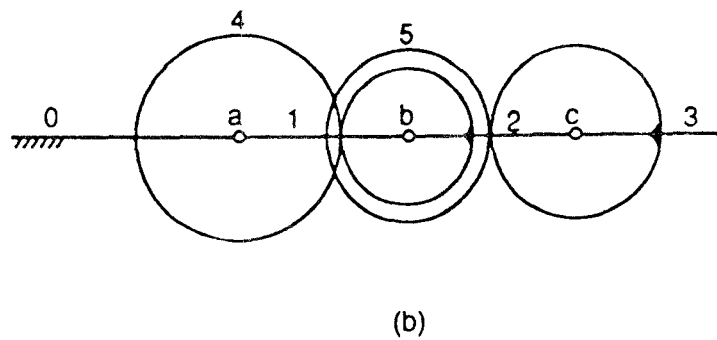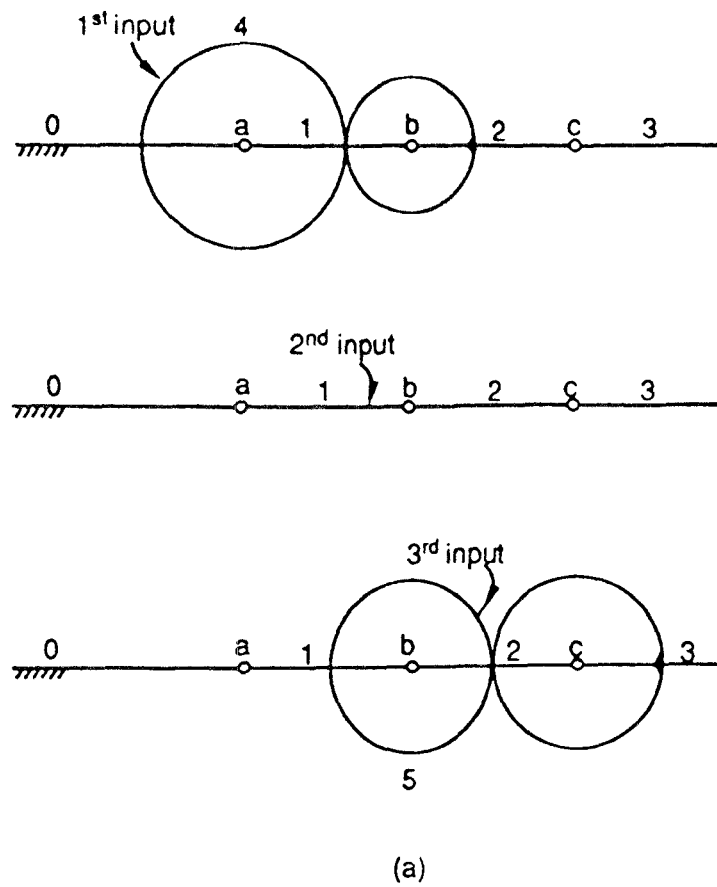
Figure 2.4: Construction of the g^2s-8 Robotic Mechanism

26

(2) Construction of planar mechanisms:

All the transmission lines constructed above can be combined, using the common open-loop chain, to form a planar mechanism. For example, the three transmission lines shown in Fig. 2.4(a) have been combined into a planar mechanism shown in Fig. 2.4(b).

(3) Addition of idler gears:

The mechanisms derived from the above two steps shall be called the *basic mechanisms*. In order to change the direction of rotation, to achieve greater gear reduction, and/or to extend the center distance between two adjacent articulation points, idler gears may be added to the basic mechanisms. For example, Fig. 2.5(a) shows a transmission line with two meshing gears, while Fig. 2.5(b) shows the addition of an idler gear, gear j. Those mechanisms with the addition of one or more idler gears are called the *derived mechanisms* as opposed to the basic mechanisms.

(4) Construction of spatial or spherical mechanisms:

Spatial and/or spherical mechanisms can be constructed by replacing the spur gears with bevel gears and the parallel joint axes with intersecting or skew joint axes. Fig. 2.5(c) shows a spatial transmission line derived from the planar schematic shown in Fig. 2.5(b). Note that idler gears are required for the construction of two nonintersecting joint axes.
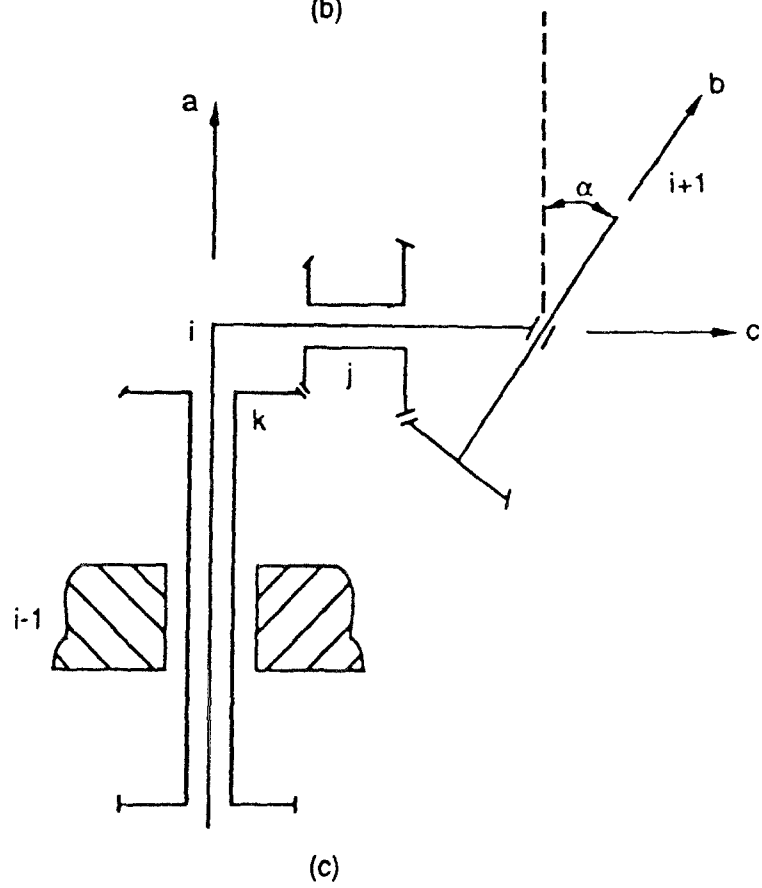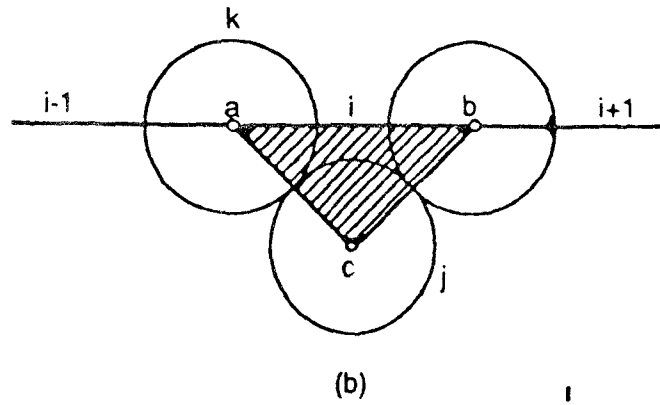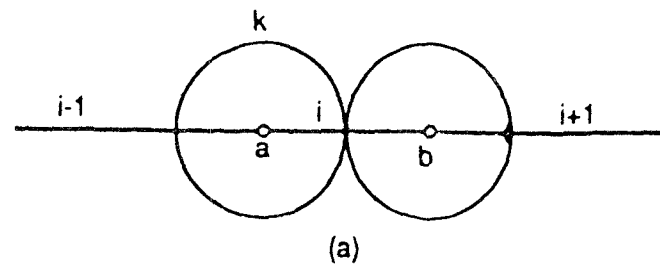
Figure 2.5: Mechanism Construction with Idler Gear and Skewed Joint Axes

2.6 The Creation of 3R Robotic Mechanisms

2.6.1 3R robot arms

All the structure matrices listed in Table 2.1 can be used to construct spatial 3R robot arms. For example, using the structure matrix $g^2s - 8$, three transmission lines and its planar basic mechanism have been sketched in Fig. 2.4(a) and (b), as discussed in the previous section. In order to convert the planar mechanism to a spatial one, the joint axes are rearranged such that the first two intersect perpendicularly, and the third is parallel to the second. Then, spur gears are replaced by bevel gears and, in addition, an idler gear is added to the third transmission line to accommodate for the large offset distance between the second and third joint axes. The resulting mechanism is shown in Fig. 2.6.

The transformation between input displacements and the joint angles for the 3R arm shown in Fig. 2.6 can be obtained by writing Eq. (2.15) three times, once for each transmission line

$$
\begin{bmatrix} \theta_{40} \\ \theta_{10} \\ \theta_{51} \end{bmatrix} = \begin{bmatrix} 1 & N_{24} & 0 \\ 1 & 0 & 0 \\ 0 & 1 & -N_{36}N_{65} \end{bmatrix} \begin{bmatrix} \theta_{10} \\ \theta_{21} \\ \theta_{32} \end{bmatrix} .
\tag{2.16}
$$

Hence, the structure matrix is

$$
A = \begin{bmatrix} 1 & 1 & 0 \\ N_{24} & 0 & 1 \\ 0 & 0 & -N_{36}N_{65} \end{bmatrix}
\tag{2.17}
$$

which is in complete agreement with the $g^2s - 8$ matrix given in Table 2.1.

In a similar manner, 3R robot arms can be constructed for each of the
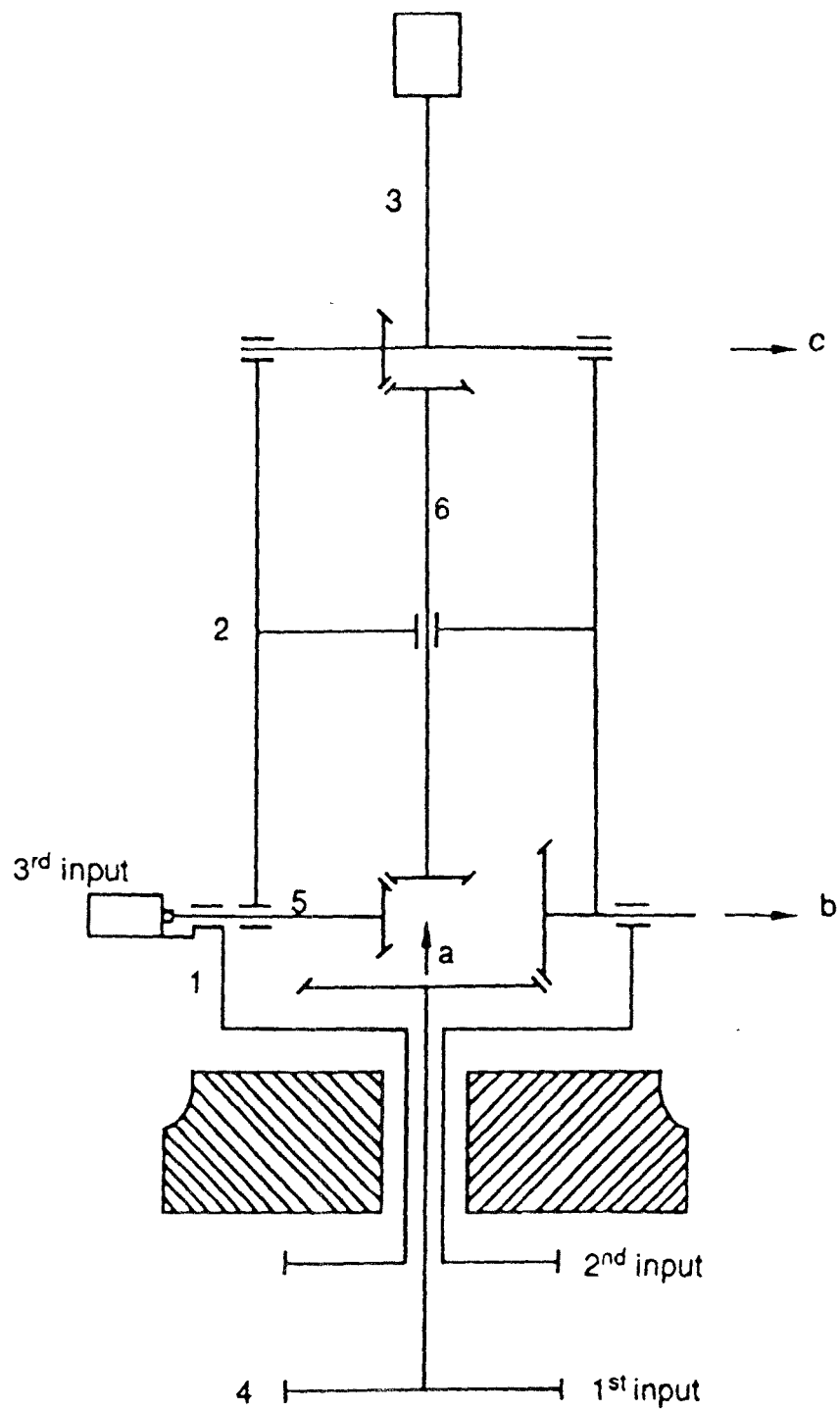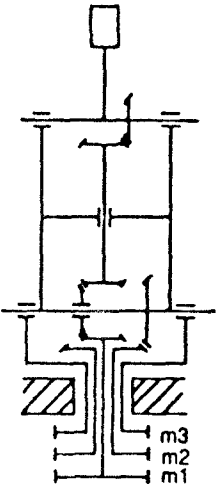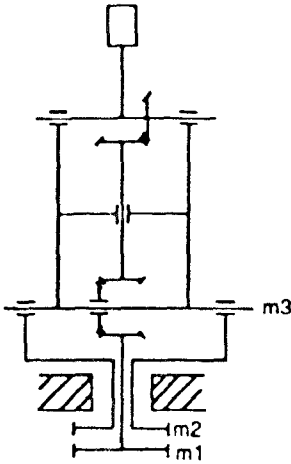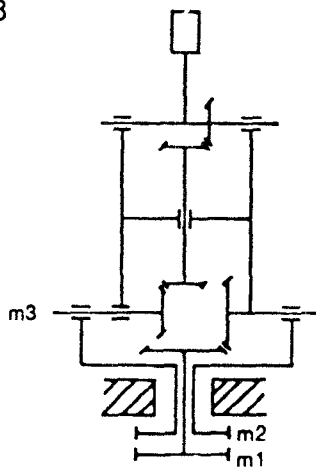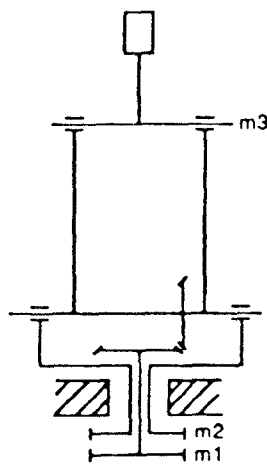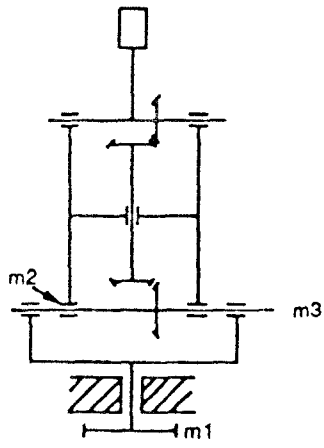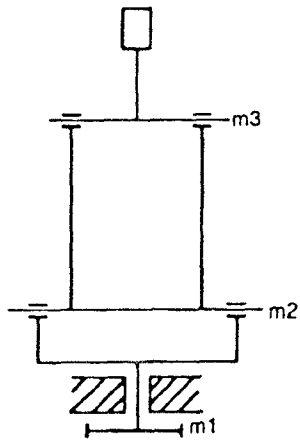
Figure 2.6: A 3-R Robot Arm Derived from Fig. 2.4(b)

structure matrices listed in Table 2.1. We note that the g^3 family permits all the motors to be ground-connected, the g^2s family permits two motors to ground-connected and the third on the shoulder joint, the g^2e family permits two motors to be ground-connected and the third on the elbow joint, the gs^2 family permits only one motor to be ground-connected and the remaining two on the shoulder joint, and finally, the gse family requires the motors to be distributed one on each joint axis. The selection of the type of family is a compromise between mechanical complexity, inertia load, and the coupling, and is not the subject of this investigation. However, suggestion can be made for the selection of designs among the structure matrices within each family. From mechanical complexity and coupling points of view, we believe the $g^3 - 5$, $g^2s - 7$ and $g^2s - 8$, $g^2e - 5$, $gs^2 - 6$, as well as $gse - 6$ are the least complex and least coupled structure matrices for the g^3, g^2s, g^2e, gs^2, and gse families, respectively. For this reason, a 3R arm corresponding to each of the aforementioned structure matrices has been constructed and listed in Table 2.2. The joint axes for each of the 3R arms listed in Table 2.2 have been arranged in a configuration similar to that of the PUMA arm. We note that the mechanism configurations $g^3 - 5$ and $gs^2 - 6$ shown in Table 2.2 were recently revealed by Tsai and Freudenstein (1989).

2.6.2 3R wrists

In practice, in order to reduce the inertia load of a manipulator, the wrist design must be compact and lightweight. The actuators of a wrist mechanism are generally preferred to be located on the base link of the wrist. The g^3 family listed in Table 2.1 permits all the actuators to be

Table 2.2: Some Recommended 3R Robot Arms

located on the base link and is recommended for the wrist design. For the purpose of demonstration, the mechanism corresponding to the structure matrix $g^3 - 5$ is constructed as an example. Three transmission lines can be constructed. The combination of these three transmission lines forms a planar basic mechanism as shown in Fig. 2.7(a). After the three joint axes are made to intersect at a point and the spur gears are replaced with bevel gears, a spherical wrist mechanism can be constructed as shown in Fig. 2.7(b). Note that the mechanism structure is identical to that of the Cincinnati Milacron T^3 wrist (Stackhouse, 1979).

As noted earlier, idler gears can be added to modify the gear ratio or to change the direction of rotation. Fig. 2.7(c) shows the addition of an idler gear 7 between the gear mesh 3-5 of the mechanism shown in Fig. 2.7(b). Note that this becomes the structure of PUMA wrist.

Following the same procedure, all the recommended basic spherical wrist mechanisms have been constructed and listed in Table 2.3. It is interesting to note that the $g^3 - 3$ mechanism is structurally the same as the Bendix wrist (Anonymous, 1982).

2.7 Summary

The concept of transmission lines has been introduced for the kinematic analysis of geared robotic mechanisms. Using the concept, a set of rules for the enumeration of structure matrices has been derived, and a procedure for the construction of basic mechanisms, planar or spatial, has been developed.

33
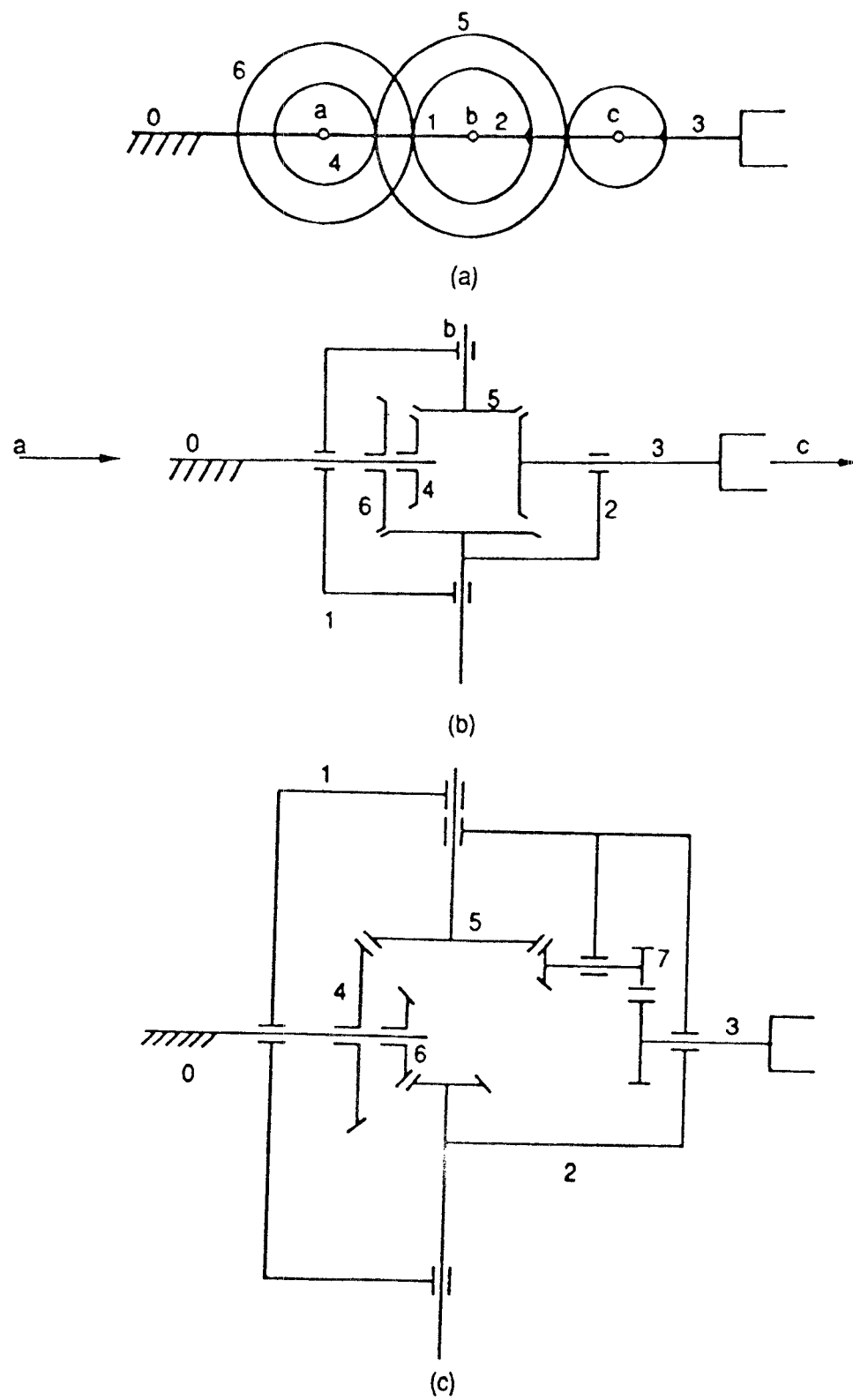
Figure 2.7: Construction of g^3-5 Wrist Mechanisms

34
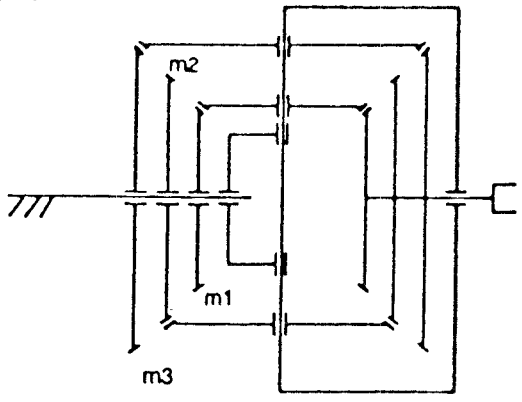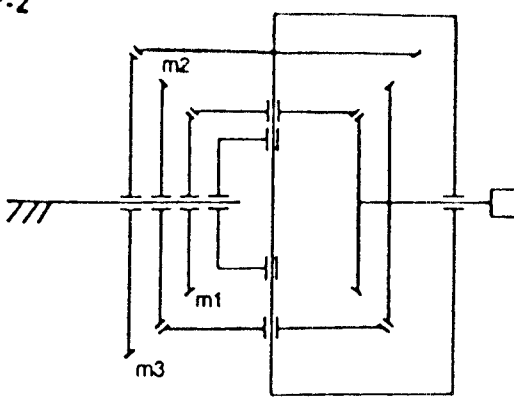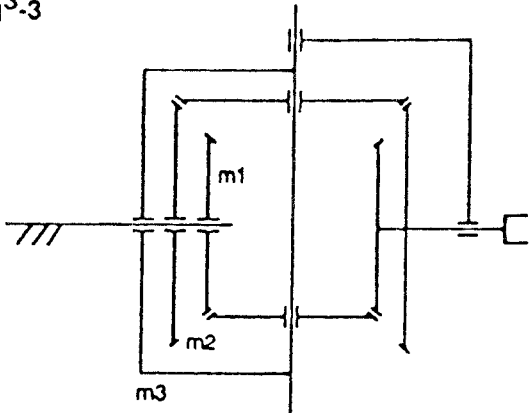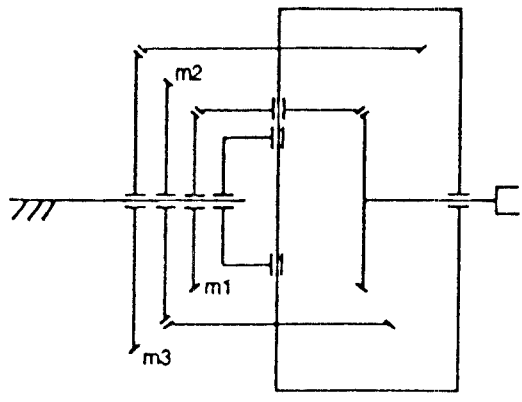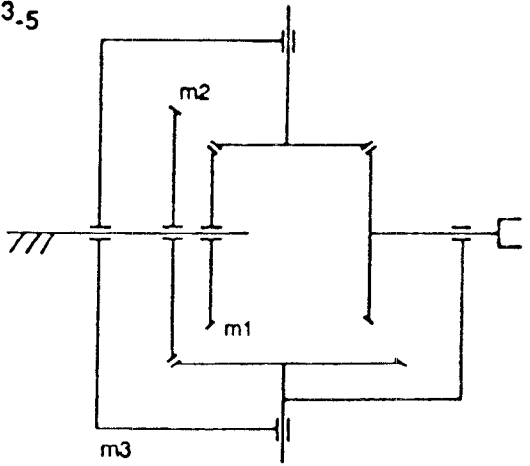
Table 2.3: A List of Basic Wrist Mechanisms

It is also shown that idler gears can be added to these basic mechanisms to form additional mechanisms. The theorem has been demonstrated by the enumeration of 3-DOF robotic arms and wrists. Some of the mechanism configurations presented are believed to be new and novel, and deserve further studies.

We believe this method of enumeration is more straightforward and more efficient than that of graph representation. The design can be started from a desired structure matrix, i.e., a desired mechanical coupling, instead of searching for all the admissible mechanisms as is the case of graph theory.

Although we have used the enumeration of 3-DOF mechanisms as an example, the methodology presented in this work is completely general and can be applied to the enumeration of 6-DOF mechanisms as well.

Chapter 3

The Creation of Redundant-Drive Backlash-Free Robotic (RBR) Mechanisms

Most industrial robots use gear trains for power transmission to allow actuators to be located in some desirable positions. Gear trains are also used for torque amplification. Backlash is provided for prevention of jamming of gear teeth due to manufacturing errors or thermal expansion. However, backlash can cause momentary loss of coupling between two mating gears whenever there is a torque reversal. It can result in motion discontinuity, position uncertainty and impact in mechanical systems which, in turn, makes accurate control of a manipulator difficult. End-effector positioning accuracy is also compromised due to backlash. Precision gears, spring-loaded split gear assemblies, and precise mechanical adjustment are often used to overcome these difficulties. However, these techniques do not completely eliminate

the backlash and can increase the cost of manufacturing and assembling. Therefore, further study on reducing or eliminating the backlash problem is urgently needed.

In this chapter, an innovative concept for the control of gear backlash in robotic mechanisms will be introduced. Fundamental rules governing the function of RBR mechanisms will be presented. Based on these fundamental rules, a number of RBR mechanisms will be enumerated.

3.1 The Concept

Fig. 3.1 shows a simple one-DOF gear train with two unidirectional drives, where D_1 and D_2 are the driving gears and F is the follower. The backlash in this mechanism can be controlled by applying torques to D_1 in a clockwise sense and D_2 in a counter-clockwise sense at all times. The resultant torque acting on F will be in the counter-clockwise or clockwise sense depending on whether torque contributed by D_1 is greater or less than that contributed by D_2. Since no torque reversal is required to drive F, the effects of gear backlash are completely eliminated.

The controllability can be analyzed from kinematic and static points of view. The kinematic equation for the mechanism shown in Fig. 3.1 can be written as:

$$\begin{bmatrix} \phi_1 \\ \phi_2 \end{bmatrix} = \begin{bmatrix} -(N_f/N_1) \\ -(N_f/N_2) \end{bmatrix} \theta, \tag{3.1}$$

where ϕ_1, ϕ_2 and θ denote the angular displacements of gears D_1, D_2 and F,
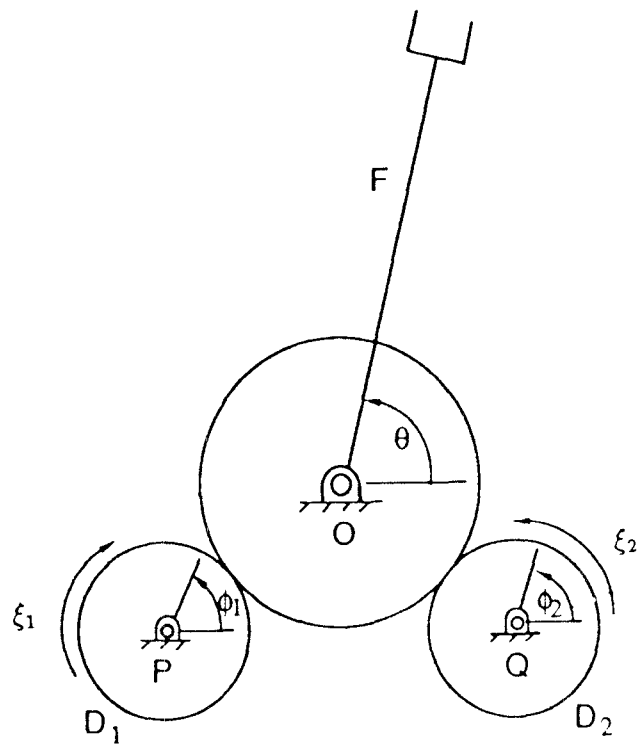
Figure 3.1: One-DOF Mechanism with Redundant Unidirectional Drives

respectively, and, N_1, N_2 and N_f represent their tooth numbers. Note that the negative sign stands for an external gear mesh.

For such a mechanical system, it can be shown that the input and output torques are related by the following equation:

$$\tau_f = \left[\begin{array}{cc} -(N_f/N_1) & -(N_f/N_2) \end{array} \right] \left[\begin{array}{c} \xi_1 \\ \xi_2 \end{array} \right], \tag{3.2}$$

where ξ_1 and ξ_2 are the torques applied to D_1 and D_2, respectively, and, τ_f is the output torque on the follower F. Thus, given the input torques ξ_1 and ξ_2, the resultant joint torque τ_f is uniquely determined. However, for a desired output torque τ_f, the required input torques are indeterminate. For example, the input torques can be expressed as:

$$\left[\begin{array}{c} \xi_1 \\ \xi_2 \end{array} \right] = \left[\begin{array}{c} -\frac{N_1 N_2^2}{N_f(N_1^2+N_2^2)} \\ -\frac{N_1^2 N_2}{N_f(N_1^2+N_2^2)} \end{array} \right] \tau_f + \lambda \left[\begin{array}{c} N_1 \\ -N_2 \end{array} \right], \tag{3.3}$$

where λ is an arbitrary real number. The first term on the right-hand-side of Eq. (3.3) is referred to as the particular solution and the second term the homogenuous solution. From Eq. (3.3), it is clear that by selecting a proper positive λ, the sense of input torques $[\begin{array}{cc} \xi_1 & \xi_2 \end{array}]^T$ can be maintained in the $[\begin{array}{cc} + & - \end{array}]^T$ direction at all times regardless of the value of τ_f. Similarly, the sense of input torques can also be maintained in the $[\begin{array}{cc} - & + \end{array}]^T$ direction by selecting a proper negative λ. Hence, the mechanism can be controlled by two unidirectional drives designed either in the $[\begin{array}{cc} + & - \end{array}]^T$ direction or in the $[\begin{array}{cc} - & + \end{array}]^T$ direction. Since the input torques can be maintained in predetermined unidirection senses at all times, backlash will never occur.

The principle illustrated in the above simple example can be extended to

the general n-DOF gear-coupled robotic mechanisms with k-unidirectional drives. For an n-DOF articulated mechanism, it can be shown that the input angular displacements and joint angles are related by the following linear transformation:

$$\underline{\phi} = B \, \underline{\theta},\tag{3.4}$$

where $\underline{\theta} = [\theta_1, \theta_2, \cdots, \theta_n]^T$ is the joint angular displacement vector,

$\underline{\phi} = [\phi_1, \phi_2, \cdots, \phi_k]^T$ is the input angular displacement vector,

and $B = [b_{ij}]$ is a k by n matrix.

Note that the word "joint" refers to the joint in the equivalent open-loop chain of a gear-coupled robotic mechanism. See Tsai (1988) for the definition of an equivalent open-loop chain.

It can also be shown that the equation relating the resultant joint torques to the input torques for an n-DOF system is given by:

$$\underline{\tau} = B^T \underline{\xi} = A \, \underline{\xi},\tag{3.5}$$

where $\underline{\tau} = [\, \tau_1, \tau_2, \cdots, \tau_n \,]^T$ denotes the resultant joint torques, and $\underline{\xi} = [\, \xi_1, \xi_2, \cdots, \xi_k]^T$ denotes the input actuator torques, and where the matrix, A, known as the structure matrix, is a function of the structural topology and gear ratios.

For a given set of desired joint torques, Eq. (3.5) constitutes n linear equations in k unknowns. In order to maintain unidirectional torques in the actuators, k should be greater than n. Thus, the solution for the actuator torques consists of a particular solution plus a $(k - n)$-dimensional

homogenous solution. The homogenous solution corresponds to certain sets of actuator torques that result in no net joint torques. It can be expressed as a sum of $(k - n)$ basis vectors, each of them being multiplied by an arbitrary constant. Hence, by adjusting the constants, unidirectional actuator torques can be maintained. Furthermore, if $k = n + 1$, then every element in the null vector should be non-zero, and the direction of input torques can be controlled either in the direction of the null vector or in the opposite direction.

For the case of $k = n + 1$, let the direction of input torques be in the direction of the null vector, then the parameter, λ, has to be positive. Theoretically, the minimum value of λ is

$$\lambda_{\min} = \text{Max}\left(-\frac{(\xi_i)_p}{\mu_i}\right) \tag{3.6}$$

where $(\xi_i)_p$ is the particular solution of ξ_i and μ_i the ith element of the null vector. Under this condition, one of the input torques is zero, i.e. only n actuators drive the system at a time. The energy consumption of this system will be equal to the energy consumption of a conventional robot plus the energy loss in the additional transmission line. However, to assure positive coupling at all times, λ is usually chosen to be the above minimum number plus a small positive number. The energy consumption will then increase slightly because of the increased friction in the system.

3.2 Creation of RBR Mechanisms

3.2.1 Enumeration of Structure Matrices

In the previous chapter, it has been shown that the topology of a gear-coupled robotic mechanism can be represented by a structure matrix. It has also been shown that gear-coupled robotic mechanisms can be created systematically in two steps: (1) the enumeration of admissible structure matrices, followed by (2) the construction of mechanisms from the structure matrices (Chang and Tsai, 1990). The methodology can also be used for the creation of RBR mechanisms. The enumeration of admissible structure matrices will be discussed in this subsection and the construction of mechanisms will be discussed in the following subsection. From mechanical simplicity and coupling points of view, only those mechanisms with the number of transmission lines greater than the number of DOF by one, i.e. $k = n + 1$, will be considered. Hence, the structure matrix obeys the following fundamental rules:

R1. The structure matrix is an $n \times (n+1)$ matrix and each row must contain at least two non-zero elements.

R2. The sub-matrix obtained by removing any column from a structure matrix is non-singular.

R3. Since actuator torque is transmitted to various joints in a consecutive manner, non-zero elements in a column of the structure matrix must be consecutive.

R4. Switching any two columns of a structure matrix results in a renum-

$$
\begin{bmatrix} \# & \# & \# \\ \# & \# & \# \end{bmatrix} \qquad \begin{bmatrix} \# & \# & \# \\ \# & \# & 0 \end{bmatrix} \qquad \begin{bmatrix} \# & \# & 0 \\ \# & \# & \# \end{bmatrix} \qquad \begin{bmatrix} \# & \# & 0 \\ \# & 0 & \# \end{bmatrix}
$$
$$
g^3 - 1 \qquad\qquad g^3 - 2 \qquad\qquad g^2 s - 1 \qquad\qquad g^2 s - 2
$$

Table 3.1: Admissible 2-DOF Structure Matrices

bering of the two corresponding input actuators. Hence, two kinematic structures are said to be isomorphic if their corresponding structure matrices become identical after one or repeated operations of column exchange.

Rules 1 and 2 ensure the unidirectional controllability of a mechanism. Applying the aboves rules, all the admissible 2-DOF and 3-DOF structure matrices suitable for the construction of RBR mechanisms have been enumerated. Table 3.1 lists four admissible structure matrices for two-DOF mechanisms, where the "#" sign denotes the existence of a non-zero element in the matrix.

Table 3.2 lists all the admissible 3-DOF structure matrices. In Table 3.2, the matrices are arranged according to the distribution of actuators. It is assumed that each transmission line has its actuator located on the joint axis nearest to the ground. The letters g, s and e denote that the actuators are to be located on the 1st, 2nd and 3rd joint axes, respectively, and the power stands for the number of actuators to be installed on that joint axis. There are five families listed in Table 3.2: g^4, $g^3 s$, $g^3 e$, $g^2 s^2$ and $g^2 se$. For example, the g^4 family allows all the actuators to be ground-connected. The selection

44

$$\begin{bmatrix} \# & \# & \# & \# \\ \# & \# & \# & \# \\ \# & \# & \# & \# \end{bmatrix} \quad \begin{bmatrix} \# & \# & \# & \# \\ \# & \# & \# & \# \\ \# & \# & \# & 0 \end{bmatrix} \quad \begin{bmatrix} \# & \# & \# & \# \\ \# & \# & \# & 0 \\ \# & \# & \# & 0 \end{bmatrix} \quad \begin{bmatrix} \# & \# & \# & \# \\ \# & \# & \# & \# \\ \# & \# & 0 & 0 \end{bmatrix}$$

$$g^4 - 1 \qquad\qquad g^4 - 2 \qquad\qquad g^4 - 3 \qquad\qquad g^4 - 4$$

$$\begin{bmatrix} \# & \# & \# & \# \\ \# & \# & \# & 0 \\ \# & \# & 0 & 0 \end{bmatrix}$$

$$g^4 - 5$$

$$\begin{bmatrix} \# & \# & \# & 0 \\ \# & \# & \# & \# \\ \# & \# & \# & \# \end{bmatrix} \quad \begin{bmatrix} \# & \# & \# & 0 \\ \# & \# & \# & \# \\ \# & \# & \# & 0 \end{bmatrix} \quad \begin{bmatrix} \# & \# & \# & 0 \\ \# & \# & \# & \# \\ \# & \# & 0 & \# \end{bmatrix} \quad \begin{bmatrix} \# & \# & \# & 0 \\ \# & \# & \# & \# \\ \# & \# & 0 & 0 \end{bmatrix}$$

$$g^3s - 1 \qquad\qquad g^3s - 2 \qquad\qquad g^3s - 3 \qquad\qquad g^3s - 4$$

$$\begin{bmatrix} \# & \# & \# & 0 \\ \# & \# & \# & \# \\ \# & 0 & 0 & \# \end{bmatrix} \quad \begin{bmatrix} \# & \# & \# & 0 \\ \# & \# & 0 & \# \\ \# & \# & 0 & \# \end{bmatrix} \quad \begin{bmatrix} \# & \# & \# & 0 \\ \# & \# & 0 & \# \\ \# & \# & 0 & 0 \end{bmatrix} \quad \begin{bmatrix} \# & \# & \# & 0 \\ \# & \# & 0 & \# \\ \# & 0 & 0 & \# \end{bmatrix}$$

$$g^3s - 5 \qquad\qquad g^3s - 6 \qquad\qquad g^3s - 7 \qquad\qquad g^3s - 8$$

$$\begin{bmatrix} \# & \# & \# & 0 \\ \# & \# & \# & 0 \\ \# & \# & \# & \# \end{bmatrix} \quad \begin{bmatrix} \# & \# & \# & 0 \\ \# & \# & \# & 0 \\ \# & \# & 0 & \# \end{bmatrix} \quad \begin{bmatrix} \# & \# & \# & 0 \\ \# & \# & 0 & 0 \\ \# & \# & 0 & \# \end{bmatrix} \quad \begin{bmatrix} \# & \# & \# & 0 \\ \# & \# & \# & 0 \\ \# & 0 & 0 & \# \end{bmatrix}$$

$$g^3e - 1 \qquad\qquad g^3e - 2 \qquad\qquad g^3e - 3 \qquad\qquad g^3e - 4$$

$$\begin{bmatrix} \# & \# & \# & 0 \\ \# & \# & 0 & 0 \\ \# & 0 & 0 & \# \end{bmatrix}$$

$$g^3e - 5$$

$$\begin{bmatrix} \# & \# & 0 & 0 \\ \# & \# & \# & \# \\ \# & \# & \# & \# \end{bmatrix} \quad \begin{bmatrix} \# & \# & 0 & 0 \\ \# & \# & \# & \# \\ \# & \# & \# & 0 \end{bmatrix} \quad \begin{bmatrix} \# & \# & 0 & 0 \\ \# & \# & \# & \# \\ \# & 0 & \# & \# \end{bmatrix} \quad \begin{bmatrix} \# & \# & 0 & 0 \\ \# & \# & \# & \# \\ \# & 0 & \# & 0 \end{bmatrix}$$

$$g^2s^2 - 1 \qquad\qquad g^2s^2 - 2 \qquad\qquad g^2s^2 - 3 \qquad\qquad g^2s^2 - 4$$

$$\begin{bmatrix} \# & \# & 0 & 0 \\ \# & \# & \# & \# \\ 0 & 0 & \# & \# \end{bmatrix} \quad \begin{bmatrix} \# & \# & 0 & 0 \\ \# & 0 & \# & \# \\ \# & 0 & \# & \# \end{bmatrix} \quad \begin{bmatrix} \# & \# & 0 & 0 \\ \# & 0 & \# & \# \\ \# & 0 & \# & 0 \end{bmatrix}$$

$$g^2s^2 - 5 \qquad\qquad g^2s^2 - 6 \qquad\qquad g^2s^2 - 7$$

$$\begin{bmatrix} \# & \# & 0 & 0 \\ \# & \# & \# & 0 \\ \# & \# & \# & \# \end{bmatrix} \quad \begin{bmatrix} \# & \# & 0 & 0 \\ \# & \# & \# & 0 \\ \# & \# & 0 & \# \end{bmatrix} \quad \begin{bmatrix} \# & \# & 0 & 0 \\ \# & \# & \# & 0 \\ \# & 0 & \# & \# \end{bmatrix} \quad \begin{bmatrix} \# & \# & 0 & 0 \\ \# & 0 & \# & 0 \\ \# & 0 & \# & \# \end{bmatrix}$$

$$g^2se - 1 \qquad\qquad g^2se - 2 \qquad\qquad g^2se - 3 \qquad\qquad g^2se - 4$$

$$\begin{bmatrix} \# & \# & 0 & 0 \\ \# & \# & \# & 0 \\ \# & 0 & 0 & \# \end{bmatrix} \quad \begin{bmatrix} \# & \# & 0 & 0 \\ \# & \# & \# & 0 \\ 0 & 0 & \# & \# \end{bmatrix} \quad \begin{bmatrix} \# & \# & 0 & 0 \\ \# & 0 & \# & 0 \\ 0 & 0 & \# & \# \end{bmatrix} \quad \begin{bmatrix} \# & \# & 0 & 0 \\ \# & 0 & \# & 0 \\ \# & 0 & 0 & \# \end{bmatrix}$$

$$g^2se - 5 \qquad\qquad g^2se - 6 \qquad\qquad g^2se - 7 \qquad\qquad g^2se - 8$$

Table 3.2: Admissible 3-DOF Structure Matrices

of structure matrix is a compromise between mechanical complexity, inertia load, and the coupling, and is not the subject of this study.

3.2.2 Construction of Mechanisms

The construction of mechanisms from a structure matrix can be accomplished by the method outlined in chapter 2. For example, we can construct a mechanism from structure matrix $g^2se - 6$ listed in Table 3.2 as follows. First, a transmission line is constructed for each column of the structure matrix as shown in Figs. 3.2(a), (b), (c) and (d). Then, these transmission lines are combined to form a basic mechanism as depicted in Fig. 3.2(e). Finally, idler gears can be added to increase the offset distance between two joint axes and/or to achieve greater gear reduction. A derived spatial 3-DOF RBR mechanism is shown in Fig. 3.3. Note that, many mechanisms can be derived from a basic mechanism as discussed earlier.

Fig. 3.4 shows some additional mechanisms constructed from the structure matrices listed in Table 3.2 where A_i denotes the ith actuator. These mechanisms are judged to be less coupled among each of the five families.

3.3 System Observer

As discussed in section 3.1, torque reversal will cause a loss of positive coupling between two mating gears and result in an end-effector position uncertainty. From mathematical point of view, this decoupling will momen-

46
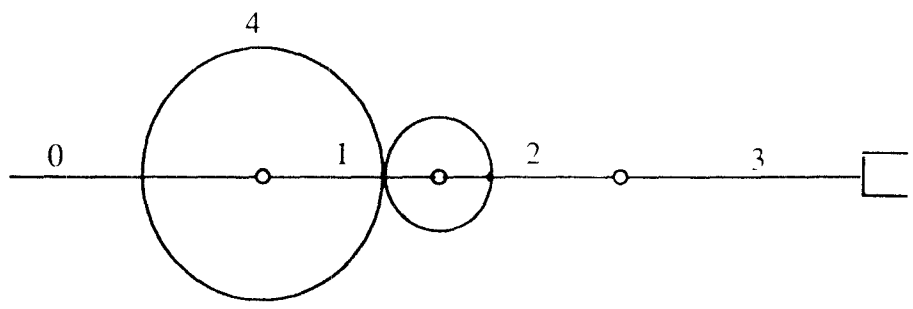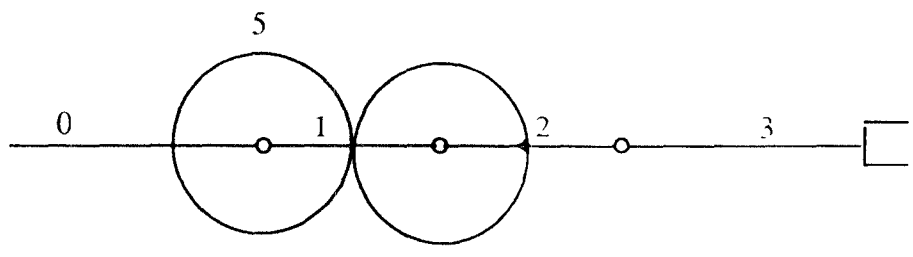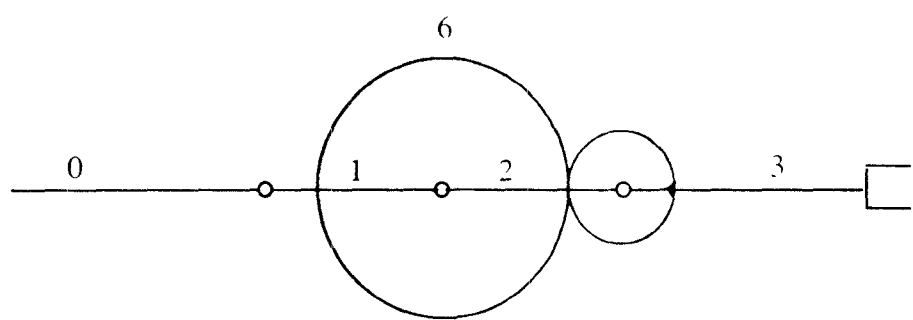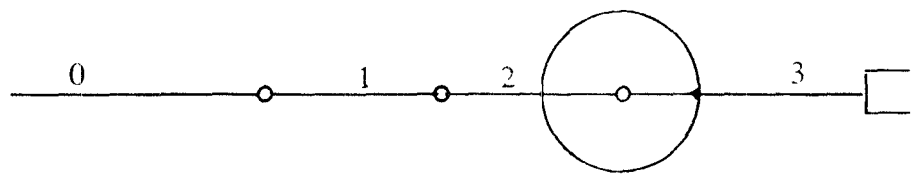
Figure 3.2: Construction of the g^2se-6 Basic Mechanism

47
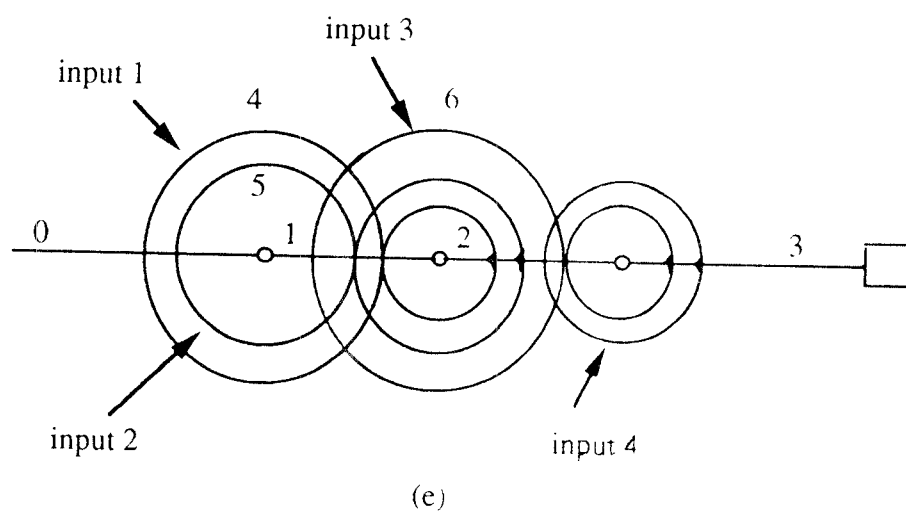
Figure 3.2: (Continued)

48
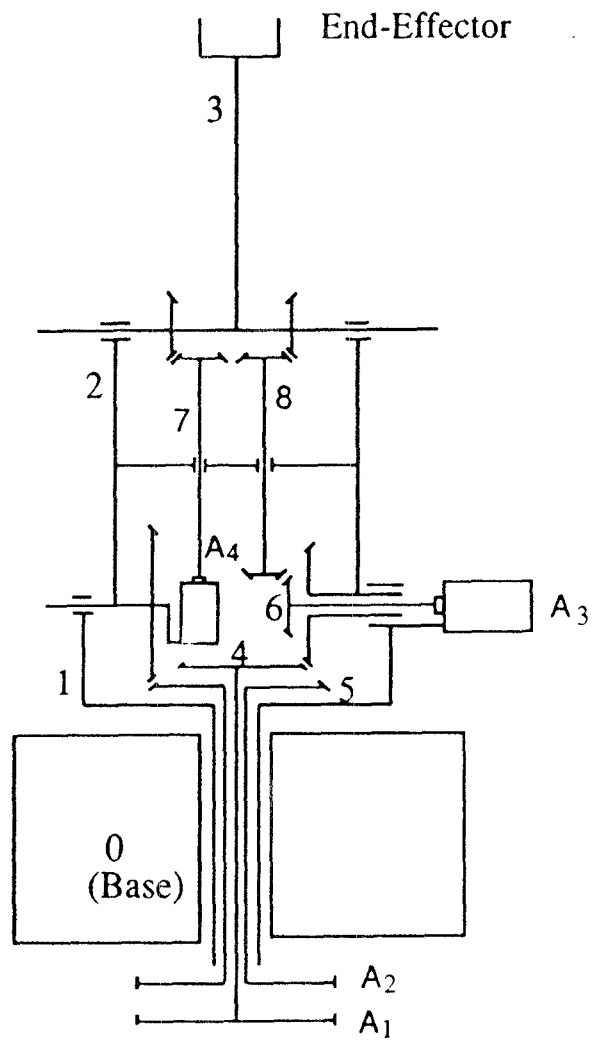
Figure 3.3: A Spatial 3-DOF RBR Arm Derived from Fig. 3.2 (e)

$g^2se\text{-}7$ $g^2se\text{-}8$ $g^2s^2\text{-}7$ $g^3e\text{-}5$

$g^3s\text{-}7$ $g^3s\text{-}8$ $g^4\text{-}5$
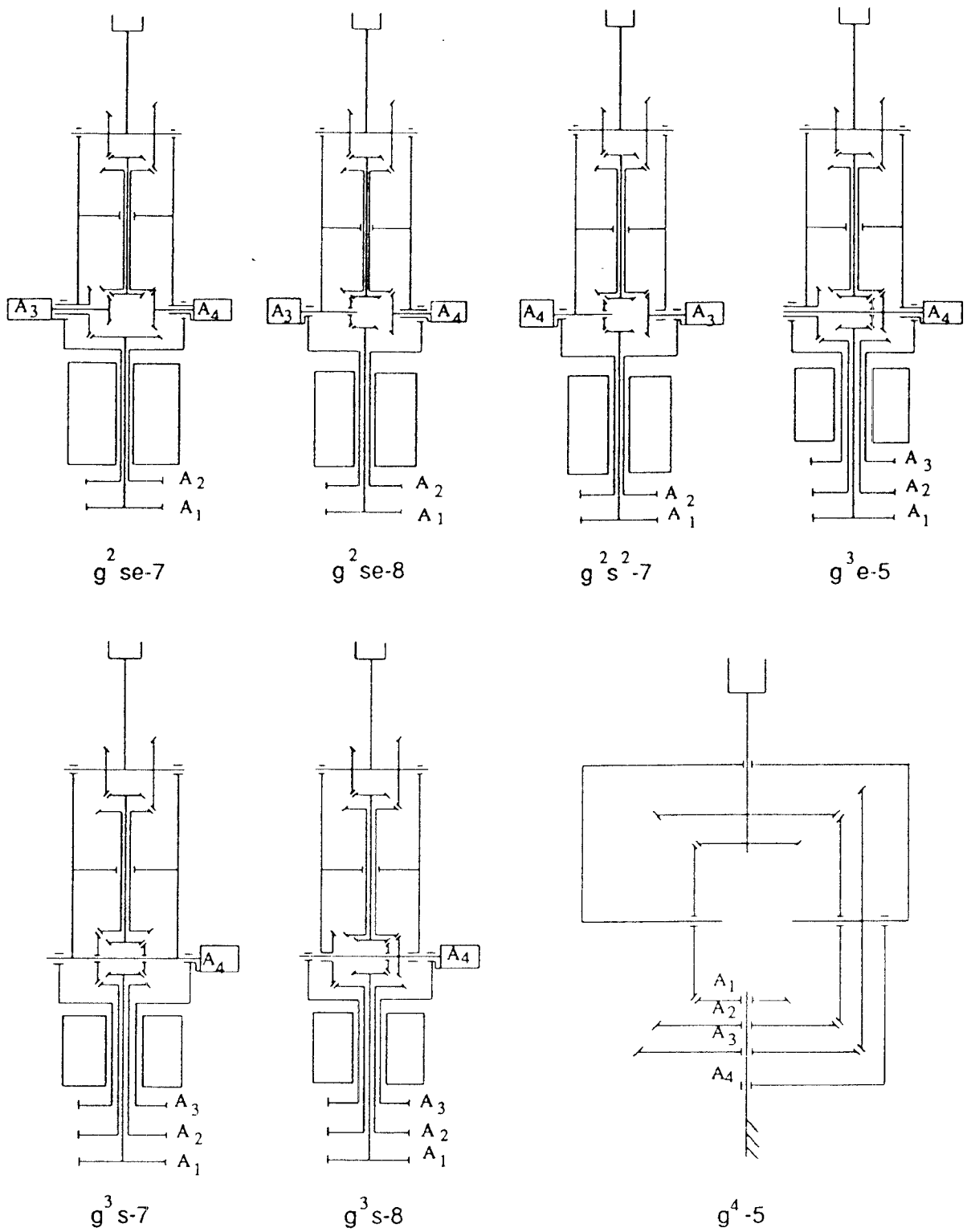
Figure 3.4: Less Coupled 3-DOF RBR Mechanisms

tarily increase the degrees of freedom in the system and lead to the state of uncertainty. This is illustrated in Fig. 3.5. The system has only one DOF when gears 1 and 2 are in positive coupling, and the angular displacement of the driven gear 2 can be predicted from that of the driving gear 1. However, when the two gears lose contact, then both gears can rotate independently and the DOF for the system is increased by one. Therefore, at least two measurements are required to tell the state of the system. One sensor or multiple dependent sensors (e.g. a position and a velocity sensors installed on one joint axis) will not be adequate to describe the system.

The RBR mechanisms created by the method discussed in this chapter will keep all the gear meshes in positive coupling. From the non-singular properties of the structure sub-matrix, it can be concluded that an RBR system can be observed if at least n sensors are installed on any n transmission lines.

3.4 Prototype Design of a Two-DOF RBR Arm

A two-DOF planar robot arm with three unidirectional drives has been designed to demonstrate the proof of this concept. The structure matrix $g^2 s - 2$ in Table 3.1 is selected for the reason of simplicity and less coupling. Its basic mechanism can be constructed by the procedures discussed in the previous section. Fig. 3.6 shows the resulting basic mechanism.

The prototype arm is designed to have both joint axes parallel to the

51
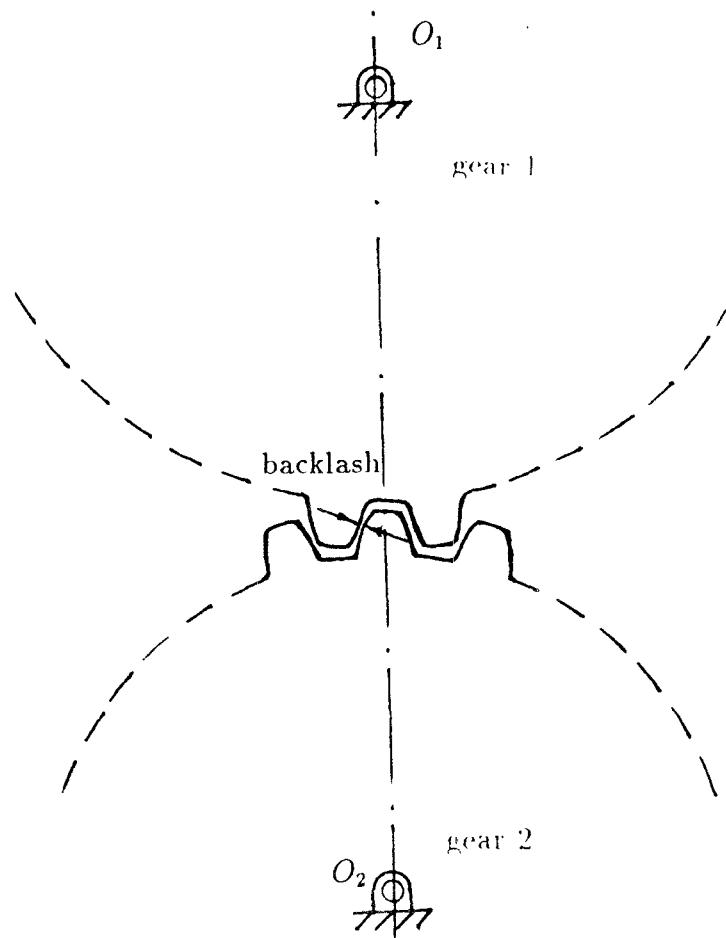
Figure 3.5: Loss of Contact Between Two Gear Teeth

52
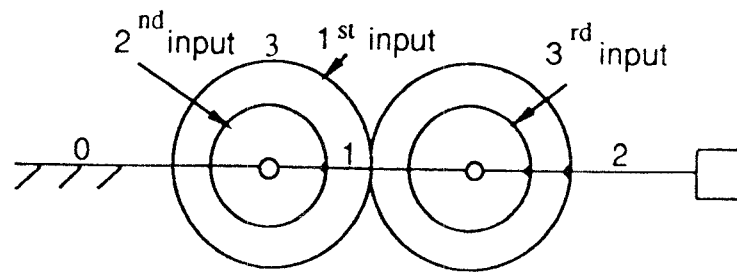
Figure 3.6: Construction of the g^2s-2 Basic Mechanism

53

direction of gravity to reduce the effect of gravitational force. Also both links are designed to have equal link lengthes to optimize its workspace. Idler gears are used to increase the offset distance between the two joint axes. The final design is shown in Fig. 3.7. There are three transmission lines and three actuators (motors). The first two motors are ground-connected and the third is installed on the rear-end of the upper-arm for the purpose of counter-balancing. Motor 1 drives both joints 1 and 2 simultaneously, motor 2 drives joint 1 and motor 3 drives joint 2, all with a two-stage gear reduction between the motor and the first joint it drives. Both actuator No. 1 and 2 use Electro-Craft 0588-33-501 DC motors and, actuator No. 3 uses the Pitman 14203 DC motor. In order to reduce the resultant torque on joint 2 due to motor 1, two step-up gear amplifications, gear pairs 3 to 4 and 5 to 6, are used in the first transmission line.

As noted previously, two measurements are enough for the description of the state for this system. Since actuators 2 and 3 drive joints 1 and 2, respectively, sensors are placed on actuators 2 and 3 to avoid the compliance problem associated with the first transmission line. In this design, the reduction gear unit of the 3rd transmission line is placed close to motor 3 to reduce the inertia of the system.

In the design, the tooth numbers for all gears are as follows: $N_3 = 64$, $N_4 = 16$, $N_{14} = N_{16} = N_{18} = N_{20} = 15$, $N_5 = N_{12} = 24$, $N_6 = 12$, $N_7 = N_{10} = 20$, $N_8 = 10$, $N_9 = 48$, $N_{11} = 120$, and, $N_{13} = N_{15} = N_{17} = N_{19} = 96$. The structure matrix can be obtained by writing Eq. (2.15) three times, once for each transmission line:

$$A = \begin{bmatrix} \frac{N_{17}N_{19}}{N_{18}N_{20}} & \frac{N_{13}N_{15}}{N_{14}N_{16}} & 0 \\ \frac{N_{17}N_{19}N_4 N_6}{N_{18}N_{20}N_3 N_5} & 0 & -\frac{N_7 N_9 N_{11}}{N_8 N_{10} N_{12}} \end{bmatrix}. \tag{3.7}$$
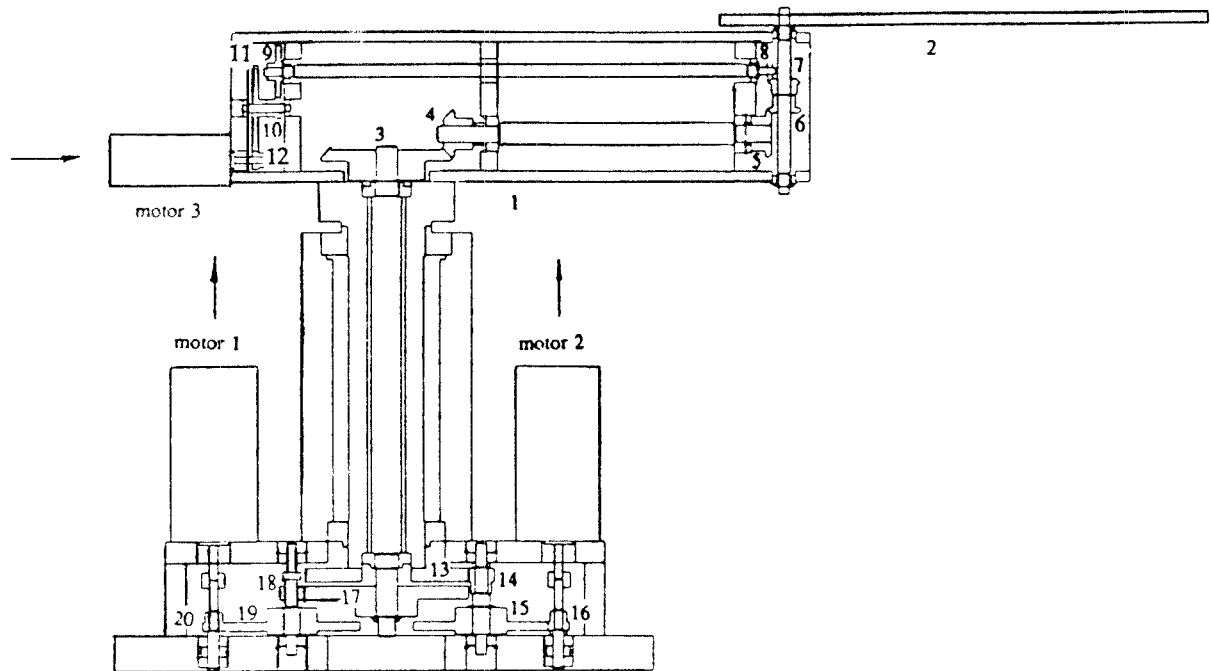
Figure 3.7: An Experimental 2-DOF Manupulator Derived from Fig. 3.6

$$\text{(3.8)}$$

$$= \begin{bmatrix} 40.96 & 40.96 & 0 \\ 5.12 & 0 & -24 \end{bmatrix}. \tag{3.9}$$

The null vector of this structure matrix is $[75, -75, 16]^T$. Hence, actuator torque can be maintained either in the direction of $[+, -, +]^T$ or $[-, +, -]^T$.

3.5 Summary

A new and innovative concept has been introduced for the control of backlash in gear-coupled robotic systems. The concept utilizes redundant unidirectional drives to assure positive coupling of gear meshes at all times.

Based on the concept, a systematic methodology has been established for the enumeration of a class of unidirectional-drive gear-coupled robotic mechanisms. Some typical two- and three-DOF robot manipulators have been sketched for the purpose of demonstration.

The main purpose of this concept is the elimination of gear backlash in a manipulator. One of the necessary conditions for the controllability of such a mechanism is that a sub-matrix obtained by deleting any column from the structure matrix is non-singular. Physically, this means that a redundantly driven manipulator has the fail-safe advantage in that, except for the loss of backlash control, it can continue to function when one of its actuators fails to work. Furthermore, if high accuracy is not important between precision points, then it is possible to control the actuators in such a way that no antagonism exist among the actuators so as to achieve optimal dynamic performance.

Elimination of gear backlash reduces noise and vibration associated with

gear trains and, at the same time, improves the accuracy and stability of a manipulator. Since gear trains are structurally much more rigid than cables and tendons, the compliance problem associated with tendon-driven manipulators is also eliminated. The result is a high precision and high performance manipulator.

Chapter 4

Actuator Sizing

In order to overcome external loads and inertia forces, the actuators of a manipulator must be designed to provide sufficient driving torques. Over-sizing the actuators will result in a sacrifice of compactness, weight, and performance of the system. Proper actuator sizing help ensure the robot arm's load capacity and its dynamic responsiveness. Therefore, actuator sizing is a very important stage in the design of manipulators. Actuator sizing has been previously studied by Thomas, et al. (1985). However, the study was concentrated on individual joint driven manipulators. For unidirectional redundant-drive manipulators, it is still completely unexplored. It should be noted that the results on this subject is equally applicable for tendon-driven manipulators.

58

4.1 Resultant Joint Torques as Functions of Dynamics Performance Criteria

The resultant joint torques as shown in Eq. (3.5) can be thought of as a set of physical torques acting on the joints of an equivalent open-loop chain. This can be illustrated from the dynamical equations of the system. The Lagrange's equations of motion for a gear-coupled robotic system can be written as:

$$\frac{d}{dt}\left(\frac{\partial L}{\partial \dot{q}_i}\right) - \frac{\partial L}{\partial q_i} = Q_i, \qquad i = 1, 2, \cdots, n \qquad (4.1)$$

$$L = K - V, \qquad (4.2)$$

where the q's denote the generalized coordinates, Q's the generalized active forces and, where K and V are the kinetic and potential energies of the system, respectively.

Using joint angles as the generalized coordinates, $q_i = \theta_i$, the generalized active forces can be expressed as:

$$Q_i = \sum_{j=1}^{k} \frac{\partial \phi_j}{\partial q_i} \xi_j, \qquad i = 1, 2, \cdots, n. \qquad (4.3)$$

where ϕ_j and ξ_j, $j = 1, 2, \ldots, n+1$, denote the angular displacements and torques of the actuators.

Taking partial derivatives of Eq. (3.4) and substituting them into (4.3), yields

$$Q_i = \sum_{j=1}^{k} b_{ji}\xi_j, \qquad i = 1, 2, \cdots, n. \qquad (4.4)$$

Comparing Eqs. (3.5) and (4.4), it can be concluded that the resultant joint torques are the generalized active forces, i.e.

$$Q_i = \tau_i, \qquad i = 1, 2, \cdots, n. \qquad (4.5)$$

The same dynamical equations would be obtained if we assume the mechanism is made up of an open-loop chain having τ_i acting on joint i. Hence, the dynamic response of the system can be completely characterized by the resultant joint torques.

For a given set of joint torques, actuator torques can be obtained by solving Eq. (3.5), using the pseudo inverse technique:

$$\underline{\xi} = A^+\underline{\tau} + \lambda\,\underline{\mu} \qquad (4.6)$$

where $\quad \underline{\mu} = [\mu_1, \mu_2, \cdots, \mu_{n+1}]^T$ is the null vector of A, i.e. $A\,\underline{\mu} = \underline{0}$,

$\qquad A^+ = A^T(A\ A^T)^{-1}$ is the pseudo inverse of A,

and where λ is an arbitrary real number (Klein and Huang, 1983). The first term on the right-hand-side of Eq. (4.6) is called the particular solution and the second term, which results in no net joint torques, is called the homogenous solution. The orthogonality property between these two terms can be shown as follows:

$$(A^+\underline{\tau})^T\ \lambda\,\underline{\mu} = \lambda\,\underline{\tau}^T\{(A\ A^T)^{-1}\}^T\ A\,\underline{\mu} = 0 \qquad (4.7)$$

60

Eq. (4.7) implies that the particular solution is a hyperplane passing through the origin and perpendicular to the null vector. To control backlash, actuator torques should be kept in a predetermined direction at all times. This can be achieved by adjusting the arbitrary constant λ. Eq. (4.6) implies that the direction of actuator torques can be kept either in the direction of the null vector or in the opposite direction.

In the design of a manipulator, sometimes it is desirable to specify the performance in terms of velocities and accelerations at the end-effector. For this purpose, the joint velocities and joint accelerations in Eq. (4.1) can be replaced by the end-effector velocities and accelerations. Using the inverse kinematic transformation, the resulting equation can be written in the following form (Thomas and Tesar, 1982):

$$\tau_i = G_i^T \, \underline{\alpha} + \underline{v}^T P_i \underline{v} + f_i, \qquad i = 1, 2, \cdots, n, \qquad (4.8)$$

where $\underline{v}$ and $\underline{\alpha}$ are velocity and acceleration vectors of a point in the end-effector, G_i and P_i are $n \times 1$ and $n \times n$ coefficient matrices relating the motion state to joint torques, and f_i is the contribution due to conservative forces. Note that $\underline{v}$ and $\underline{\alpha}$ contain both linear and angular components, and that matrices G_i and P_i are both position dependent.

Hence, joint torques can be calculated from a set of velocity and acceleration specifications. Since the maximum achievable velocity and acceleration are position dependent, the performance of a manipulator can only be specified at certain position(s) of the end-effector. Since, at a given position, the maximum achievable velocity and acceleration are also direction dependent, we may specify the performance of a manipulator in terms of its ability to

reach

$$\underline{v}^T W_v \underline{v} = v_s^2,$$

and $\quad \underline{\alpha}^T W_\alpha \underline{\alpha} = a_s^2,$ \hfill (4.9)

for all directions of motion, where v_s and a_s are the desired magnitudes for the velocity and acceleration, and where W_α and W_v are $n \times n$ symmetric matrices used as weighting functions. If W_α and W_v are chosen to be identity matrices, then Eq. (4.9) implies that the end-effector can achieve a maximum velocity and acceleration of v_s and a_s, respectively at the specified location. Thomas, et al. (1985) studied the minimum joint torque requirement for optimal actuator sizing based on local dynamic criteria. The study of Thomas, et al. can be applied to individual joint-drive manipulators. However, for gear-coupled mechanisms with unidirectional drives, the theory for actuator sizing is still unexplored. In what follows, actuator sizing requirement will be studied.

4.2 Actuator Sizing in Terms of Joint Torques Requirement

Let D_j be the joint torque working domain, in which a manipulator is intended to operate. This working domain must be transformed into the actuator torque domain, D_ξ, in order to size the actuators properly. The transformation from joint torques to input torques can be accomplished in two steps, namely a transformation from the joint torque domain, D_j, to a particular solution hyperplane, D_p, followed by a transformation from the

62

particular solution domain to the actuator torque domain, D_ξ. Fig. 4.1(a) and (b) show the transformation between D_j, D_p, and D_ξ in graphical form. Note that, using Eq. (4.6), the transformation from D_j to D_p is unique and D_ξ is obtained by extending D_p along the null vector of the structure matrix to plus and minus infinity. For a given set of joint torques $\underline{\tau}^*$ in D_j, there is a particular solution $\underline{\xi}_p^*$ in D_p, and the required motor torques can be any point on the line passing through $\underline{\xi}_p^*$ and parallel to the null vector. To eliminate backlash effects, motor torques must lie in a predetermined quadrant. The actuator sizes can be determined by selecting a proper multiplier, λ, such that corresponding to every point in the joint torque domain, D_j, the required motor torque falls within the predetermined quadrant. Unfortunately, both domains of the working joint torques, D_j, and the particular solution hyperplane, D_p, cannot be described in concise mathematical forms. This method is, therefore, judged to be impractical for actuator sizing. In what follows, an alternate approach will be presented.

The actuators can be sized in a reverse manner. This can be illustrated by taking the 2-DOF mechanism shown in Fig. 3.7 as an example. The structure matrix of the mechanism shown in Fig. 3.7 is given by:

$$A = \begin{bmatrix} \dfrac{N_{17}N_{19}}{N_{18}N_{20}} & \dfrac{N_{13}N_{15}}{N_{14}N_{16}} & 0 \\[2ex] \dfrac{N_{17}N_{19}N_4N_6}{N_{18}N_{20}N_3N_5} & 0 & -\dfrac{N_7N_9N_{11}}{N_8N_{10}N_{12}} \end{bmatrix}. \tag{4.10}$$

Substituting $N_3 = 64$, $N_4 = 16$, $N_{14} = N_{16} = N_{18} = N_{20} = 15$, $N_5 = N_{12} = 24$, $N_6 = 12$, $N_7 = N_{10} = 20$, $N_8 = 10$, $N_9 = 48$, $N_{11} = 120$, and, $N_{13} = N_{15} = N_{17} = N_{19} = 96$ into Eq. (4.10), yields

$$A = \begin{bmatrix} 40.96 & 40.96 & 0 \\ 5.12 & 0 & -24 \end{bmatrix}. \tag{4.11}$$

63
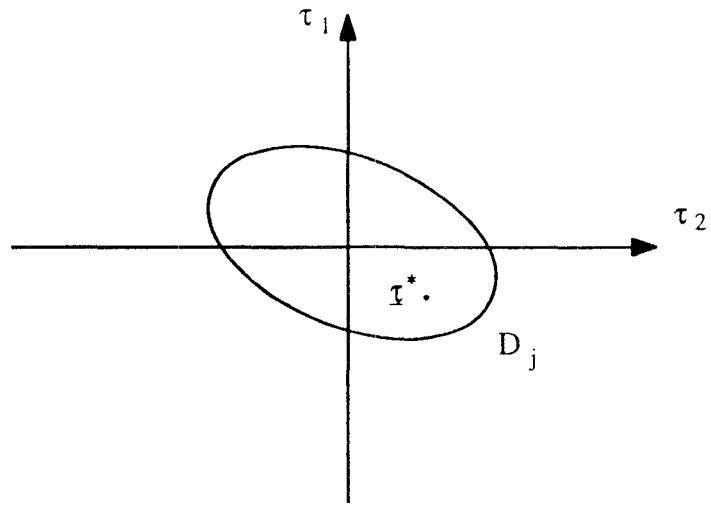
(a)
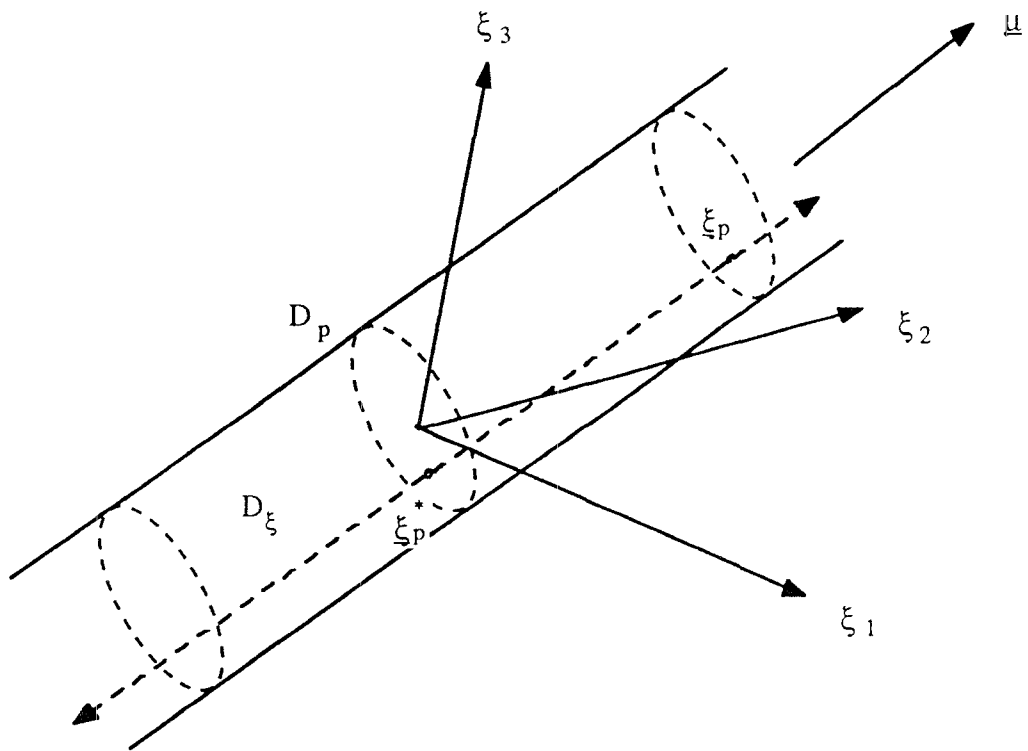
(b)

Figure 4.1: The Relationship between Joint Torques and Input Torques

The null vector of this structure matrix is $[75, -75, 16]^T$. To simplify the analysis, the positive direction of rotation for the 2nd motor axis is redefined in the opposite direction so that the structure matrix becomes

$$A = \begin{bmatrix} 40.96 & -40.96 & 0 \\ 5.12 & 0 & -24 \end{bmatrix}, \qquad (4.12)$$

and the null vector becomes $[75, 75, 16]^T$. Assuming that the actuators chosen for the mechanism have nominal torques in the range of $[\ \pm\hat{\xi}_1,\ \pm\hat{\xi}_2,\ \pm\hat{\xi}_3]^T$, then the domain of actuator torques, $\hat{D}_\xi$, will be a rectangular solid in the first quadrant as shown in Fig. 4.2. Note that a hat, $\hat{\ }$, is used to denote nominal torque available from the chosen actuators. Projecting $\hat{D}_\xi$ along the direction of the null vector results in a domain, $\hat{D}_p$, in the particular solution hyperplane. The corresponding available joint torque domain, $\hat{D}_j$, can then be obtained by a transformation using Eq. (3.5). The domain of available joint torques, $\hat{D}_j$, should contain the domain of desired joint torques, D_j, as a subset. To obtain $\hat{D}_p$, all 12 edges of the rectangular solid are projected onto the particular solution hyperplane along the direction of the null vector. But, six of them fall inside the boundary of the others. Hence, only six edges constitute the boundary of $\hat{D}_p$ as shown in Fig. 4.2. Each of them can be expressed as the intersection of two planes as shown below:

$$\begin{cases} \xi_i = \hat{\xi}_i, & i = 1, 2, 3 \\ \xi_j = 0, & j = 1, 2, 3, \quad j \neq i. \end{cases} \qquad (4.13)$$

Substituting Eqs. (4.12) and (4.13) into (3.5) for each combination of (i, j), yields two equations linear in ξ_k, $k \neq i \neq j$. Eliminate ξ_k from the two equations results in one equation which serves as one of the boundary lines for the $\hat{D}_j$ domain. Repeating the above process for all combinations of (i, j),
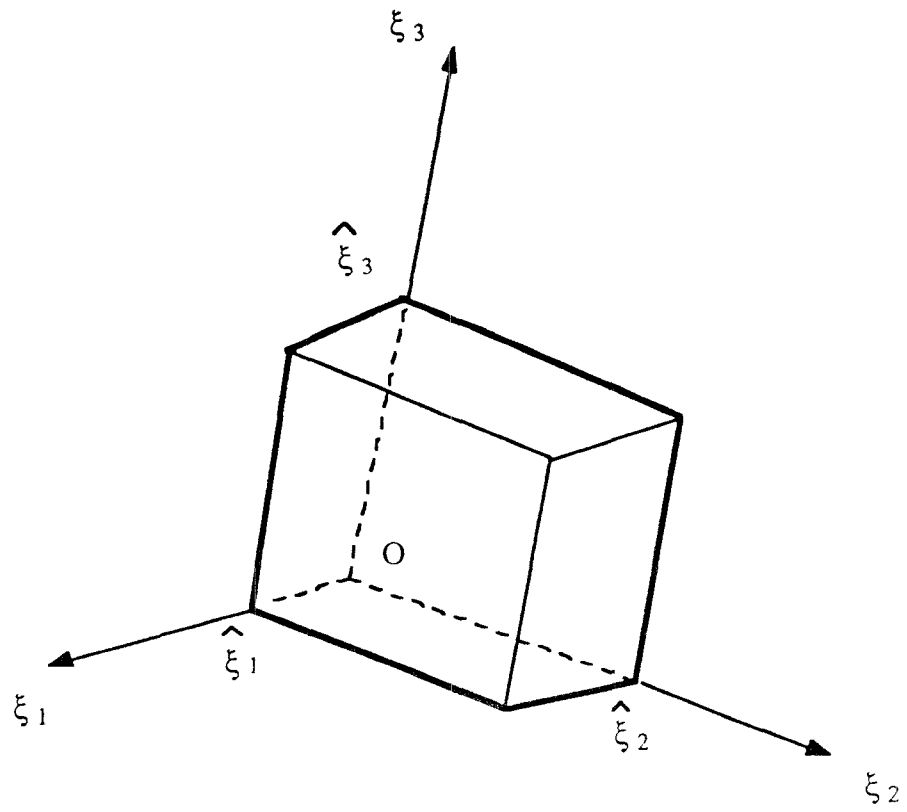
Figure 4.2: Available Actuator Torque Domain Projected on the Particular Solution Hyperplane

the boundary of the available joint torque domain, $\hat{D}_j$, are obtained as shown below:

$$\begin{cases} \tau_1 \geq -40.96 \; \hat{\xi}_2 \\ \tau_1 \leq 40.96 \; \hat{\xi}_1 \\ \tau_2 \geq -24 \; \hat{\xi}_3 \\ \tau_2 \leq 5.12 \; \hat{\xi}_1 \\ \tau_1 - 8 \; \tau_2 \leq 192 \; \hat{\xi}_3 \\ \tau_1 - 8 \; \tau_2 \geq -40.96 \; \hat{\xi}_2 \end{cases} \qquad (4.14)$$

This domain is sketched in Fig. 4.3 for the purpose of illustration.

For example, assuming the 2-DOF RBR arm as shown in Fig. 3.7 requires the following joint torque specifications:

$$\begin{cases} -25 & \leq \tau_1 \leq 25 \text{ N-m} \\ -6 & \leq \tau_2 \leq 6 \text{ N-m} \end{cases} \qquad (4.15)$$

Then, the actuator torque requirements can be obtained from Eq. (4.14) as

$$\begin{cases} \hat{\xi}_2 \geq 0.61 \text{ N-m} \\ \hat{\xi}_1 \geq 0.61 \text{ N-m} \\ \hat{\xi}_3 \geq 0.25 \text{ N-m} \\ \hat{\xi}_1 \geq 1.17 \text{ N-m} \\ \hat{\xi}_3 \geq 0.38 \text{ N-m} \\ \hat{\xi}_2 \geq 1.78 \text{ N-m} \end{cases} \qquad (4.16)$$

Therefore, actuators having nominal torques $\hat{\xi}_1 \geq 1.17$ N-m, $\hat{\xi}_2 \geq 1.78$ N-m, and $\hat{\xi}_3 \geq 0.38$ N-m of the desired operating speeds would be sufficient for the design.

The above methodology can be extended to a general n-DOF robot arm. For the reason of simplicity, it is assumed that positive directions of rotation for the actuators have been defined in such a way that all elements in the null

67
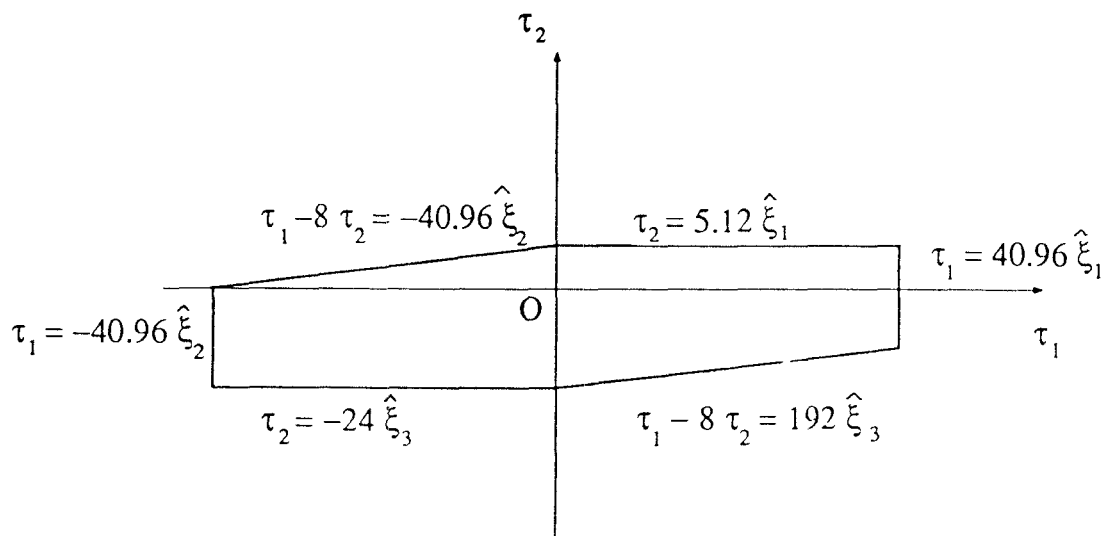
Figure 4.3: Domain of Available Joint Torque

vector of the structure matrix are positive. Thus, the domain of available motor torques, $\hat{D}_\xi$, can be represented by an $(n+1)$-dimensional rectangular solid in the first quadrant.

There are $2n(n+1)$ edges in an $(n+1)$-dimensional rectangular solid. After transformation, only $n(n+1)$ edges form the boundary of $\hat{D}_p$, and each of them can be represented as the intersection of two planes:

$$\begin{cases} \xi_i = 0, & i = 1, 2, \cdots, n+1 \\ \xi_j = \hat{\xi}_j, & j = 1, 2, \cdots, n+1, \quad j \neq i, \end{cases} \tag{4.17}$$

where $\hat{\xi}_j$ is the nominal torque available from the jth actuator. Substituting Eq. (4.17) into (3.5) for each combination of (i, j), we obtain:

$$\underline{\tau} = A_{ij}\underline{\xi}_{ij} + \hat{\xi}_j \ A_j, \tag{4.18}$$

where A_{ij} is the matrix obtained by deleting the ith and j^{th} columns from the structure matrix A, $\underline{\xi}_{ij}$ is the column matrix obtained by deleting the ith and j^{th} elements from $\underline{\xi}$, and A_j denotes the jth column of the matrix A.

Equation (4.18) represents n linear equations in $(n-1)$ unknowns, $\underline{\xi}_{ij}$, and the compatibility condition for non-trivial solutions to exist is:

$$\left| \underline{\tau} - \hat{\xi}_j A_j \quad A_{ij} \right| = \sum_{l=1}^{n} (-1)^{l-1}(\tau_l - \hat{\xi}_j a_{lj}) \left| A_{ij}^l \right| = 0, \tag{4.19}$$

where $|(\ )|$ denotes the determinant of $(\ )$, a_{lj} denotes the (l, j) element of A, and A_{ij}^l denotes a sub-matrix of A_{ij} with the lth row omitted. Rearranging Eq. (4.19) yields the following boundary hyperplanes:

$$\sum_{l=1}^{n} (-1)^{l-1} \tau_l \left| A_{ij}^l \right| = \hat{\xi}_j \sum_{l=1}^{n} (-1)^{l-1} a_{lj} \left| A_{ij}^l \right| = \hat{\xi}_j (-1)^s \left| \hat{A}_i \right|, \tag{4.20}$$

69

where $\hat{A}_i$ denotes a sub-matrix of A with the ith column omitted, and where

$$
\begin{cases}
s = j - 1, & if \ i > j \\
s = j, & if \ i < j.
\end{cases}
\tag{4.21}
$$

Hence, the actuator torque requirements can be written as:

$$
\hat{\xi}_j \geq (-1)^s \frac{\sum_{l=1}^{n} (-1)^{l-1} \tau_l \left| A_{ij}^l \right|}{\left| \hat{A}_i \right|},
\tag{4.22}
$$

where $i = 1, 2, \cdots, n + 1$; $j = 1, 2, \cdots, n + 1$; and $j \neq i$. There are $n(n + 1)$ such equations.

Hence, corresponding to a set of joint torques, Eq. (4.22) yields the minimum torque requirement for each actuator.

4.3 Actuator Sizing in Terms of End-Effector Performance Criteria

The actuator torque requirements can also be written as functions of end-effector performance criteria. Substituting Eq. (4.8) into (4.22), yields:

$$
\hat{\xi}_j \geq (-1)^s \frac{\sum_{l=1}^{n} (-1)^{l-1} \left| A_{ij}^l \right| (G_l^T \underline{\alpha} + \underline{v}^T P_l \underline{v} + f_l)}{\left| \hat{A}_i \right|},
\tag{4.23}
$$

or

$$
\hat{\xi}_j \geq F_j^T \underline{\alpha} + \underline{v}^T H_j \underline{v} + g_j, \qquad j = 1, 2, \cdots, n
\tag{4.24}
$$

70

where

$$F_j^T = (-1)^s \frac{\sum_{l=1}^n (-1)^{l-1} \left| A_{ij}^l \right| G_l^T}{\left| \hat{A}_i \right|} \tag{4.25}$$

$$H_j = (-1)^s \frac{\sum_{l=1}^n (-1)^{l-1} \left| A_{ij}^l \right| P_l}{\left| \hat{A}_i \right|} \tag{4.26}$$

$$g_j = (-1)^s \frac{\sum_{l=1}^n (-1)^{l-1} \left| A_{ij}^l \right| f_l}{\left| \hat{A}_i \right|} \tag{4.27}$$

and

$$i = 1, 2, \cdots, n+1, \qquad i \neq j.$$

The actuators should be selected to satisfy Eq. (4.9), i.e.

$$\underline{v}^T W_v \underline{v} = v_s^2$$

and

$$\underline{\alpha}^T W_\alpha \underline{\alpha} = a_s^2$$

Since the maximum value of the three terms in the right-hand-side of Eq. (4.24) can occur simultaneously, actuators should be chosen such that their available torques, $\hat{\underline{\xi}}$, are equal to the sum of the maximum value of each term. The maximum value of each term can be obtained as follows:

(a) 1st term:

$$Max \quad \xi_j^\alpha = F_j^T \underline{\alpha}, \quad subject \ to \quad \underline{\alpha}^T W_\alpha \underline{\alpha} = a_s^2 \tag{4.28}$$

where ξ_j^α denotes the maximum torque required to produce a desired acceleration, $\underline{\alpha}$. Define J as

$$J = F_j^T \underline{\alpha} + h \left(\underline{\alpha}^T W_\alpha \underline{\alpha} - a_s^2 \right), \tag{4.29}$$

where h is a Lagrange multiplier. Equating $\frac{\partial J}{\partial \underline{\alpha}}$ and $\frac{\partial J}{\partial h}$ to zero, yields:

$$F_j + 2 \ h \ W_\alpha \underline{\alpha} = \underline{0}, \tag{4.30}$$

and

$$\underline{\alpha}^T W_\alpha \underline{\alpha} = a_s^2, \tag{4.31}$$

Premultiplying Eq. (4.30) by $\underline{\alpha}^T$ and substituting (4.31) into the resulting equation, yields

$$F_j^T \underline{\alpha} + 2 \ h \ a_s^2 = 0. \tag{4.32}$$

Thus, the maximum value of ξ_j^α occurs at

$$h = -\frac{F_j^T \underline{\alpha}}{2a_s^2} = -\frac{\xi_j^\alpha}{2a_s^2}. \tag{4.33}$$

Substituting Eq. (4.33) into (4.30) and simplifying, yields:

$$\underline{\alpha} = \frac{a_s^2 W_\alpha^{-1} F_j}{\xi_j^\alpha} \tag{4.34}$$

Premultiplying Eq. (4.34) by F_j^T and simplifying, yields the maximum value of ξ_j^α,

$$\xi_j^\alpha = a_s(F_j^T W_\alpha^{-1} F_j)^{\frac{1}{2}}. \qquad (4.35)$$

(b) 2nd term:

$$Max \qquad \xi_j^v = \underline{v}^T H_j \underline{v}, \qquad subject \ to \qquad \underline{v}^T W_v \underline{v} = v_s^2. \qquad (4.36)$$

Define J as

$$J = \underline{v}^T H_j \underline{v} + h \ (\underline{v}^T W_v \underline{v} - v_s^2), \qquad (4.37)$$

where h is a Lagrange multiplier. By the same method, equating $\frac{\partial J}{\partial \underline{v}}$ and $\frac{\partial J}{\partial h}$ to zero, yields:

$$(H_j + H_j^T) \ \underline{v} + 2 \ h \ W_v \underline{v} = \underline{0}, \qquad (4.38)$$

and

$$\underline{v}^T W_v \underline{v} = v_s^2. \qquad (4.39)$$

From Eq. (4.38), it can be shown that $h = -\frac{1}{2}$ eigenvalue of $W_v^{-1}(H_j + H_j^T)$, and $\underline{v} =$ eigenvector of $W_v^{-1}(H_j + H_j^T)$. Premultiplying Eq. (4.38) by $\underline{v}^T$ and substituting (4.39) into the resulting equation, yields

$$\underline{v}^T(H_j + H_j^T) \ \underline{v} + 2 \ h \ v_s^2 = 0. \qquad (4.40)$$

Thus, ξ_j^v has a maximum value of

$$\xi_j^v = \underline{v}^T H_j \underline{v} = - \ h \ v_s^2. \qquad (4.41)$$

(c) 3rd term:

The third term is position dependent and can be obtained directly from Eq. (4.27).

Finally, the actuactor sizes can be determined by summing Eqs. (4.35), (4.41) and (4.27).

4.4   Example

At the initial design stage actuator torque requirement has to be estimated. Then, gears are selected according to the torque and speed capacity of actuators. The system is updated with new data and the process is repeated until a satisfactory design is reached.

For the design of the 2-DOF prototype RBR arm, the dynamic analysis will be approximated by an equivalent three-link chain connected by two revolute joints as shown in Fig. 4.4. Both moving links are assumed to have uniformly distributed mass of m_1 and m_2, and, equal link length l. Since this planar mechanism has its joint axes parallel to the gravitational field, the potential energy of the system will be constant. The kinetic energy of the system can be written as

$$
\begin{aligned}
K \;=\; & \frac{1}{6}(m_1 + 3m_2)l^2\dot{\theta}_1^2 + \frac{1}{6}m_2 l^2(\dot{\theta}_1 + \dot{\theta}_2)^2 \\
& + \frac{1}{2}m_2 l^2 \dot{\theta}_1(\dot{\theta}_1 + \dot{\theta}_2)\,\cos\theta_2
\end{aligned}
\tag{4.42}
$$
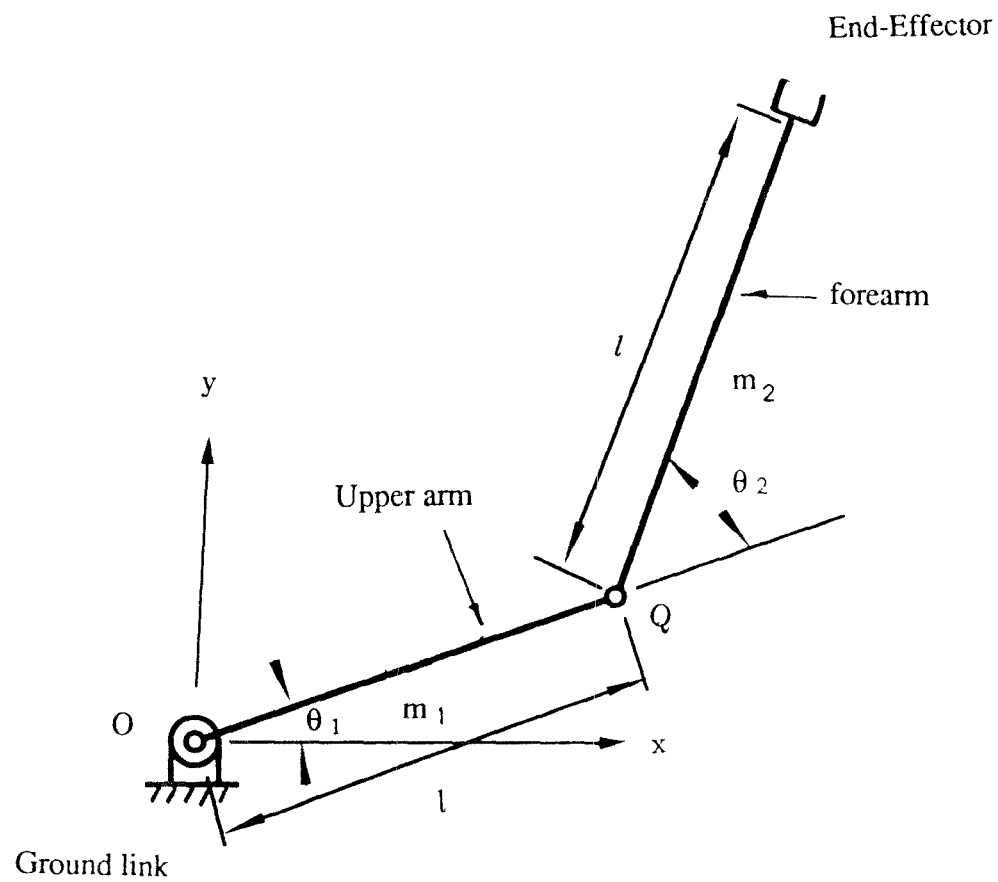
Figure 4.4: An Equivalent Three-link Chain

By applying Eq. (4.1), we can obtain the dynamical equations as

$$\tau_1 = l^2(\frac{1}{3}m_1 + \frac{4}{3}m_2 + m_2\cos\theta_2)\ddot{\theta}_1 + l^2(\frac{1}{3}m_2 + \frac{1}{2}m_2\cos\theta_2)\ddot{\theta}_2$$
$$- \frac{1}{2}m_2l^2\sin\theta_2\ (2\dot{\theta}_1 + \dot{\theta}_2)\dot{\theta}_2 \tag{4.43}$$

$$\tau_2 = \frac{1}{6}m_2l^2(2 + 3\cos\theta_2)\ddot{\theta}_1 + \frac{1}{3}m_2l^2\ddot{\theta}_2 + \frac{1}{2}m_2l^2(\sin\theta_2)\dot{\theta}_1^2 \tag{4.44}$$

Suppose we want to choose the actuators such that at $\theta_2 = 60°$, the end-effector can reach a velocity of $v_s = 0.8$ m/s with an acceleration of $a_s = 9.8$ m/s^2 in all direction. This means W_v and W_α in Eq. (4.9) are identity matrices, i.e.

$$W_v = W_\alpha = I \tag{4.45}$$

And suppose that for the prototype design, $l = 0.3048$ m, $m_1 = 7$ kg and $m_2 = 0.7$ kg. Then, at $\theta_2 = 60°$, Eqs. (4.43) and (4.44) become

$$\tau_1 = 0.3360\ddot{\theta}_1 + 0.03794\ddot{\theta}_2 - 0.02816(2\dot{\theta}_1 + \dot{\theta}_2)\dot{\theta}_2 \tag{4.46}$$

$$\tau_2 = 0.03794\ddot{\theta}_1 + 0.02168\ddot{\theta}_2 + 0.02816\dot{\theta}_1^2 \tag{4.47}$$

Since θ_1 has no effect on the dynamic performance, we can choose an arbitrary number, say $\theta_1 = 0°$ for the analysis to follow. At $\theta_1 = 0°$ and $\theta_2 = 60°$, the X-Y coordinates of the end-effector can be written as

$$x = l\ \cos\theta_1 + l\ \cos(\theta_1 + \theta_2) \tag{4.48}$$
$$y = l\ \sin\theta_1 + l\ \sin(\theta_1 + \theta_2) \tag{4.49}$$

76

Taking the time derivatives of Eqs. (4.48) and (4.49), yields the velocity of the end-effector as:

$$\dot{x} = -l\,\dot{\theta}_1\,\sin\theta_1 - l\,(\dot{\theta}_1 + \dot{\theta}_2)\,\sin(\theta_1 + \theta_2)$$

$$= -0.264(\dot{\theta}_1 + \dot{\theta}_2) \tag{4.50}$$

$$\dot{y} = l\,\dot{\theta}_1\,\cos\theta_1 + l\,(\dot{\theta}_1 + \dot{\theta}_2)\,\cos(\theta_1 + \theta_2)$$

$$= 0.4572\,\dot{\theta}_1 + 0.1524\,\dot{\theta}_2 \tag{4.51}$$

and the acceleration of the end-effector as:

$$\frac{\ddot{x}}{l} = -\sin\theta_1\,\ddot{\theta}_1 - \cos\theta_1\dot{\theta}_1^2 - \sin(\theta_1 + \theta_2)\,(\ddot{\theta}_1 + \ddot{\theta}_2)$$

$$- \cos(\theta_1 + \theta_2)\,(\dot{\theta}_1 + \dot{\theta}_2)^2$$

$$= -\frac{\sqrt{3}}{2}(\ddot{\theta}_1 + \ddot{\theta}_2) - \frac{3}{2}\dot{\theta}_1^2 - \dot{\theta}_1\dot{\theta}_2 - \frac{1}{2}\dot{\theta}_2^2 \tag{4.52}$$

$$\frac{\ddot{y}}{l} = \cos\theta_1\,\ddot{\theta}_1 - \sin\theta_1\,\dot{\theta}_1^2 + \cos(\theta_1 + \theta_2)\,(\ddot{\theta}_1 + \ddot{\theta}_2)$$

$$- \sin(\theta_1 + \theta_2)\,(\dot{\theta}_1 + \dot{\theta}_2)^2$$

$$= \frac{3}{2}\ddot{\theta}_1 + \frac{1}{2}\ddot{\theta}_2 - \frac{\sqrt{3}}{2}(\dot{\theta}_1 + \dot{\theta}_2)^2 \tag{4.53}$$

Solving Eqs. (4.50) and (4.51) for $\dot{\theta}_1$ and $\dot{\theta}_2$, yields

$$\dot{\theta}_1 = 1.894\,\dot{x} + 3.281\,\dot{y} \tag{4.54}$$

$$\dot{\theta}_2 = -5.683\,\dot{x} - 3.281\,\dot{y} \tag{4.55}$$

Solving Eqs. (4.52) and (4.53) for $\ddot{\theta}_1$ and $\ddot{\theta}_2$, yields

$$\ddot{\theta}_1 = 1.894\,\ddot{x} + 3.281\,\ddot{y} + 18.644\,\dot{x}^2 + 6.215\,\dot{y}^2 + 7.176\,\dot{x}\dot{y} \tag{4.56}$$

$$\ddot{\theta}_2 = -5.683\,\ddot{x} - 3.281\,\ddot{y} - 31.073\,\dot{x}^2$$

$$-18.644\,\dot{y}^2 - 21.528\,\dot{x}\dot{y} \tag{4.57}$$

77

Substituting Eqs. (4.54), (4.55), (4.56) and (4.57) into (4.46) and (4.47), yields

$$\tau_1 = \begin{bmatrix} 0.421 & 0.978 \end{bmatrix} \begin{bmatrix} \ddot{x} \\ \ddot{y} \end{bmatrix} + \begin{bmatrix} \dot{x} & \dot{y} \end{bmatrix} \begin{bmatrix} 4.782 & 0.972 \\ 0.972 & 1.684 \end{bmatrix} \begin{bmatrix} \dot{x} \\ \dot{y} \end{bmatrix} \qquad (4.58)$$

$$\tau_2 = \begin{bmatrix} -0.051 & 0.053 \end{bmatrix} \begin{bmatrix} \ddot{x} \\ \ddot{y} \end{bmatrix} + \begin{bmatrix} \dot{x} & \dot{y} \end{bmatrix} \begin{bmatrix} 0.135 & 0.078 \\ 0.078 & 0.135 \end{bmatrix} \begin{bmatrix} \dot{x} \\ \dot{y} \end{bmatrix} \qquad (4.59)$$

Hence, the coefficient matrices in Eq. (4.8) are

$$G_1^T = \begin{bmatrix} 0.421 & 0.978 \end{bmatrix}, \qquad (4.60)$$

$$G_2^T = \begin{bmatrix} -0.051 & 0.053 \end{bmatrix}, \qquad (4.61)$$

$$P_1 = \begin{bmatrix} 4.782 & 0.972 \\ 0.972 & 1.684 \end{bmatrix}, \qquad (4.62)$$

and

$$P_2 = \begin{bmatrix} 0.135 & 0.078 \\ 0.078 & 0.135 \end{bmatrix} \qquad (4.63)$$

Assuming the system has the structure matrix given by Eq. (4.12), then the actuator torques requirement can be written in term of the end-effector performance criteria. Substituting Eqs. (4.60)-(4.63) into (4.25), (4.26) and then the resulting equations into Eqs. (4.35) and (4.41) respectively for $i = 1, 2, 3$ and $j = 1, 2, 3$, $i \neq j$, yields the following results:

(a) $i = 2$, $j = 1$

$$F_1 = G_1/40.96$$

$$H_1 = P_1/40.96$$

$$\xi_1^\alpha = a_s(G_1^T G_1)^{\frac{1}{2}}/40.96$$

$$= 9.8 \times (0.421^2 + 0.978^2)^{\frac{1}{2}}/40.96$$

$$= 0.2548 \text{ N-m}$$

$$\xi_1^v = 0.8^2 \times (\frac{1}{2} \text{ eigenvalue of } (P_1 + P_1^T))/40.96$$

$$= 0.0791 \text{ N-m}$$

Hence, $\hat{\xi}_1 \geq \xi_1^\alpha + \xi_1^v = 0.3339$ N-m

(b) $i = 3, \ j = 1$

$$F_1 = G_2/5.12$$

$$H_1 = P_2/5.12$$

$$\xi_1^\alpha = a_s(G_2^T G_2)^{\frac{1}{2}}/5.12$$

$$= 9.8 \times (0.051^2 + 0.053^2)^{\frac{1}{2}}/5.12$$

$$= 0.1408 \text{ N-m}$$

$$\xi_1^v = 0.8^2 \times (\frac{1}{2} \text{ eigenvalue of } (P_2 + P_2^T))/5.12$$

$$= 0.1675 \text{ N-m}$$

Hence, $\hat{\xi}_1 \geq \xi_1^\alpha + \xi_1^v = 0.3083$ N-m

(c) $i = 1, \ j = 2$

$$F_2 = -G_1/40.96$$

$$H_2 = -P_1/40.96$$

$$\xi_2^\alpha = a_s(G_1^T G_1)^{\frac{1}{2}}/40.96$$

$$= 9.8 \times (0.421^2 + 0.978^2)^{\frac{1}{2}}/40.96$$

$$= 0.2548 \text{ N-m}$$

$$\xi_2^v = 0.8^2 \times (\frac{1}{2} \text{ eigenvalue of } (-P_1 - P_1^T))/40.96$$

79

$$= -0.0009 \text{ N-m}$$

Hence, $\hat{\xi}_2 \geq \xi_2^\alpha + 0 = 0.2548$ N-m

(d) $i = 3, \ j = 2$

$$F_2 = -(G_1 - 8G_2)/40.96$$

$$H_2 = -(P_1 - 8P_2)/40.96$$

$$\xi_2^\alpha = a_s(F_2^T F_2)^{\frac{1}{2}}$$

$$= 9.8 \times (0.829^2 + 0.554^2)^{\frac{1}{2}}/40.96$$

$$= 0.2386 \text{ N-m}$$

$$\xi_2^v = 0.8^2 \times (\frac{1}{2} \text{ eigenvalue of } (H_2 + H_2^T))$$

$$= -0.0088 \text{ N-m}$$

Hence, $\hat{\xi}_2 \geq \xi_2^\alpha + 0 = 0.2386$ N-m

(e) $i = 1, \ j = 3$

$$F_3 = -G_2/24$$

$$H_3 = -P_2/24$$

$$\xi_3^\alpha = a_s(G_2^T G_2)^{\frac{1}{2}}/24$$

$$= 1.8 \times (0.051^2 + 0.053^2)^{\frac{1}{2}}/24$$

$$= 0.0300 \text{ N-m}$$

$$\xi_3^v = 0.8^2 \times (\frac{1}{2} \text{ eigenvalue of } (-P_2 - P_2^T))/24$$

$$= -0.0015 \text{ N-m}$$

Hence, $\hat{\xi}_3 \geq \xi_3^\alpha + 0 = 0.0300$ N-m

(f) $i = 2, \ j = 3$

$$F_3 = (G_1 - 8G_2)/192$$

$$H_3 = (P_1 - 8P_2)/192$$

$$\xi_3^\alpha = a_s(F_3^T F_3)^{\frac{1}{2}}$$

$$= 9.8 \times (0.829^2 + 0.554^2)^{\frac{1}{2}}/192$$

$$= 0.0508 \text{ N-m}$$

$$\xi_3^v = 0.8^2 \times (\frac{1}{2} \text{ eigenvalue of } (H_3 + H_3^T))$$

$$= 0.0125 \text{ N-m}$$

Hence, $\hat{\xi}_3 \geq \xi_3^\alpha + \xi_3^v = 0.0633$ N-m

Therefore, the actuators are chosen so that $\hat{\xi}_1 \geq 0.3339$ N-m, $\hat{\xi}_2 \geq 0.2548$ N-m, and $\hat{\xi}_3 \geq 0.0633$ N-m

In the prototype design, the characteristics of actuators 1, 2 and 3 are as follows:

characteristics	actuators 1 & 2	actuator 3
continuous stall torque	0.353 N-m	N/A
peak torque	2.47 N-m	1.13 N-m
torque constant	83.34 mN-m/A	65.4 mN-m/A
max speed	6000 rpm	3420 rpm

4.5   Summary

A methodology for actuator sizing has been established for RBR mechanisms. The actuator torques requirement was first derived as functions of joint torques. Then, dynamical equations were applied to derive the actuator torque requirement based on end-effector dynamic performance criteria. With this method, the actuators sizing can be performed in a straightforward method instead of recursive calculations. An example was also presented in

this chapter. The methodology is also applicable for tendon-driven manipulators.

Chapter 5

Dynamics of Gear-Coupled Robotic Mechanisms

In the area of robotics, we are constantly concerned with controlling the position and orientation of the end-effector as well as the posture of a manipulator itself. In order to generate a desired motion, actuator torques should be applied properly. The first step for controlling such a system is to predict its response due to applied torques, i.e. to study the dynamics of the robotic system. The dynamics of manipulators has been studied thoroughly by many researchers (Thomas and Tesar, 1982; Paul, 1981). Usually, frictional force is neglected in dynamics modeling of a manipulator. However, frictional force in gear-coupled robotic mechanisms can have significant effects on the manipulator dynamics and control. Therefore, it is imperative to take it into consideration in the formulation of dynamical equations. This subject is important for precise motion control of an end-effector and is still

relatively unexplored. Without knowing the exact form of dynamical equations, system parameters identification and adaptive control law cannot be implemented (Craig et al., 1986; Han et al., 1987).

In this chapter, frictional force in the system dynamics of gear-coupled robotic mechanisms will be studied.

5.1 Dynamical Equations without Frictional Forces

The dynamical equations of a manipulator can be derived by several methods. In the study of kinematics, Tsai (1988) defined an equivalent open-loop chain for gear-coupled robotic mechanisms. All links contained in the equivalent open-loop chain are called the major links or the carriers, and those not included in the equivalent open-loop chain are called the carried links. Using this concept, Chen et al. (1990) developed a systematic methodology for the dynamic analysis of such systems. The method is very efficient and will be used in the study that follow. By this method, first, the equivalent open-loop chain is identified, the carried links are treated as being rigidly attached to their corresponding carriers, and the kinetic energy of the resulting equivalent open-loop chain is formulated. Then, the additional kinetic energy contributed by the relative rotations of the carried links is added.

It has been shown that for a link i performing a fixed-axis-rotation with respect to its carrier j, the additional kinetic energy $K'_{i,j}$ is given by:

$$K'_{i,j} = \frac{1}{2}J_i(\dot{\theta}_{i,j})^2 + J_i\dot{\theta}_{i,j}(\underline{w}_j \cdot \underline{e}_i) \tag{5.1}$$

where J_i is the moment of inertia of the carried link i about its axis of rotation, $\underline{e}_i$ is a positive unit vector defined along the axis of relative rotation, $\underline{w}_j$ is the angular velocity of link j with respect to the inertia frame, and $\dot{\theta}_{i,j}$ is the relative rotation of link i with respect to link j. Finally, dynamical equations can be derived by substituting the kinetic energy of the system into the Lagrange's equation of motion.

For the prototype arm shown in Fig. 3.7, either the rotation axis of a carried link is perpendicular to the rotation axis of its carrier or the carrier is stationary (ground link). Hence,

$$\underline{w}_j \cdot \underline{e}_i = 0 \tag{5.2}$$

and Eq. (5.1) reduces to:

$$K'_{i,j} = \frac{1}{2}J_i \, (\dot{\theta}_{i,j})^2 \tag{5.3}$$

To simplify the formulation of dynamical equations, two or more components keyed together with a common shaft are considered as one rigid link. Fig. 5.1 shows the numbering of the rigid links, where links A and B are two major moving links and link 0 is the ground link. Link 0 carries links 1, 6, 7, 8, and 9; link A carries links 2, 3, 4 and 5; while link B does not carry any links. Fig. 5.2 shows its equivalent open-loop chain.

The kinetic energy of this system comprises two parts, K_m, contributed from major links A and B and, K' contributed from the relative rotation of the carried links. That is
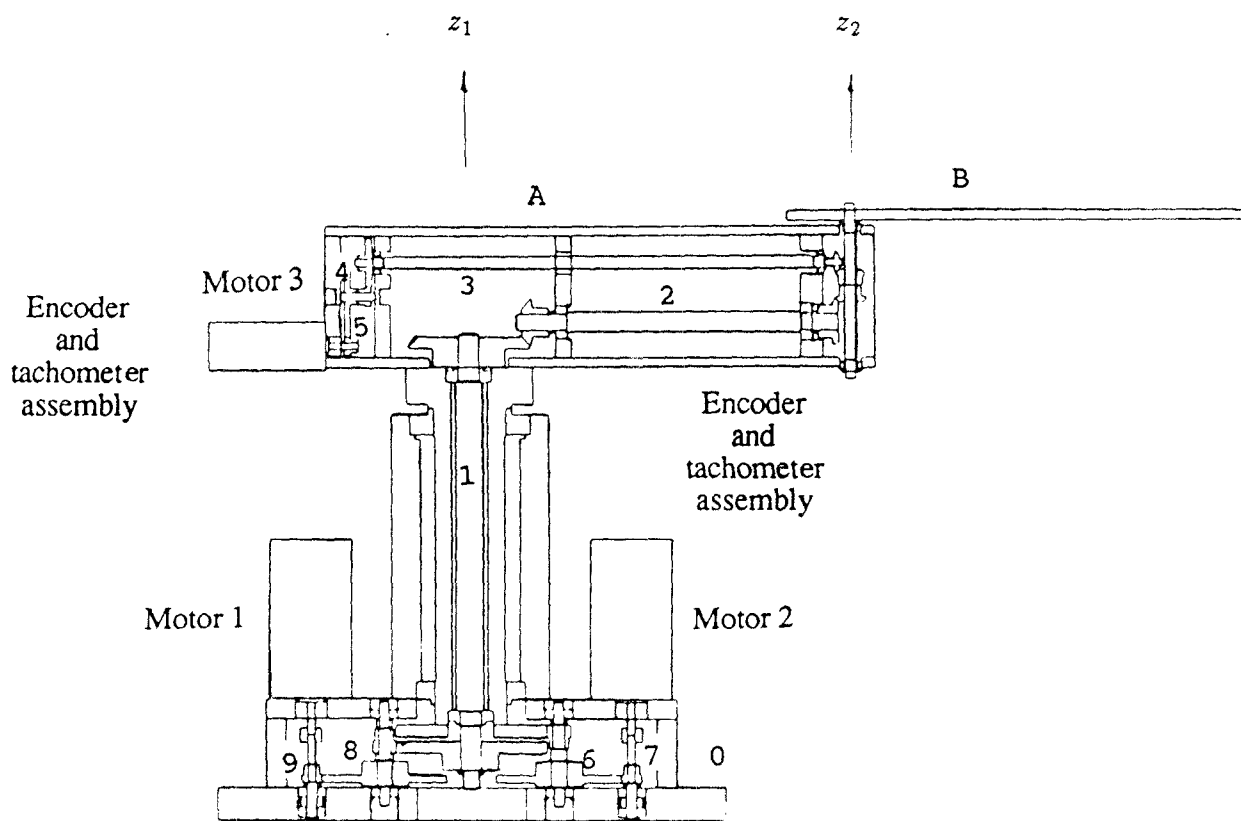
Figure 5.1: Prototype RBR Arm
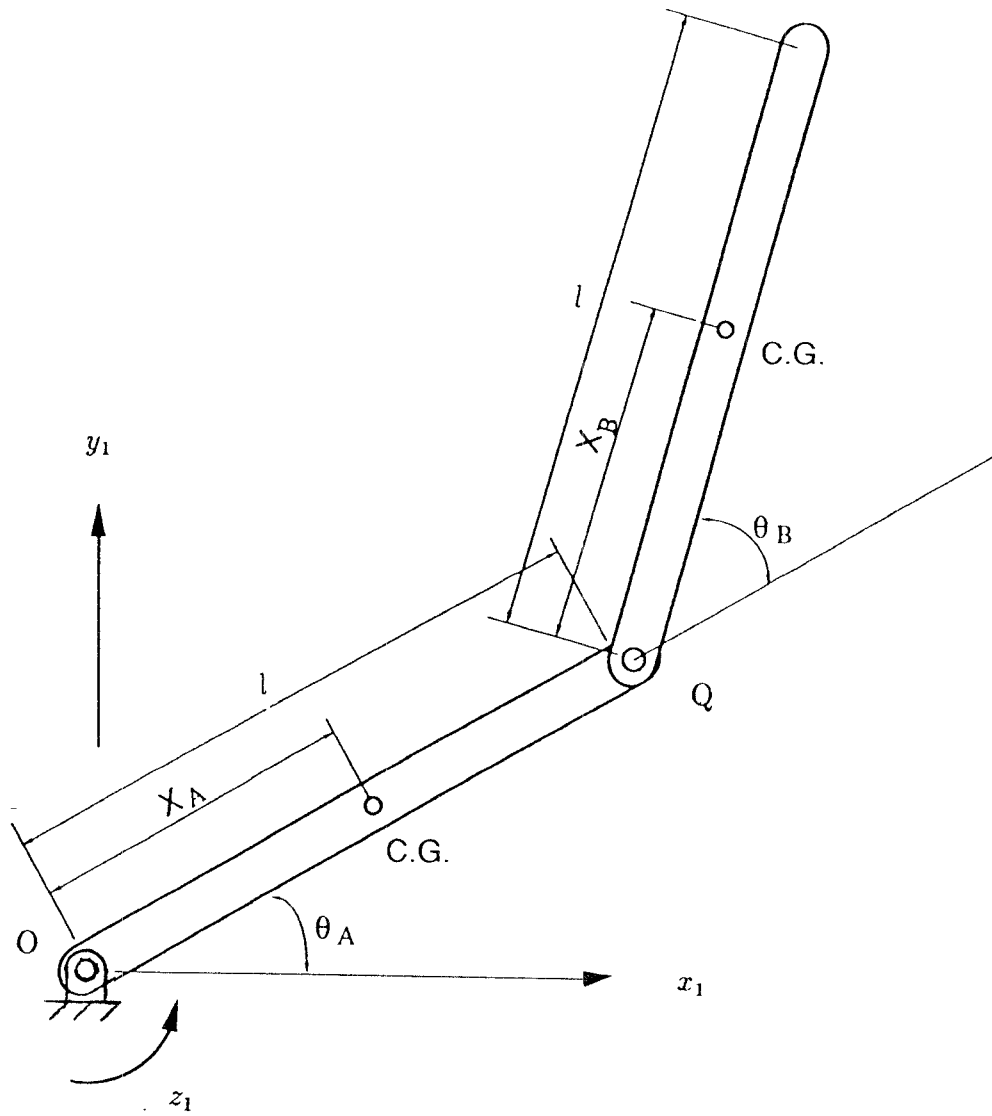
Figure 5.2: The Equivalent Open-loop Chain of Fig. 5.1

$$K = K_m + K'$$ (5.4)

The first part of the above equation K_m can be written as

$$K_m = \frac{1}{2}J'_A\dot{\theta}_A^2 + \frac{1}{2}m_A x_A^2 \dot{\theta}_A^2 + \frac{1}{2}J'_B(\dot{\theta}_A + \dot{\theta}_B)^2$$
$$+\frac{1}{2}m_B[l^2\dot{\theta}_A^2 + 2lx_B\dot{\theta}_A(\dot{\theta}_A + \dot{\theta}_B) \cos\theta_B + x_B^2(\dot{\theta}_A + \dot{\theta}_B)^2]$$ (5.5)

where l denotes the link length, θ the joint angle, m the combined mass of a major link and its carried links, x the length from the combined center of mass to its preceeding joint, J' the combined moment of inertia of an equivalent link about an axis passing through its center of mass and parallel to the joint axes, and where the subscripts A and B refer to the major links, A and B, respectively.

Rearranging Eq. (5.5), yields

$$K_m = \frac{1}{2}J_A\dot{\theta}_A^2 + \frac{1}{2}J_B(\dot{\theta}_A + \dot{\theta}_B)^2$$
$$+\frac{1}{2}m_B(l^2\dot{\theta}_A^2 + 2lx_B\dot{\theta}_A^2 \cos\theta_B + 2lx_B\dot{\theta}_A\dot{\theta}_B \cos\theta_B)$$ (5.6)

where J denotes the moment of inertia of an equivalent major link about its preceeding joint axis.

The relative rotational rate of carried links with respect to their corresponding major links can be obtained by applying fundamental circuit equations and coaxiality conditions stated in Chapter 2. Using the gear teeth numbers given in section 3.4, the results are shown below:

$$\dot{\theta}_{10} = \dot{\theta}_A + 0.125\dot{\theta}_B$$ (5.7)

$$\dot{\theta}_{2A} = 0.5\,\dot{\theta}_B$$ (5.8)

$$\dot{\theta}_{3A} = -2\dot{\theta}_B$$ (5.9)

$$\dot{\theta}_{4A} = 4.8\dot{\theta}_B \tag{5.10}$$

$$\dot{\theta}_{5A} = -24\dot{\theta}_B \tag{5.11}$$

$$\dot{\theta}_{60} = -6.4\dot{\theta}_A \tag{5.12}$$

$$\dot{\theta}_{70} = 40.96\dot{\theta}_A \tag{5.13}$$

$$\dot{\theta}_{80} = -6.4\dot{\theta}_A - 0.8\dot{\theta}_B \tag{5.14}$$

$$\dot{\theta}_{90} = 40.96\dot{\theta}_A + 5.12\dot{\theta}_B \tag{5.15}$$

where $\dot{\theta}_{ij}$ denotes the relative rotational rate of link i with respect to link j. The additional kinetic energy, K', can then be obtained by substituting Eq. (5.7)-(5.15) into (5.3) and summing them. The result is

$$
\begin{aligned}
K' = \ & \frac{1}{2}[J_1(\dot{\theta}_A + 0.125\dot{\theta}_B)^2 + J_2(0.5\ \dot{\theta}_B)^2 \\
& + J_3(-2\dot{\theta}_B)^2 + J_4(4.8\dot{\theta}_B)^2 \\
& + J_5(-24\dot{\theta}_B)^2 + J_6(-6.4\dot{\theta}_A)^2 \\
& + J_7(40.96\dot{\theta}_A)^2 + J_8(-6.4\dot{\theta}_A - 0.8\dot{\theta}_B)^2 \\
& + J_9(40.96\dot{\theta}_A + 5.12\dot{\theta}_B)^2]
\end{aligned}
\tag{5.16}
$$

where J_i denotes the moment of inertia of link i with respect to its rotation axis. The dynamical equations can be derived by substituting Eqs. (5.6) and (5.16) into (5.4) and then substituting the resulting equation into Eq. (4.1). The resulting equations are

$$
\begin{aligned}
\tau_1 = \ & (r + 2k\ \cos\theta_B)\ddot{\theta}_A + (s + k\ \cos\theta_B)\ddot{\theta}_B \\
& -2k\ (\sin\theta_B)\ \dot{\theta}_A\dot{\theta}_B - k\ (\sin\theta_B)\ \dot{\theta}_B^2
\end{aligned}
\tag{5.17}
$$

$$\tau_2 = (s + k\ \cos\theta_B)\ddot{\theta}_A + t\ \ddot{\theta}_B + k\ \sin\theta_B\ \dot{\theta}_A^2 \tag{5.18}$$

where

$$r = J_A + J_B + J_1 + 40.96J_6 + 40.96^2 J_7$$

89

$$+40.96 J_8 + 40.96^2 J_9 + m_B l^2 \qquad (5.19)$$

$$s = J_B + 0.125 J_1 + 5.12 J_8 + 5.12 \times 40.96 J_9 \qquad (5.20)$$

$$t = J_B + 0.125^2 J_1 + 0.25 J_2 + 4 J_3$$
$$+23.04 J_4 + 576 J_5 + 0.64 J_8 + 5.12^2 J_9 \qquad (5.21)$$

$$k = m_B l x_B \qquad (5.22)$$

Note that the dynamical equations contain only four independent parameters, r, s, t and k. If the J's and m's are completely known, then r, s, t and k can be calculated. On the other hand, if the J's and m's are not completely known, then r, s, t and k must be estimated experimentally. In general, J_A and J_B are a few order of magnitude greater than that of the rotors, gears, and shafts. However, the effect of rotors can be as large as the arms since they are multiplied by the square of the gear ratio as shown in Eqs. (5.19)-(5.22).

5.2   Sliding Motion in a Gear Mesh

The relative sliding velocity at the point of contact in two meshing gears can be determined by the velocity difference of the contact points. The frictional force acts in the opposite direction of the relative sliding velocity. Fig. 5.3 shows two teeth in contact, where X is the line of action, C is the contact point and, R_1 and R_2 are the radii of the base circle of gears 1 and
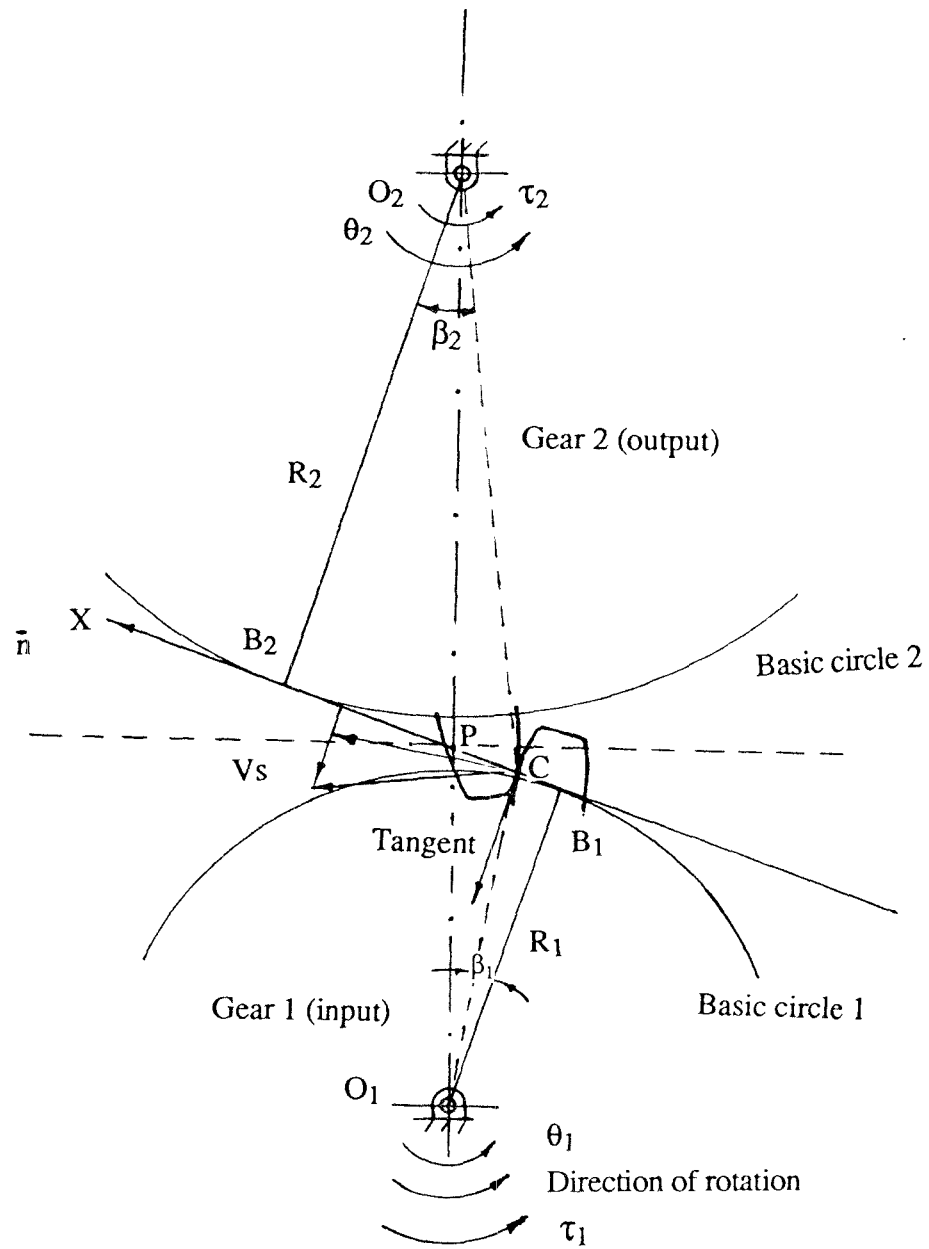
Figure 5.3: A Spur Gear Mesh

91

2, respectively. Let gear 1 be the driving gear and gear 2 the driven gear. Then, when gear 1 rotates counter-clockwise, the contact point C will travel along the line of action X with a speed of

$$V_c = R_1 \dot{\theta}_1 = -R_2 \dot{\theta}_2, \qquad (5.23)$$

where θ_1 and θ_2 are the angular displacements of gears 1 and 2, respectively. Note that a positive displacement represents a counter-clockwise rotation. Since the line of action is perpendicular to the contact surface, the velocity components along the line of action of the contact points C_1 on gear 1 and C_2 on gear 2 should be identical. And the sliding velocity of the driving gear 1 with respect to the driven gear 2 is the difference of their components along the tangent at the contact surface. It can be written as

$$
\begin{aligned}
v_s &= O_1 C \ \dot{\theta}_1 \ \sin\beta_1 + O_2 C \ \dot{\theta}_2 \ \sin\beta_2 \\
&= B_1 C \ \dot{\theta}_1 + B_2 C \ \dot{\theta}_2 \\
&= (B_1 B_2 - B_2 C) \ \dot{\theta}_1 + B_2 C \ \dot{\theta}_2 \qquad (5.24)
\end{aligned}
$$

Note that we have defined the positive direction of the tangent at the contact point to be pointing toward the center of the driving gear O_1, as shown in Fig. 5.3. Let P be the point of intersection between the line of action X and the line $O_1 O_2$. Let $|B_1 P| = a$, $|B_2 P| = b$, and $x = B_1 C - a$. Note that x is defined as the distance measured from point P to C, positive or negative depending on whether PC points in the direction of $\bar{n}$ or in the opposite direction as shown in Fig. 5.3. Since

$$\dot{\theta}_2 = -N_{12} \ \dot{\theta}_1, \qquad (5.25)$$

Eq. (5.24) can be rewritten as

$$\begin{aligned}
v_s &= (B_1 B_2 - B_2 C - N_{12} B_2 C)\, \dot{\theta}_1 \\
&= [a + x - (b - x)\, N_{12}]\, \dot{\theta}_1 \\
&= (1 + N_{12}) x\, \dot{\theta}_1
\end{aligned} \tag{5.26}$$

Note that in arriving at Eq. (5.26), the relationship $a - bN_{12} = 0$ has been used. From Eq. (5.26), we can conclude that the sliding velocity is negative in the approaching period, positive in the recess period and zero at the pitch point P. Also, it is proporational to the rotational speed of the driving gear relative to their carrier.

5.3 Dry Friction Between Two Meshing Gears

5.3.1 The dynamical equation of a simple gear pair

In this dissertation, frictional effect at revolute joints will be neglected. However, the friction due to gearing will be considered. Referring to Fig. 5.3, let gear 1 be the driving gear with an applied torque τ_1 and gear 2 the driven gear with a loading torque τ_2, and let gear 1 be rotating in the counter-clockwise direction. When the contact point falls within the angle of approach, the dynamical equations can be written as:

$$I_1 \ddot{\theta}_1 = \tau_1 + \mu F_n (a + x) - F_n R_1, \tag{5.27}$$

$$I_2 \ddot{\theta}_2 = \tau_2 + \mu F_n (b - x) - F_n R_2, \tag{5.28}$$

where F_n is the normal force at the contact point, μ is the friciton coefficient, I_1 and I_2 are the moments of inertia of gears 1 and 2 about O_1 and O_2 axes, respectively, and where x is a negative number.

Solving Eqs. (5.27) and (5.28) for F_n, yields

$$F_n = \frac{I_1\ddot{\theta}_1 - \tau_1}{\mu(a + x) - R_1} \tag{5.29}$$

and

$$F_n = \frac{I_2\ddot{\theta}_2 - \tau_2}{\mu(b - x) - R_2} \tag{5.30}$$

Equating Eqs. (5.29) and (5.30), yields

$$\frac{I_1\ddot{\theta}_1 - \tau_1}{\mu(a + x) - R_1} = \frac{I_2\ddot{\theta}_2 - \tau_2}{\mu(b - x) - R_2} \tag{5.31}$$

Therefore,

$$\frac{I_1\ddot{\theta}_1 - \tau_1}{I_2\ddot{\theta}_2 - \tau_2} = \frac{\mu(a + x) - R_1}{\mu(b - x) - R_2} \tag{5.32}$$

Substituting $a = N_{12}b$ and $R_1 = N_{12}R_2$ into Eq. (5.32) and rearranging it, yields

$$\frac{I_1\ddot{\theta}_1 - \tau_1}{I_2\ddot{\theta}_2 - \tau_2} = N_{12}\frac{\mu(b - N_{21}x) - R_2}{\mu(b - x) - R_2} = N_{12}\beta \tag{5.33}$$

where

$$\beta = \frac{\mu(b - N_{21}x) - R_2}{\mu(b - x) - R_2} \tag{5.34}$$

Note that β is a positive number. Assuming positive coupling between mating gears is maintained at all times, then

$$\ddot{\theta}_2 = -N_{12}\ddot{\theta}_1, \tag{5.35}$$

Substituting Eq. (5.35) into (5.33) and rearranging it, yields

$$(I_1 + \beta N_{12}^2 I_2)\ddot{\theta}_1 = \tau_1 - \beta N_{12}\tau_2 \tag{5.36}$$

Equation (5.36) is the equation of motion for the system when the carrier is fixed and when θ_1 is used as the generalized coordinate. Comparing Eq. (5.36) with the dynamical equation of a frictionless model

$$(I_1 + N_{12}^2 I_2)\ddot{\theta}_1 = \tau_1 - N_{12}\tau_2, \tag{5.37}$$

it can be said that the moment of inertia of gear 2 reflected on the drive shaft of gear 1 is changed from $N_{12}^2 I_2$ to $\beta N_{12}^2 I_2$, while the loading torque reflected on the drive shaft of gear 1 is changed from $-N_{12}\tau_2$ to $-\beta N_{12}\tau_2$, i.e. they are amplified by β.

Eq. (5.36) and (5.37) can be also rewritten, using θ_2 as the generalized coordinate, as

$$(I_2 + \frac{N_{21}^2}{\beta} I_1)\ddot{\theta}_2 = \tau_2 - \frac{N_{21}}{\beta}\tau_1, \tag{5.38}$$

and

$$(I_2 + N_{21}^2 I_1)\ddot{\theta}_2 = \tau_2 - N_{21}\tau_1 \tag{5.39}$$

From the above two equations, it can be said that the moment of inertia and the applied torque of gear 1 reflected on the driven shaft are amplified by $\frac{1}{\beta}$.

By the same method, when contact point falls within the angle of recess, i.e. $x > 0$, we have

$$\beta = \frac{\mu(b - N_{21}x) + R_2}{\mu(b - x) + R_2} \tag{5.40}$$

And, the dynamical equation (5.36) still applys.

5.3.2   Gearing efficiency

The input power, P_i, and output power, P_o, of the system shown in Fig. 5.3 are given by

$$P_i = \tau_1 \dot{\theta}_1 \tag{5.41}$$

and

$$P_o = -\tau_2 \dot{\theta}_2 = \tau_2 N_{12} \dot{\theta}_1 \tag{5.42}$$

where τ_2 is related to τ_1 by the dynamical equation (5.36). The increasing rate of the system energy can be written as

$$P_e = \frac{d}{dt}(\frac{1}{2}I_1\dot{\theta}_1^2 + \frac{1}{2}I_2\dot{\theta}_2^2) = I_1\dot{\theta}_1\ddot{\theta}_1 + I_2\dot{\theta}_2\ddot{\theta}_2. \tag{5.43}$$

Therefore, the instantaneous gearing efficiency of this system is given by

$$\eta = \frac{P_o + P_e}{P_i}$$

96

$$= \frac{N_{12}\tau_2\dot{\theta}_1 + I_1\dot{\theta}_1\ddot{\theta}_1 + I_2\dot{\theta}_2\ddot{\theta}_2}{\tau_1\dot{\theta}_1}$$

$$= \frac{\frac{\dot{\theta}_1}{\beta}[\tau_1 - (I_1 + \beta N_{12}^2 I_2)\ddot{\theta}_1] + \dot{\theta}_1\ddot{\theta}_1(I_1 + N_{12}^2 I_2)}{\tau_1\dot{\theta}_1}$$

$$= \frac{1}{\beta} + \frac{(1 - \frac{1}{\beta})I_1\ddot{\theta}_1}{\tau_1} \tag{5.44}$$

For constant angular velocity,

$$\eta_c = \frac{1}{\beta} \tag{5.45}$$

Assuming $-x_i \leq x \leq x_f$, then the average gearing efficiency can be written as

$$\bar{\eta} = \frac{1}{x_i + x_f}\int_{-x_i}^{x_f} \eta_c dx$$

$$= \frac{1}{x_i + x_f}\left(\int_{-x_i}^{0} \frac{\mu(b - x) - R_2}{\mu(b - N_{21}x) - R_2}dx + \int_{0}^{x_f} \frac{\mu(b - x) + R_2}{\mu(b - N_{21}x) + R_2}dx\right)$$

$$= \frac{1}{N_{21}} - \frac{(N_{21} - 1)}{\mu N_{21}^2(x_i + x_f)}\left((R_2 - \mu b)\ln\frac{R_2 - \mu b}{-\mu N_{21}x_i + R_2 - \mu b}\right.$$

$$\left. + (R_2 + \mu b)\ln\frac{-R_2 - \mu b}{\mu N_{21}x_f - R_2 - \mu b}\right) \tag{5.46}$$

All the foregoing discussion is based on the assumption that the driving gear rotates in the same direction as the applied torque. If the torque applied to gear 1 is a braking torque, i.e. the driving gear rotates in the opposite direction of its applied torque, then it can be shown that the dynamical eq. (5.36) and (5.38) remain the same. However, due to the change in the direction of frictional force, the definition of β becomes

$$\beta = \frac{\mu(b - N_{21}x) + R_2}{\mu(b - x) + R_2}, \qquad \text{for } x < 0$$

and

$$\beta = \frac{\mu(b - N_{21}x) - R_2}{\mu(b - x) - R_2}, \qquad \text{for } x > 0 \tag{5.47}$$

which is equivalent to replacing μ by $-\mu$ in equations (5.34) and (5.40), respectively. Note that this is essentially the same as interchanging the driving and driven gears. In what follows, we shall only consider the case for which the driving gear rotates in the direction of applied torque.

All the equations derived above are based on the assumption that all the gears and shafts are axially symmetric. If a gear is not axially symmetric, then the inertia force due to the offset of mass center will create an inertia torque about its axis of rotation.

5.3.3 Power loss

The normal force F_n can be obtained by solving Eq. (5.36) for $\ddot{\theta}_1$ and substituting it into Eq. (5.29). This yields

$$F_n = -\frac{N_{12}\beta(N_{12}I_2\tau_1 + I_1\tau_2)}{(\mu(a + x) - R_1)(I_1 + \beta N_{12}^2 I_2)}, \qquad \text{for } x \leq 0 \tag{5.48}$$

Similarly,

$$F_n = \frac{N_{12}\beta(N_{12}I_2\tau_1 + I_1\tau_2)}{(\mu(a + x) + R_1)(I_1 + \beta N_{12}^2 I_2)}, \qquad \text{for } x > 0 \tag{5.49}$$

The frictional force can be written as

$$f = \mu F_n \tag{5.50}$$

98

The power loss of this system is

$$P_l = - |f \ v_s| \tag{5.51}$$

Substituting Eqs. (5.48) or (5.49) into (5.50), and then the resulting equation and (5.26) into (5.51), yields

$$P_l = (p_1(x)\tau_1 + p_2(x)\tau_2) \ \dot{\theta}_1, \tag{5.52}$$

where

$$p_1(x) = \frac{-\mu\beta I_2 N_{12}^2 (1 + N_{12})x}{(\mu(a + x) - R_1)(I_1 + \beta N_{12}^2 I_2)}, \qquad \text{for } x \ \leq \ 0$$

$$p_1(x) = \frac{-\mu\beta I_2 N_{12}^2 (1 + N_{12})x}{(\mu(a + x) + R_1)(I_1 + \beta N_{12}^2 I_2)}, \qquad \text{for } x \ \geq \ 0 \tag{5.53}$$

and

$$p_2(x) = \frac{I_1}{I_2} N_{21} p_1(x) \tag{5.54}$$

The dynamical equation including friction term can be also derived by Lagrange's equation of motion, where the generalized active force due to friction is given by

$$Q_j = \frac{\partial P_l}{\partial \dot{q}_j}, \qquad j = 1, 2, \cdots \tag{5.55}$$

where q_j is the generalized coordinate. The resulting dynamical equation would be the same as Eq. (5.36) or (5.38).

Note that τ_1 or τ_2 in Eq. (5.52) can be replaced by the angular acceleration of gear 1 or 2. Solving Eq. (5.27) for F_n, yields

$$F_n = -\frac{-\tau_1 + I_1\ddot{\theta}_1}{\mu(a+x) - R_1} \tag{5.56}$$

Substituting Eq. (5.56) into (5.50) and then substituting the resulting equation and (5.26) into (5.51), yields

$$P_l = (-\tau_1 + I_1\ddot{\theta}_1)\left(\frac{1 + N_{12}x}{\mu(a+x) - R_1}\right)\dot{\theta}_1, \quad \text{for } x \leq 0$$

$$P_l = (-\tau_1 + I_1\ddot{\theta}_1)\left(\frac{1 + N_{12}x}{\mu(a+x) + R_1}\right)\dot{\theta}_1, \quad \text{for } x \geq 0 \tag{5.57}$$

5.4 Two Meshing Gears Mounted on a Moving Carrier

The derivations given in the previous section are valid for situations where the carrier is fixed. In this section, we shall discuss the effect of carrier motion on friction between two meshing gears. Obviously, translational motion of the carrier does not have any effect on the normal contact force between two meshing gears. And, the frictional effect in such a system would be the same as the one with stationary carrier. In what follows, we shall discuss the case when the carrier has rotational motion.

Fig. 5.4 shows such a mechanism, where two mating gears 1 and 2 with applied torques τ_1 and τ_2, respectively, are supported by a moving carrier, A. For such a system, the dynamical equations (5.27) and (5.28), and the combined equation, (5.33), remain valid. However, θ_1 and θ_2 are not related by Eq. (5.35). Assuming positive coupling is maintained, they are related by

$$\dot{\theta}_{2A} = -N_{12}\dot{\theta}_{1A} \tag{5.58}$$

100
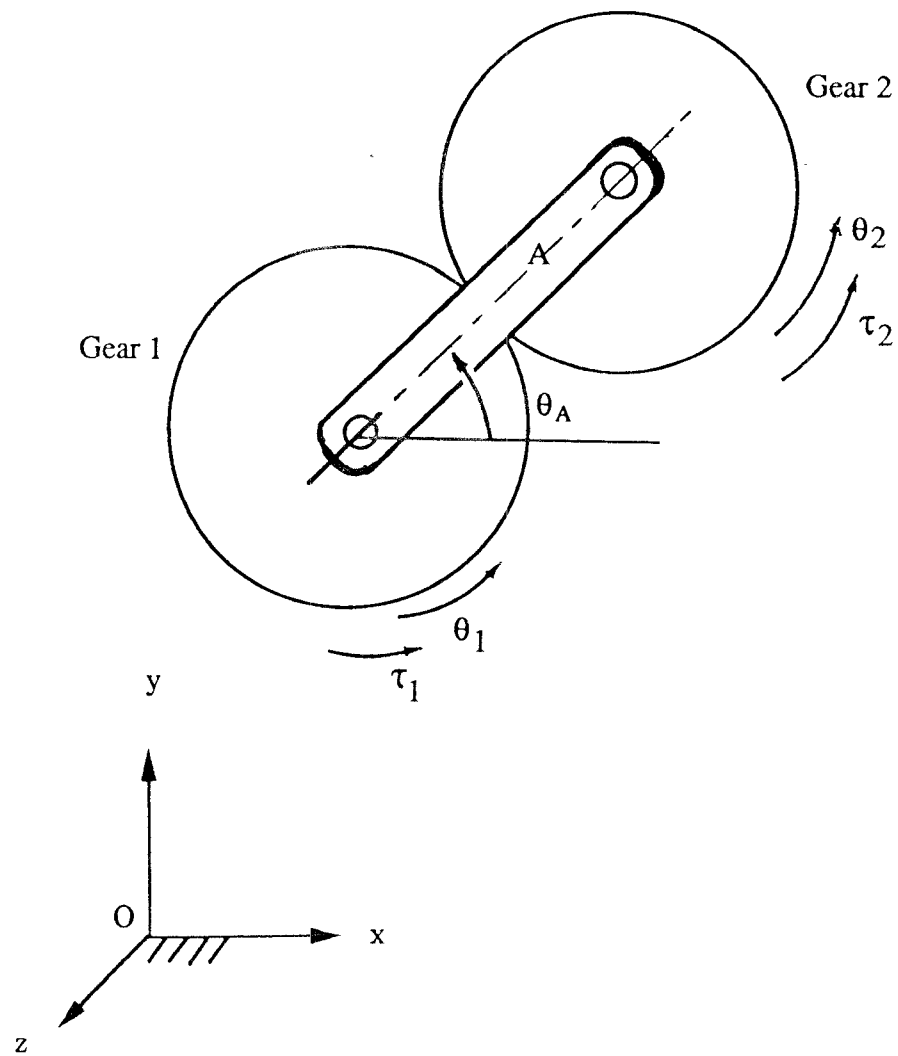
Figure 5.4: A Simple Gear Pair with Moving Carrier

where

$$\dot{\theta}_{iA} = \dot{\theta}_i - \dot{\theta}_A, \qquad i = 1, 2 \tag{5.59}$$

where $\dot{\theta}_A$ is the angular velocity of the carrier, and $\dot{\theta}_{iA}$ is the angular velocity of gear i relative to its carrier A. Substituting the time derivative of Eqs. (5.58) and (5.59) into (5.33), yields

$$(I_1 + N_{12}^2 \beta I_2)\ddot{\theta}_{1A} = \tau_1 - N_{12}\beta\tau_2 + (N_{12}\beta I_2 - I_1)\ddot{\theta}_A \tag{5.60}$$

or in terms of θ_{2A} and θ_A,

$$(I_2 + \frac{N_{21}^2}{\beta}I_1)\ddot{\theta}_{2A} = \tau_2 - \frac{N_{21}}{\beta}\tau_1 + (\frac{N_{21}I_1}{\beta} - I_2)\ddot{\theta}_A \tag{5.61}$$

From Eqs. (5.60) and (5.61), it can be said that the angular acceleration of the carrier $\ddot{\theta}_A$ produces an effective torque of $(N_{12}\beta I_2 - I_1)\ddot{\theta}_A$ about the drive shaft of gear 1. On the other hand, it can also be said that $\ddot{\theta}_A$ produces an effective torque $(\frac{N_{21}I_1}{\beta} - I_2)\ddot{\theta}_A$ about the driven shaft of gear 2.

The normal contact force between these two gears can be obtained by solving Eqs. (5.59) and (5.60) for $\ddot{\theta}_1$ and substituting the result into Eq. (5.29). This yields

$$F_n = \frac{N_{12}\beta I_1 I_2 (1 + N_{12})\ddot{\theta}_A - \beta N_{12}(N_{12}I_2\tau_1 + I_1\tau_2)}{(I_1 + N_{12}^2\beta I_2)(\mu(a + x) - R_1)} \tag{5.62}$$

The power loss of this system can be obtained by substituting Eq. (5.62) and $v_s = (1 + N_{12})x\dot{\theta}_{1A}$ into Eq. (5.51). This gives

$$P_l = [p_1(x)\tau_1 + p_2(x)\tau_2 + p_\theta(x)\ddot{\theta}_A]\dot{\theta}_{1A} \tag{5.63}$$

102

where $p_1(x)$ and $p_2(x)$ are given by Eqs. (5.53) and (5.54), and where

$$p_\theta(x) = \frac{\mu N_{12}\beta I_1 I_2 (1 + N_{12})^2 x}{(I_1 + N_{12}^2 \beta I_2)(\mu(a+x) - R_1)} , \qquad \text{for } x \leq 0$$

$$p_\theta(x) = \frac{\mu N_{12}\beta I_1 I_2 (1 + N_{12})^2 x}{(I_1 + N_{12}^2 \beta I_2)(\mu(a+x) + R_1)} , \qquad \text{for } x \geq 0 \qquad (5.64)$$

5.5 Gear Train

Fig. 5.5 shows a gear train having three gears mounted on one carrier, where τ_1, τ_2 and τ_3 are torques applied on gears 1 ,2 and 3, respectively.

As discussed in section 5.3, the effective moment of inertia of gears 2 and 3 reflected on the axis of gear 2 can be written as:

$$(I_2)_{eff} = I_2 + \beta_{23} N_{23}^2 I_3. \qquad (5.65)$$

The effective torque due to τ_2 and τ_3 and reflected on the axis of gear 2 can be written as:

$$(\tau_2)_{eff} = \tau_2 - \beta_{23} N_{23} \tau_3 \qquad (5.66)$$

where β_{ij} is defined by Eqs. (5.34) and (5.40) and where the subscript (23) denotes the gear pair (2,3). Hence, the effective moment of inertia of gears 1, 2 and 3 and the effective torque due to τ_1, τ_2 and τ_3 reflected on the axis of gear 1 can be written as

$$\begin{aligned}
(I_1)_{eff} &= I_1 + \beta_{12} N_{12}^2 (I_2)_{eff} \\
&= I_1 + \beta_{12} N_{12}^2 I_2 + \beta_{12}\beta_{23} N_{12}^2 N_{23}^2 I_3 \qquad (5.67)
\end{aligned}$$

103
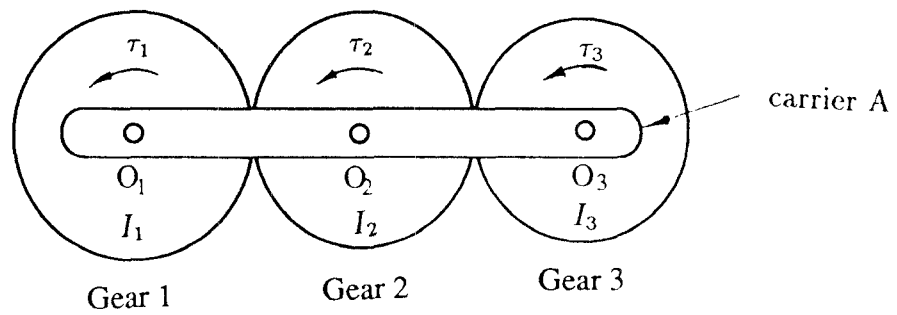
Figure 5.5: Three Gears Mounted on One Carrier

and

$$(\tau_1)_{eff} = \tau_1 - \beta_{12}N_{12}(\tau_2)_{eff}$$
$$= \tau_1 - \beta_{12}N_{12}\tau_2 + \beta_{12}\beta_{23}N_{12}N_{23}\tau_3 \tag{5.68}$$

Hence, using θ_1 as generalized coordinate, the dynamical equation for this gear train can be written as

$$(I_1)_{eff}\ddot{\theta}_1 = (\tau_1)_{eff} \tag{5.69}$$

or

$$(I_1 + \beta_{12}N_{12}^2 I_2 + \beta_{12}\beta_{23}N_{12}^2 N_{23}^2 I_3)\ddot{\theta}_1$$
$$= \tau_1 - \beta_{12}N_{12}\tau_2 + \beta_{12}\beta_{23}N_{12}N_{23}\tau_3 \tag{5.70}$$

The power loss between gears 1 and 2 can be obtained by replacing τ_2 with $(\tau_2)_{eff}$ and I_2 with $(I_2)_{eff}$ in Eq. (5.52). The result is

$$P_l^{12} = \left(p_1^{12}(x_{12}, x_{23})\tau_1 + p_2^{12}(x_{12}, x_{23})\tau_2 + p_3^{12}(x_{12}, x_{23})\tau_3\right)\dot{\theta}_1, \tag{5.71}$$

where

$$p_1^{12}(x_{12}, x_{23}) = \frac{-\mu\beta_{12}N_{12}^2(1 + N_{12})x_{12}(I_2 + \beta_{23}N_{23}^2 I_3)}{(\mu(a_{12} + x_{12}) - R_1)(I_1 + \beta_{12}N_{12}^2(I_2 + \beta_{23}N_{23}^2 I_3))},$$

$$x_{12} \leq 0;$$

$$p_1^{12}(x_{12}, x_{23}) = \frac{-\mu\beta_{12}N_{12}^2(1 + N_{12})x_{12}(I_2 + \beta_{23}N_{23}^2 I_3)}{(\mu(a_{12} + x_{12}) + R_1)(I_1 + \beta_{12}N_{12}^2(I_2 + \beta_{23}N_{23}^2 I_3))},$$

$$x_{12} \geq 0; \tag{5.72}$$

$$p_2^{12}(x_{12}, x_{23}) = \frac{-\mu \beta_{12} I_1 N_{12}(1 + N_{12})x_{12}}{(\mu(a_{12} + x_{12}) - R_1)(I_1 + \beta_{12}N_{12}^2(I_2 + \beta_{23}N_{23}^2 I_3))},$$

$$x_{12} \leq 0;$$

$$p_2^{12}(x_{12}, x_{23}) = \frac{-\mu \beta_{12} I_1 N_{12}(1 + N_{12})x_{12}}{(\mu(a_{12} + x_{12}) + R_1)(I_1 + \beta_{12}N_{12}^2(I_2 + \beta_{23}N_{23}^2 I_3))}$$

$$x_{12} \geq 0 \tag{5.73}$$

and

$$p_3^{12}(x_{12}, x_{23}) = -\beta_{23} N_{23} p_2^{12} \tag{5.74}$$

Similarly, the power loss between gears 2 and 3 can be written in the following form:

$$P_l^{23} = \left(p_1^{23}(x_{12}, x_{23})\tau_1 + p_2^{23}(x_{12}, x_{23})\tau_2 + p_3^{23}(x_{12}, x_{23})\tau_3 \right) \dot{\theta}_1 \tag{5.75}$$

The power loss of the overall system can be written as follows:

$$\begin{aligned} P_l &= P_l^{12} + P_l^{23} \\ &= (p_1\tau_1 + p_2\tau_2 + p_3\tau_3)\dot{\theta}_1 \end{aligned} \tag{5.76}$$

where

$$p_1 = p_1^{12} + p_1^{23} \tag{5.77}$$

$$p_2 = p_2^{12} + p_2^{23} \tag{5.78}$$

and

106

$$p_3 = p_3^{12} + p_3^{23} \tag{5.79}$$

The above method of effective moment of inertia and effective applied torque can be extended to a gear train with any number of gears mounted on a common stationary or moving carrier. In general, we can conclude that for a gear train with n gears sharing a common moving carrier, the power loss can be written in the following form:

$$P_l = \left(p_\theta \ddot{\theta}_A + \sum_{i=1}^{n} p_i \tau_i \right) \dot{\theta}_{1A} \tag{5.80}$$

where p_θ and p_i are functions of contact point, but are independent of $\dot{\theta}_{1A}$. Note that Eq. (5.80) can also be written in terms of τ_k ($k = 1, 2, \cdots, n-1$), $\ddot{\theta}_A$ and $\ddot{\theta}_{nA}$ as discussed in section 5.3.3. That is

$$P_l = \left(p_\theta \ddot{\theta}_A + p_n \ddot{\theta}_{nA} + \sum_{i=1}^{n-1} p_i \tau_i \right) \dot{\theta}_{1A} \tag{5.81}$$

5.6   Dynamical Equations with Friction Term

In this section, we shall demonstrate the effect of friction on the dynamics of gear coupled manipulators. We shall use the two-DOF prototype arm shown in Fig. 5.1 as an example. The dynamical equations for the prototype arm can be obtained by adding the generalized active forces contributed from frictional forces into Eqs. (5.17) and (5.18).

In a gear-coupled robotic mechanism, every column in the structure matrix represents a transmission line. A transmission line may start from one link and end at the following link, which results in only one non-zero element

107

in the column. It may also start from one link and go through several links and joints, which results in several consecutive non-zero elements. Every transmission line can be broken into several sections, such that all gears in a section share a common carrier.

There are three transmission lines in the prototype design. The first starts from the ground link and goes through two major links, A and B. This transmission line can be broken into two sections. The first section contains two gear pairs mounted on links 9 and 8, and 8 and 1; the second section also contains two gear pairs mounted on links 1 and 2, and 2 and B, respectively. The power loss in the first section can be written as

$$P_l^{(1)} = (p_1 \xi_1 + p_2 \ddot{\theta}_{10}) \dot{\theta}_{90} \tag{5.82}$$

where ξ_1 is torque applied by motor 1, and where p_1 and p_2 are functions of x_{98} and x_{81} as well as the rotational direction of $\dot{\theta}_{90}$, i.e. the sign of $(40.96\dot{\theta}_A + 5.12\dot{\theta}_B)$. Since the third transmission line contains gear pairs (5,4), (4,3) and (3,B) with link A as the carrier, power can be circulated through (5,4), (4,3), (3,B), (B,2) and (2,1) gear pairs. And, since they all share the common carrier A, the power loss in the third transmission line can be combined with the second section of the first transmission line. Note that the inertia force from the motion of link B has an equivalent torque ξ_i applied on the second axis of link B. The inertia torque is given as

$$\xi_i = -(J_B + m_B l x_B \cos \theta_B) \ddot{\theta}_A - J_B \ddot{\theta}_B - m_B l x_B \sin \theta_B \dot{\theta}_A^2 \tag{5.83}$$

where J_B is the moment of inertia of link B about its rotation axis, Z_2. Hence, the power loss can be written as

108

$$P_l^{(2)} = (p_3\xi_3 + p_4\xi_i + p_5\ddot{\theta}_{1A})\dot{\theta}_{5A} \tag{5.84}$$

where ξ_3 is the torque applied by motor 3, and where p_3, p_4 and p_5 are functions of x_{54}, x_{43}, x_{3B}, x_{B2} and x_{21} as well as the rotational direction of $\dot{\theta}_{5A}$, i.e. the sign of $\dot{\theta}_B$. The second transmission line starts from the ground link and ends at link A. There is only one section in the transimission line, making up of gear pairs (7,6) and (6,A). The power loss due to this section can be written as

$$P_l^{(3)} = (p_6\xi_2 + p_7\ddot{\theta}_A)\dot{\theta}_{70} \tag{5.85}$$

where ξ_2 is torque applied by motor 2, and where p_6 and p_7 are functions of x_{76} and x_{6A} as well as the direction of rotation of $\dot{\theta}_{70}$, i.e. the sign of $\dot{\theta}_A$. The total power loss of this system can be obtained by summing Eqs. (5.82), (5.84) and (5.85) as

$$
\begin{aligned}
P_l = {}& (p_1\xi_1 + p_2\ddot{\theta}_{10})\dot{\theta}_{90} \\
& + (p_3\xi_3 + p_4\xi_i + p_5\ddot{\theta}_{1A})\dot{\theta}_{5A} \\
& + (p_6\xi_2 + p_7\ddot{\theta}_A)\dot{\theta}_{70}
\end{aligned} \tag{5.86}
$$

The generalized active force can be obtained by substituting Eqs. (5.83), (5.7)-(5.15) into (5.86) and the resulting equation into Eq. (5.55). This yields

$$
\begin{aligned}
Q_1 = {}& 40.96(p_2 + p_7)\ddot{\theta}_A + 5.12p_2\ddot{\theta}_B + 40.96p_1\xi_1 \\
& + 40.96p_6\xi_2 + 48m_Blx_Bp_4 \sin\theta_A \ \dot{\theta}_A\dot{\theta}_B
\end{aligned} \tag{5.87}
$$

and

$$
\begin{aligned}
Q_2 = {}& (5.12p_2 + 24p_4(J_B + m_Blx_B \cos\theta_B))\ddot{\theta}_A \\
& + (0.64p_2 - 3p_5 + 24p_4J_B)\ddot{\theta}_B \\
& + 24p_4m_Blx_B \sin\theta_B\dot{\theta}_A^2 + 5.12p_1\xi_1 - 24p_3\xi_3
\end{aligned} \tag{5.88}
$$

109

The overall dynamical equations can be obtained by adding Q_1 and Q_2 into left hand side of Eqs. (5.17) and (5.18), respectively. This yields

$$\xi_1 + 40.96p_1\xi_1 + 40.96p_6\xi_2$$

$$= (r + 2k \ \cos\theta_B - 40.96(p_2 + p_7))\ddot{\theta}_A + (s + k \ \cos\theta_B - 5.12p_2)\ddot{\theta}_B$$

$$+ (48m_B l x_B p_4 \ \sin\theta_A - 2k \ \sin\theta_B)\dot{\theta}_A\dot{\theta}_B - k \ \sin\theta_B \ \dot{\theta}_B^2 \qquad (5.89)$$

and

$$5.12p_1\xi_1 + \xi_2 - 24p_3\xi_3$$

$$= (s + k \ \cos\theta_B - 5.12p_2 - 24p_4(J_B + m_B l x_B \cos\theta_B))\ddot{\theta}_A$$

$$+ (t - 0.64p_2 + 3p_5 - 24p_4 J_B)\ddot{\theta}_B$$

$$- (24p_4 m_B l x_B \ \cos\theta_B - k \ \sin\theta_B)\dot{\theta}_A^2 \qquad (5.90)$$

Note that x_{ij}'s are periodic functions. Usually, their frequencies are much higher than that of the mechanical system. Hence, p_i can be approximated by a constant for a designated rotational direction and another constant for the reverse direction. Equations. (5.89) and (5.90) can be used for more accurate modeling of the system.

5.7 Summary

The dynamical equations of motion for a typical RBR robot have been derived. It is shown that rotor inertia can have significant effect on the dynamics of such gear-coupled mechanical systems. Frictional force can also have significant effect on the dynamics and control of gear-coupled manipulators. The effect of friction has been investigated for two meshing gears

with a stationary or moving carrier, and for a gear train with a common stationary or moving carrier. The inclusion of friction in the dynamic model makes precise control of a manipulator more feasible.

Chapter 6

Computed Torque Control and the Experimental Results

6.1 Computed Torque Control Law

Computed torque technique together with PD control can be implemented for the control of RBR arms. This control algorithm has been employed in the experimental RBR arm shown in Fig. 6.1. The dynamical equations, (5.17) and (5.18), for this two-DOF RBR arm can be written in the following form

$$\underline{G}\,\ddot{\underline{\theta}} + \underline{f}_r(\dot{\underline{\theta}}, \underline{\theta}) = \underline{\tau} \tag{6.1}$$

where

$$\underline{\theta} = \begin{bmatrix} \theta_A \\ \theta_B \end{bmatrix} = \quad \text{generalized coordinates,} \tag{6.2}$$

112
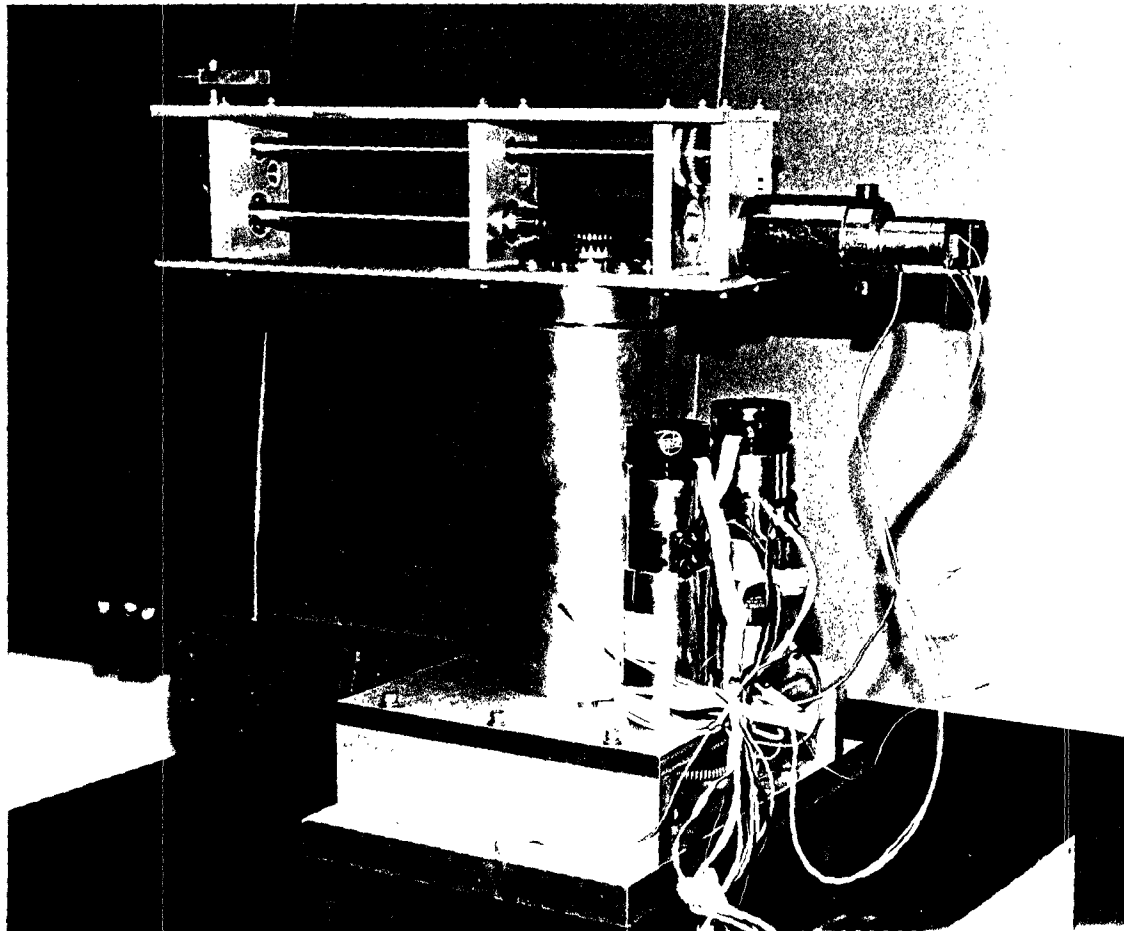
Figure 6.1: The Picture of the Experimental Arm

$$\underline{G} = \begin{bmatrix} r + 2k \ \cos\theta_B & s + k \ \cos\theta_B \\ s + k \ \cos\theta_B & t \end{bmatrix} = \text{mass matrix,} \qquad (6.3)$$

$$\underline{f}_r = -k \ \sin\theta_B \begin{bmatrix} 2\dot{\theta}_A\dot{\theta}_B + \dot{\theta}_B^2 \\ \dot{\theta}_A^2 \end{bmatrix}$$
$$= \quad \text{coriolis and centrifugal forces,} \qquad (6.4)$$

and

$$\underline{\tau} = \begin{bmatrix} \tau_1 \\ \tau_2 \end{bmatrix} = \text{generalized active forces,} \qquad (6.5)$$

and where r, s, t and k are given by Eqs. (5-19) through (5.22). Since joint angles are used as the generalized coordinates, the generalized active forces are the resultant joint torques about joint axes Z_1 and Z_2, respectively. If frictional forces are considered, $\underline{G}$ and $\underline{f}_r$ have to be modified according to Eqs. (5.89) and (5.90).

In the computed torque technique, the generalized active forces are computed in every sampling period by using the following equation:

$$\underline{\tau} = \underline{f}_r(\dot{\underline{\theta}}, \underline{\theta}) + \underline{G}\ddot{\underline{\theta}}_d + \underline{G}\underline{k}_v\dot{\underline{e}} + \underline{G}\underline{k}_p\underline{e} \qquad (6.6)$$

where $\underline{\theta}_d$ is the desired joint angles, $\underline{k}_p$ and $\underline{k}_v$ are matrices representing positional and velocity feedback gains, respectively, and where

$$\underline{e} = \underline{\theta}_d - \underline{\theta} \qquad (6.7)$$

is the error signal obtained by substracting the measured displacement, $\underline{\theta}$, from the desired displacement, $\underline{\theta}_d$. Substituting Eq. (6.6) into (6.1), yields

114

$$\underline{G}\, \underline{\ddot{\theta}} = \underline{G}\, \underline{\ddot{\theta}_d} + \underline{G}\, \underline{k_v}\, \underline{\dot{e}} + \underline{G}\, \underline{k_p}\, \underline{e} \tag{6.8}$$

Rearranging the above equation and pre-multipling it by $\underline{G}^{-1}$, yields

$$\underline{\ddot{e}} + \underline{k_v}\, \underline{\dot{e}} + \underline{k_p}\, \underline{e} = 0 \tag{6.9}$$

The position feedback gain, $\underline{k_p}$, and velocity feedback gain, $\underline{k_v}$, must be chosen such that all the poles in Eq. (6.9) locate on the left-hand-side of the complex plane. This ensures the position error, $\underline{e}$, will converge to zero, and the arm will follow the desired path, θ_d.

For the 2-DOF prototype arm design, the inertia properties of the rotors, gears, shafts, and the two major links were estimated from their sizes and materials to be as follows:

J_1	44195	gm-cm^2	J_2	205	gm-cm^2
J_3	189	gm-cm^2	J_4	111	gm-cm^2
J_5	470	gm-cm^2	J_6	10102	gm-cm^2
J_7	1223	gm-cm^2	J_8	10102	gm-cm^2
J_9	1223	gm-cm^2	J_A	1195685	gm-cm^2
J_B	124005	gm-cm^2	m_A	5770	gm
m_B	515	gm	l	30.48	cm
x_B	11.04	cm			

Hence,

$$r = 6773598 \text{ gm-cm}^2, \tag{6.10}$$

$$s = 437732 \text{ gm-cm}^2, \tag{6.11}$$

$$t = 437307 \text{ gm-cm}^2,$$ (6.12)

$$k = 173297 \text{ gm-cm}^2,$$ (6.13)

$$\underline{G} = \begin{bmatrix} 6773598 + 346594 \ \cos\theta_B & 437732 + 173297 \ \cos\theta_B \\ 437732 + 173297 \ \cos\theta_B & 437307 \end{bmatrix}$$ (6.14)

and

$$\underline{f}_r = -173297 \ \sin\theta_B \begin{bmatrix} 2\dot{\theta}_A\dot{\theta}_B + \dot{\theta}_B^2 \\ \dot{\theta}_A^2 \end{bmatrix}$$ (6.15)

In this experimrntal arm, $\underline{k}_p = \begin{bmatrix} 0.84 & 0 \\ 0 & 0.84 \end{bmatrix}$ and $\underline{k}_v = \begin{bmatrix} 1.833 & 0 \\ 0 & 1.833 \end{bmatrix}$ were chosen so that the system is critically damped.

6.2   System Parameters Estimation

The values of r, s, t and k in Eqs. (6.10) - (6.13) were calculated from the size and material used for each mechanical part in the system. To obtain a more accurate dynamical model, the system parameters can also be estimated by experiments.

In the first experiment, the second joint was mechanically locked at $\theta_B = 0$ and then 180 degrees. A sinusoidal input torque τ_1 was applied to joint 1, where τ_1 is generated by applying proper current to motor 1 with a small biased current to motor 2 when its value is positive, and applying current to motor 2 with a small biased current to motor 1 when its value is negative. The circuit to motor 3 is kept open. This ensures positive coupling of the gear meshes.

116

Substituting $\theta_B = 0°$ into Eq. (5.17), yields

$$\tau_1 = (r + 2k)\ddot{\theta}_A \qquad (6.16)$$

Substituting $\theta_B = 180°$ into Eq. (5.17), yields

$$\tau_1 = (r - 2k)\ddot{\theta}_A \qquad (6.17)$$

Under constant frequency excitation, the following equations can be obtained from Eqs. (6.16) and (6.17)

$$r + 2k = \frac{\Gamma_1}{\omega^2 \Theta_A}, \qquad \text{for } \theta_B = 0°, \qquad (6.18)$$

$$r - 2k = \frac{\Gamma_1}{\omega^2 \Theta_A}, \qquad \text{for } \theta_B = 180° \qquad (6.19)$$

where Γ_1 and Θ_A are the amplitude of τ_1 and θ_A, respectively, and where ω is the frequency of the sinusoidal input. Figs. 6.2 and 6.3 show the experimental results, the output displacement θ_A and input torque τ_1 versus time for $\theta_B = 0°$ and $\theta_B = 180°$, respectively. From these two figures, we obtain

$$r + 2k = 6478446 \text{ gm-cm}^2 \qquad (6.20)$$

and

$$r - 2k = 5417242 \text{ gm-cm}^2 \qquad (6.21)$$

Summing Eqs. (6.20) and (6.21) and dividing the result by 2, yields

117
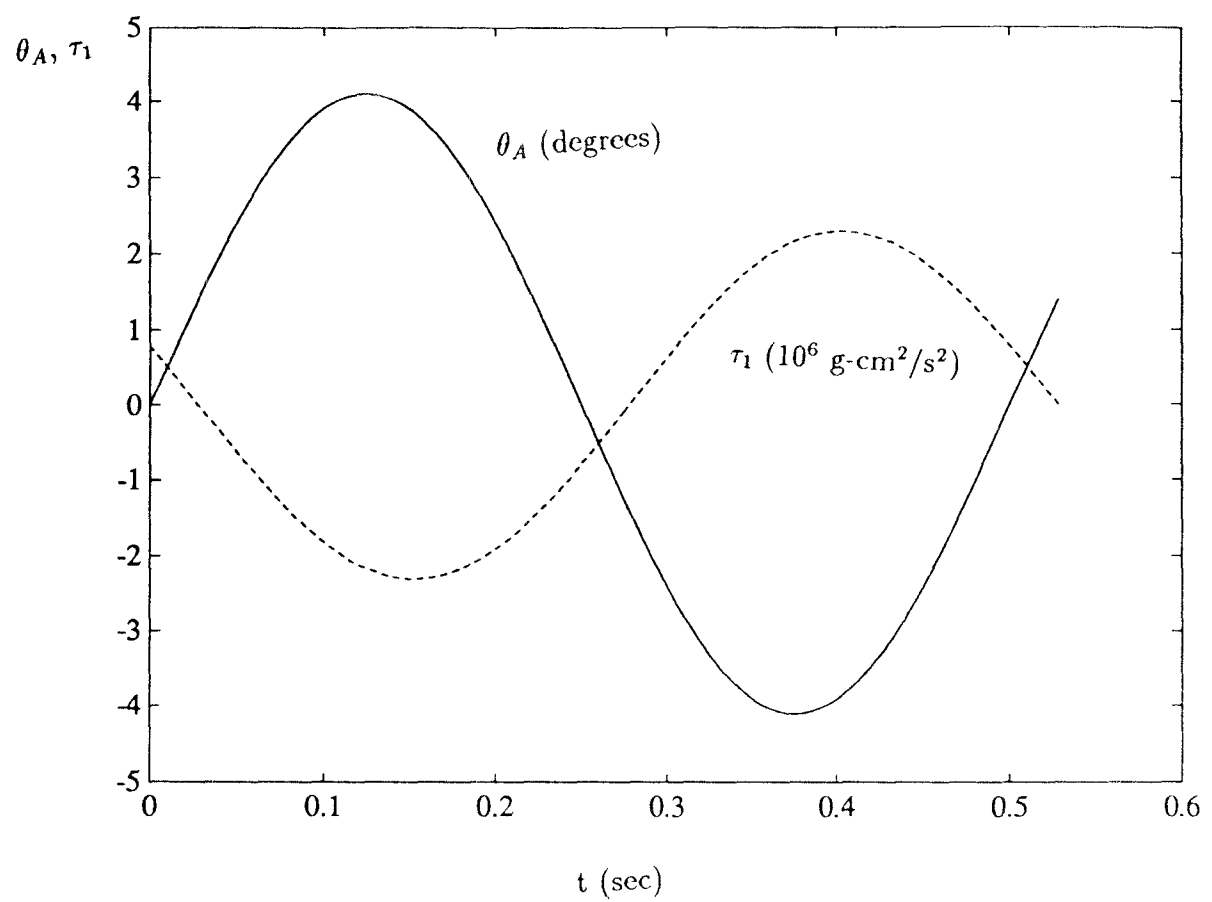
Figure 6.2: Sinusoidal Response ($\theta_B = 0°$)

118
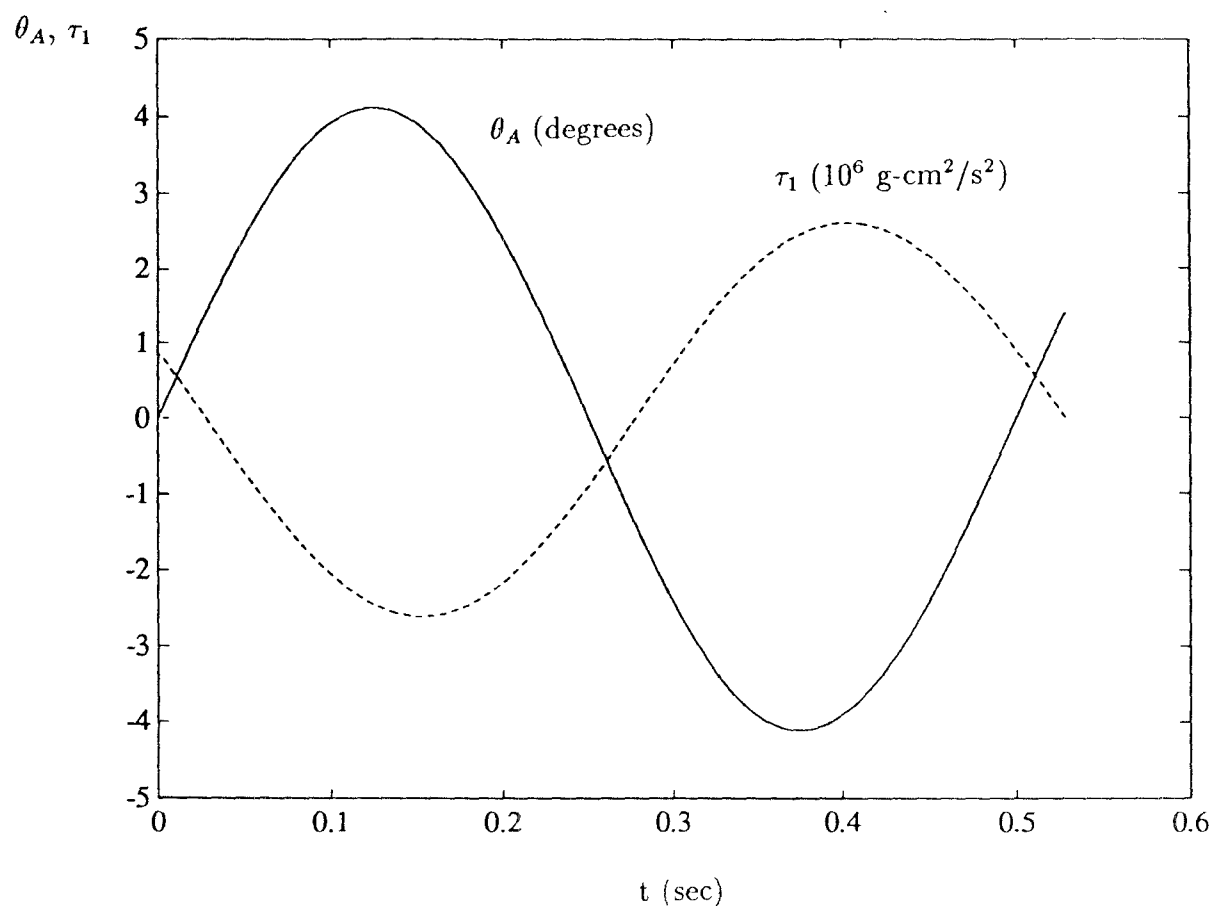
Figure 6.3: Sinusoidal Response (θ_B=180°)

119

$$r = 5947844 \text{ gm-cm}^2 \qquad (6.22)$$

Subtracting Eq. (6.21) from (6.20) and dividing the result by 4, yields

$$k = 191051 \text{ gm-cm}^2 \qquad (6.23)$$

In the second experiment, the first joint axis, θ_A, was mechanically locked. The second joint was driven by a sinusoidal torque τ_2, to estimate the value of t, where τ_2 was generated by applying current to motor 3 plus a small biased current to motor 1 when its value is positive, and applying current to motor 1 with a small biased current to motor 3 when it is negative. The circuit to motor 1 is kept open. Substituting $\dot{\theta}_A = 0$ and $\ddot{\theta}_A = 0$ into Eq. (5.18), yields

$$\tau_2 = t\, \ddot{\theta}_B \qquad (6.24)$$

Hence, under constant frequency excitation, we obtain

$$t = \frac{\Gamma_2}{\omega^2 \Theta_B} \qquad (6.25)$$

where Γ_2 and Θ_B are the amplitude of τ_2 and θ_B, respectively, and where ω is the frequency of the sinusoidal input. The output displacement θ_B and input torque τ_2 versus time of this experiment is shown in Fig. 6.4. This results in

$$t = 510262 \text{ gm-cm}^2 \qquad (6.26)$$

In the third experiment, none of the joints were mechanically locked, and the input torques $\tau_1 = \Gamma_1 \sin(\omega t)$ and $\tau_2 = 0$ were used for the estimation
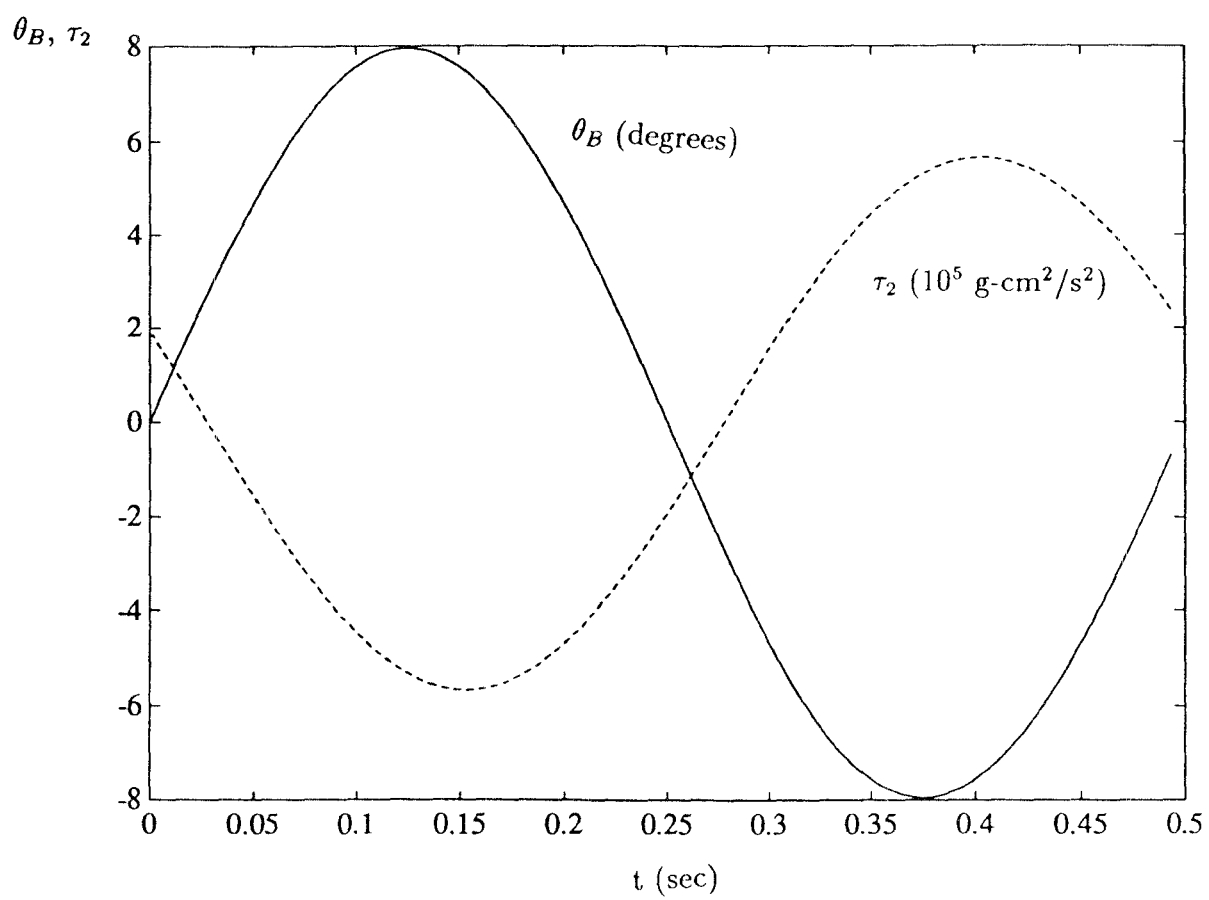
Figure 6.4: Sinusoidal Response ($\theta_A=0°$)

of s. The input torques were generated by applying current to all the three motors by using Eq. (4.6) in which minimum value of λ to keep all the motor torques unidirectional was used. In this experiment, Γ_1 and ω were chosen so that both θ_A and θ_B are much smaller than 1 rad, and both $\dot{\theta}_A$ and $\dot{\theta}_B$ are much smaller than 1 rad/sec. Hence, Eqs. (5.17) and (5.18) can be approximated by

$$\tau_1 = (r + 2k)\ddot{\theta}_A + (s + k)\ddot{\theta}_B \tag{6.27}$$

$$0 = (s + k)\ddot{\theta}_A + t\ddot{\theta}_B \tag{6.28}$$

Solving Eq. (6.28) for $\ddot{\theta}_B$, yields

$$\ddot{\theta}_B = -\frac{s + k}{t}\ddot{\theta}_A \tag{6.29}$$

Substituting Eq. (6.29) into (6.27), yields

$$\tau_1 = \left(r + 2k - \frac{(s + k)^2}{t}\right)\ddot{\theta}_A \tag{6.30}$$

Hence, under constant frequency excitation,

$$r + 2k - \frac{(s + k)^2}{t} = \frac{\Gamma_1}{\omega^2 \, \Theta_A} \tag{6.31}$$

or

$$s = \sqrt{t\left(r + 2k - \frac{\Gamma_1}{\omega^2 \, \Theta_A}\right)} - k \tag{6.32}$$

Fig. 6.5 shows the result of this experiment. From this figure, we obtained

122
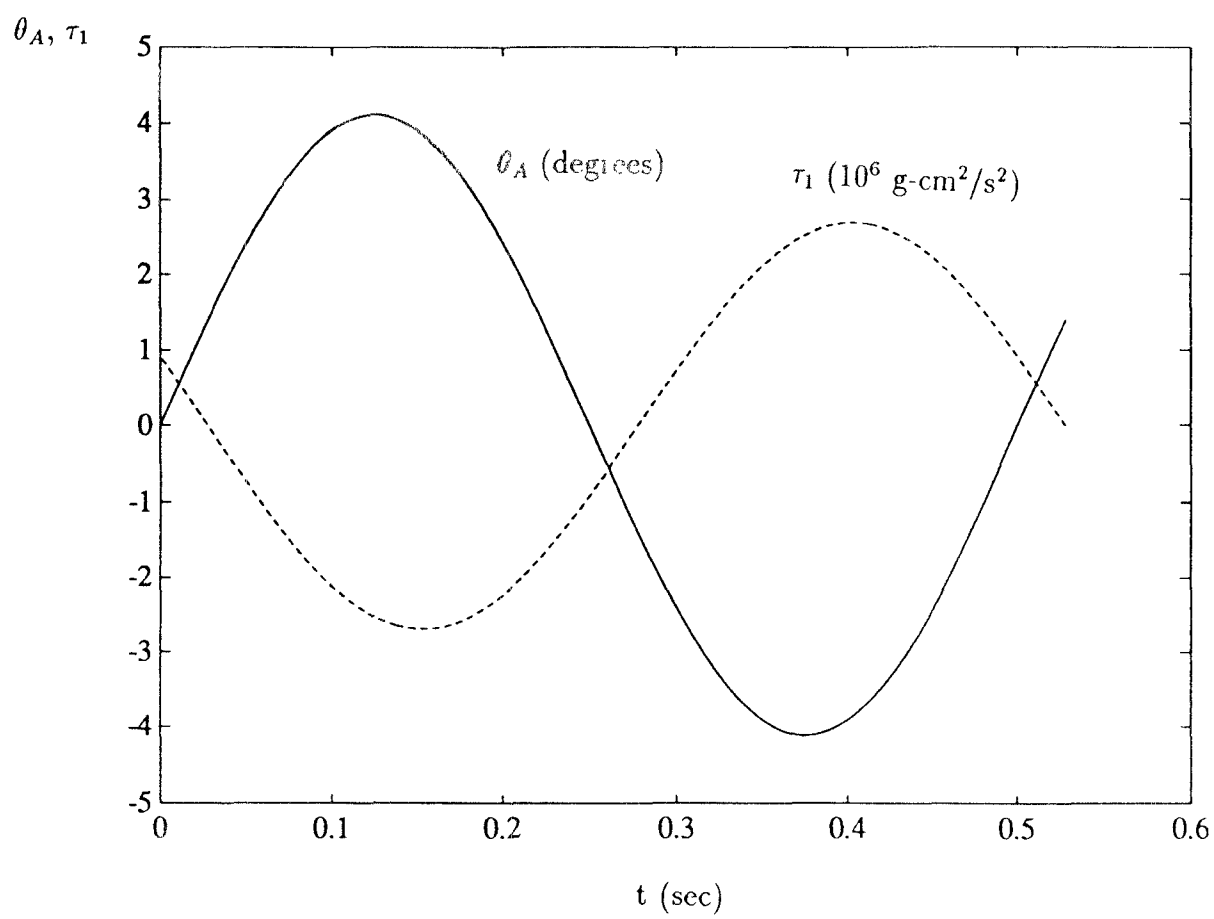
Figure 6.5: Sinusoidal Response ($\tau_2=0$)

123

$$s = 593852 \tag{6.33}$$

Because $\theta_B \neq 0$ at all times, it can be expected that the estimated value of s will have a larger error. The estimated parameters r, s, t and k were used in the dynamic model for controlling the 2-DOF experimental arm.

6.3 Actuator Torques Computation and Power Comsumption Optimization

As discussed in Chapter 4, there are infinite many sets of actuator torques, $\underline{\xi}$, corresponding to a set of desired joint torques. To keep all the gear meshes in contact at all times, the parameter λ in Eq. (4.6) should be chosen properly. From power consumption point of view, λ can be selected in such a manner that energy consumption is minimized. Using DC motors as actuators, the power consumption for the jth motor can be written as

$$E_j = z_j \, i_j^2 \tag{6.34}$$

where z_j is the internal impedence of motor j, and i_j is its armature current. The output torque of a DC motor is given by

$$\xi_j = (K_\xi)_j \, i_j \tag{6.35}$$

where K_ξ is the torque constant. Eliminating i_j from Eqs. (6.34) and (6.35), yields

$$E_j = Z_j \, \xi_j^2 \tag{6.36}$$

124

where

$$Z_j = \frac{z_j}{(K_\xi)_j^2} \tag{6.37}$$

The total energy consumption for an N-DOF RBR system, with (N+1) unidirectional drives, can be written as

$$E = \sum_{j=1}^{N+1} E_j = \sum_{j=1}^{N+1} Z_j \, \xi_j^2 \tag{6.38}$$

Substituting Eq. (4.6) into (6.38), yields

$$E = \sum_{j=1}^{N+1} Z_j \, (X_j + \lambda \, \mu_j)^2 \tag{6.39}$$

where X_j and μ_j denote the particular solution and the homogenous solution of ξ_j, respectively.

The problem of minimizing power consumption can now be stated as minimizing the objective function E subject to the following constraints:

$$0 \leq \xi_j \leq \hat{\xi}_j, \qquad j = 1, 2, \cdots, N+1 \tag{6.40}$$

where ξ_j is the required torque of the jth motor and $\hat{\xi}_j$ the maximum torque available from the jth motor.

The objective function is a positive-definite, second-degree polynominal function of λ. Without considering the constraints, the minimum value occurs at

$$\frac{\partial E}{\partial \lambda} = 2 \sum_{j=1}^{N+1} Z_j \, \mu_j \, (X_j + \lambda \, \mu_j) = 0 \tag{6.41}$$

125

Solving the above equation for λ, yields

$$\lambda_{opt} = -\frac{\sum_{j=1}^{N+1} Z_j \, \mu_j \, X_j}{\sum_{j=1}^{N+1} Z_j \, \mu_j^2} \qquad (6.42)$$

Since the objective function is a second-degree polynomial, its function is symmetric with respect to $\lambda = \lambda_{opt}$ as shown in Fig. 6.6.

Substututing

$$\xi_j = X_j + \lambda \, \mu_j \qquad (6.43)$$

into Eq. (6.40), yields

$$g_j \leq \lambda \leq h_j, \qquad j = 1, 2, \cdots, N+1 \qquad (6.44)$$

where

$$g_j = \frac{X_j}{\mu_j} \qquad (6.45)$$

$$h_j = \frac{\hat{\xi}_j - X_j}{\mu_j} \qquad (6.46)$$

From the properties of a parabolic function, the minimum value of E can be found as follows:

1. If $max(g_j) > min(h_j)$, the desired joint torques are out of the available motor torque region $\hat{D}_j$.

2. If $max(g_j) > \lambda_{opt}$, the minimum occurs at $\lambda = max(g_j)$.

126
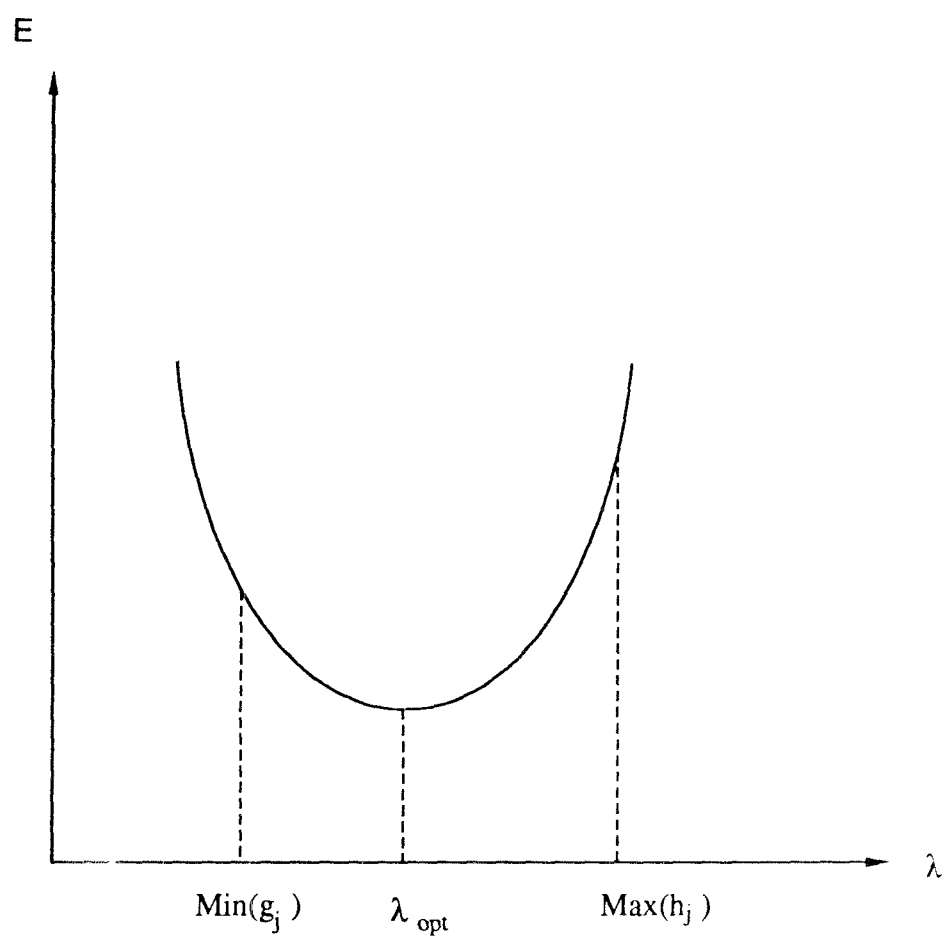
Figure 6.6: Power Consumption as a Function of the Free Parameter λ

3. If $max(g_j) \leq \lambda_{opt} \leq min(h_j)$, the minimum occurs at $\lambda = \lambda_{opt}$.

4. If $min(h_j) < -\lambda_{opt}$, the minimum occurs at $\lambda = min(h_j)$.

For the control of the prototype arm, actuator torques will be computed using the above procedure. To correct the steady-state error, the integration of position error is also added to the controller. The computed torque control flow chart for the RBR arm is shown in Fig. 6.7, where k_i is the gain of the integration feedback.

6.4 Experiment

To establish a proof of the concept of RBR mechanisms, experiments were performed with and without backlash control. Although the protoype arm were designed for unidirectional redundant drives, it can also be driven without backlash control.

In the first experiment backlash was not controlled. Since actuators 2 and 3 directly drive joints 1 and 2, respectively, these two actuators were selected as the drivers while the third motor was disconnected. In this case, the actuator torques $[\xi_1, \xi_2]^T$ were given by $[\tau_1/40.96, 0, -\tau_2/24]^T$.

In the second experiment, backlash was controlled. The value of λ was calculated using the procedure outlined in the previous section. Actuator torques were then calculated by using Eq.(4.6). Appendix A shows details of the controller design implemented on an IBM Model 55, 80386SX personal computer. Appendix B shows the computer program developed for the

128
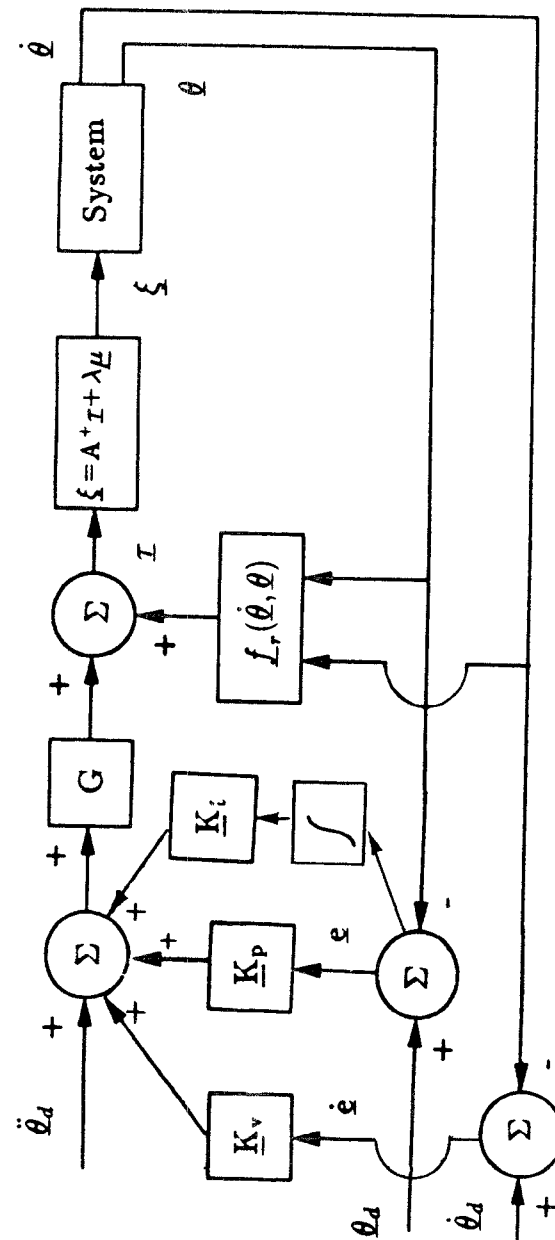
Figure 6.7: Computed Torque Control Flowchart

129

purpose of motion planning.

A laser tracking system developed by NIST (National Institute of Standard and Technology) was used to measure the Cartensian coordinates of a reference point at the end of the second moving link. The experiments were performed at four different postures of the robot arm to ensure a good coverage of the workspace. For each psoture, a target point was selected by servoing the end-effector to a predetermined position. Then the robot was commanded to approach the target point from four different directions (four orthogonal directions in the joint space). Fifteen measurements were made for each approach. The experimental data measured at NIST is given in Appendix C.

The radius of the smallest sphere containing the fifteen data points is defined as the *unidirectional repeatability* for that direction of approach. The radius of the smallest sphere containing the sixty data points taken from four directions of approach is defined as the *overall repeatability* for the posture. A graphical definition of repeatability is shown in Fig. 6.8.

Tables 6.1 through 6.4 show the differences in repeatability calculated from the experimental measurements made at NIST. From these tables, we can summarize the experiment results as follows:

1. With redundant drives, the unidirectional repeatability and the overall repeatability have same order of magnitude. This indicates that backlash has been successfully controlled by using redundant drives.

2. Without redundant control, the unidirectional repeatability can be quite random. Since the robot arm was driven slowly to a target point in

130
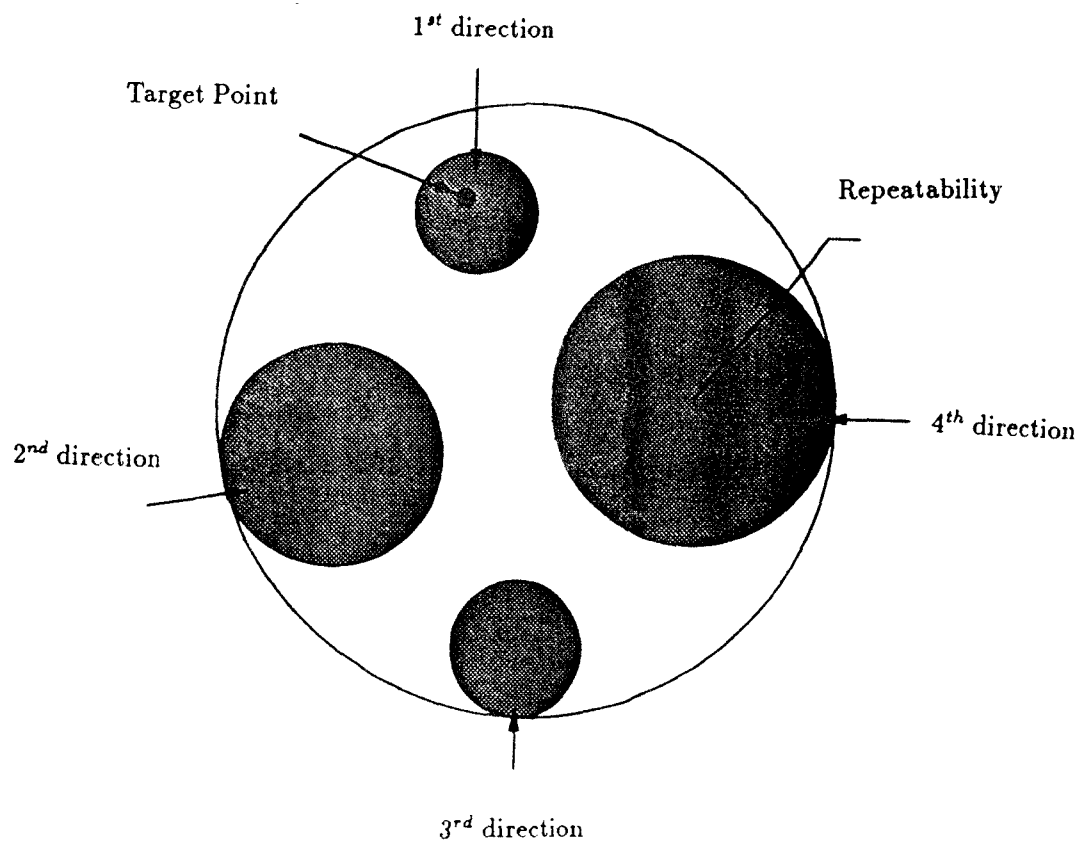
Figure 6.8: Definition of Repeatability

the same manner fifteen times, free play in gear meshes tends to occur at the same side of the teeth most of the times. The unidirectional repeatability will be as good as that with redundant control if free play does occur at the same side in all fifteen measurements. However, in some cases, noise can cause free play to occur at different side of gear meshes, and therefore increase the repeatability dramatically. This can be seen from the experimental data in Appendix C. For example, the first approach of the first direction in page 157 is far from the other fourteen approaches. This causes a big increase of repeatability. The overall repeatability without redundant control is always very large, because of the changes in the direction of approach.

3. The overall repeatability for the experiment without redundant drives is one order of magnitude greater than that with redundant drives.

Direction	Repeatability (mm)	
of Approach	Conventional Control	Redundant Control
1	1.989341	0.3218217
2	1.417662	0.1772752
3	0.2244366	0.2746798
4	0.3008665	0.2892615
Overall	6.388480	0.3985681

Table 6.1: Comparison of Repeatability at the First Target Position

| Direction | Repeatability (mm) | |
of Approach	Conventional Control	Redundant Control
1	1.950774	0.1821312
2	4.589997	7.6511331E-02
3	1.510194	0.1207631
4	0.3899245	0.2032410
Overall	6.611162	0.4786238

Table 6.2: Comparison of Repeatability at the Second Target Position

| Direction | Repeatability (mm) | |
of Approach	Conventional Control	Redundant Control
1	0.1618994	0.1525680
2	0.1601167	0.3175775
3	0.2431160	0.1664969
4	0.1678905	0.1501162
Overall	3.195182	0.4188084

Table 6.3: Comparison of Repeatability at the Third Target Position

| Direction | Repeatability (mm) | |
of Approach	Conventional Control	Redundant Control
1	0.4496819	0.1955256
2	0.1075683	0.1361130
3	0.1414595	0.1861271
4	0.2858933	0.1170794
Overall	2.593668	0.3054367

Table 6.4: Comparison of Repeatability at the Fourth Target Position

6.5 Summary

The system parameters were estimated experimentally. The computed torque technique and PD control algorithm were employed in this experimental RBR arm. This algorithm, first, computes joint torques according to a desired end-effector performance requirement. Then, joint torques are converted into actuator torques based on minimum power consumption.

Experiments on verifying the concept of backlash control were performed. The results of the experiments show that the improvement in repeatability for the redundant drive robot is one order-of-magnitude better than that without backlash control.

Chapter 7

Summary and Future Work

In this thesis, we have presented a new concept for controlling gear backlash of an articulated robotic mechanism. It has been shown that through proper arrangement of a minimum number of N+1 transmission lines, gear backlash of an N-DOF robotic mechanism can be completely eliminated.

We have started this subject from the concept of transmission lines. Using this concept, a methodology for the creation and analysis of geared robotic mechanisms has been established. Using this methodology, all the admissible structure matrices for RBR mechanisms have been enumerated. A two-DOF RBR arm has been built for the demonstration of gear backlash elimination. The dynamics and control algorithm for this class of mechanisms have been also studied. An experiment has been made for the verification of this theorem.

The major results of this study can be summarized as follows:

7.1 The Concept of Transmission Lines

A transmission line is a gear train which transmits actuator torque through consecutive joints of an articulated gear-mechanism. It is represented by a series of numbers. Each number of the transmission line stands for the amplification factor of the actuator torque at its corresponding joint. The structure matrix, which consists of all the transmission lines as its columns, will relate input torques and joint torques.

A set of rules for the enumeration of structure matrices of conventional gear-coupled robotic mechanisms has been established. The correspondence between structure matrices and basic mechanisms has also been derived. By using these rules, all the admissible two- and three-DOF structure matrices have been enumerated. A basic mechanism corresponding to each structure matrix has been constructed. Furthermore, we have also shown that idler gear(s) can be added to a basic mechanism to form derived mechanisms without changing its structural topology.

7.2 The Creation of RBR Mechanisms

A new concept has been conceived for the control of backlash in gear-coupled robotic mechanisms. The concept utilizes redundant unidirectional drives to assure positive coupling of gear meshes at all times. Consolidating this concept and the methodologies of mechanism creation and analysis using transmission lines, we have shown that through proper arrangement,

136

a minimum number of N+1 transmission lines is required for the control of an N-DOF robotic mechanism. Based on this concept, a systematic methodology has been established for the enumeration of a class of RBR mechanisms. Typical two- and three-DOF RBR mechanisms have been derived. A two-DOF experimental RBR arm has been designed and constructed for the purpose of demonstration.

The main purpose of this class of mechanism is to eliminate gear backlash in mechanical systems. One side-benefit of this class of mechanisms is that it is fail-safe, i.e., unless there is loss of backlash control, the mechanisms can continue to function when one of its actuators fails to work. This can be easily observed from the necessary conditions of controllability incorporated in the structure matrix. A sub-matrix obtained by deleting any one column from the structure matrix of a controllable RBR mechanism is non-singular. Physically, this sub-matrix is indeed a structure matrix of the mechanism, if one removes the transmission line corresponding to that column. Since the structure matrix of this new mechanism is non-singular, it is still a drivable mechanism.

7.3   Actuator Sizing

The actuator sizing for unidirectional redundant-drive manipulators has been studied in this dissertation. Using the relationship between input and output torques which is described by the structure matrix, the actuator torque requirements were first derived as functions of joint torques. Then,

137

dynamical equations were applied to derive the actuator torque, a derivation based on the velocity and acceleration of the end-effector. Finally, the minimum actuator torques are calculated by an optimization scheme. Using this method, the actuator sizing can be performed in a straightforward way instead of by means of recursive calculations. The methodology is equally applicable for tendon-driven manipulators.

7.4 Dynamics

The dynamical equations of motion for a typical gear-coupled robotic mechanism, including the inertia effect of gears and rotors, have been derived. From the dynamical equations of motion, it can be seen that the inclusion of rotors and gears in the equations could be imperative. We have also considered the gearing friction in dynamics analysis. First, the frictional force, power loss, and dynamical equations of a simple gear pair are studied. Then, the dynamics and power loss of a gear train with a common carrier are studied. It is shown that, by incorporating the power loss into the formulation of Lagrange's equations, the generalized forces due to frictional forces can be derived.

The inclusion of gearing friction in the dynamical equations can furnish more information about its influence on dynamic behavior and make precise control of a RBR mechanism more feasible.

7.5 Control and Experiment

The computed torque technique and PD control law are implemented in the two-DOF RBR experimental arm. In this control algorithm, the required joint torques are computed first. Then, motor torques are calculated based on minimum power consumption of the system.

The experiments included both conventional and redundant-drive control methods. For each control method, four target points were chosen. For each target point, the arm was commanded to approach the target point from four orthogonal directions fifteen times each. It is shown that the improvement in repeatability for the redundantly driven robot is one-order-of-magnitude better than that of conventional control.

7.6 Future Research

The improvement in manipulator repeatability has been verified by the experimental RBR arm. However, the work presented in this dissertation is only initial groundwork. The following topics are considered worth further study.

(1) Adaptive Control

The experiments made in this study demonstrate an improvement in repeatability. However, this is not the only advantage of RBR mechanisms. Since backlash can be completely eliminated in RBR mechanisms, the sta-

bility of such mechanisms can also be improved. Additional experiments on dynamic tracking is, therefore, encouraged. The employment of adaptive control using dynamical equations including gearing friction is suggested.

(2) Mechanism Creation

The concept of transmission lines has been used to enumerate all admissible articulated gear-mechanisms whose articulation points are equal in number to the number of degree-of-freedom of the mechanism. Mechanisms whose number of DOFs is greater than that of the articulation points such as the soft hand, have been employed in some special applications. Those mechanisms with a number of DOFs smaller than that of the articulation points, on the other hand, have the advantage of singularity avoidance. The concept of transmission lines can also be applied to the creation and analysis of these two classes of mechanisms. This will be the subject of future study.

Bibliography

1. Ahmad, S., 1985, "Second order nonlinear kinematic effects and their compensation," *Proc. of the 1985 IEEE Int. Conf. on Robotics and Automation* (St. Louis, MO), vol. 2, pp. 307-314.

2. Anonymous, 1982, "Bevel gear make robot's 'wrist' more flexible," *Machine Design*, vol. 54, no. 18, pp. 55.

3. Buchsbaum, F., and Freudenstein, F., 1970, "Synthesis of kinematic structure of geared kinematic chains and other mechanisms," *J. Mechanisms*, vol. 5, pp.357-392.

4. Calson, J. H., 1985, "Harmonic drives for servomechanisms," *Machine Design*, vol. 57, no. 1, pp. 102-106.

5. Chang, S. L., and Tsai, L. W., 1990, "Topological synthesis of articulated gear mechanisms," *IEEE J. Robotics Automation*, vol. 6, no. 1, pp. 97 - 103.

6. Chen, J., Chen, D.Z., and Tsai, L.W., 1990, "A systematic methodology for the dynamic analysis of articulated gear-mechanisms," *Proc. of Japan-U.S.A. Symposium on Flexible Automation. Kyoto, Japan.*

7. Craig, J., Hsu, P., and Sastry, S., 1986, "Adaptive control of mechanical manipulators," *Proceedings of IEEE International Conf. on Robotics and Automation*, San Francisco, CA, pp. 190-195.

8. Dagalakis, N. G., and Myers, D. R., 1985, "Adjustment of robot joint gear backlash using robot joint test excitation technique," *The International J. of Robotics Research*, vol. 4, no. 2.

9. Freudenstein, F., 1971, "An application of boolean algebra to the motion of epicyclic drives," *ASME J. Engineering for Industry*, vol. 93, ser. B, pp.176-182.

10. Freudenstein, F., and Maki, E.R., 1979, "The creation of mechanisms according to kinematic structure and function," *International. J. of Architecture Design, Environment, Planning*, vol. 6, pp.375-391.

11. Han, J-Y., Hemamai, H, and Yurkovich, S, 1987, "Nonlinear adaptive control of an N-link robot with unknown load," *The International J. of Robotics Research*, vol. 6, no. 3.

12. Hartenberg, R.S., and Denavit, J., 1964, *Kinematic Synthesis of linkages*. New York, McGraw-Hill.

13. Kleinn, C. A., and Huang, C. H., 1983, "Review of pseudo-inverse control for use with kinematically redundant manipulators," *IEEE Trans. on System, Man, and Cybernetics*, vol,SM513, pp. 245-250.

14. Michalec, G. W., 1966, *Precision Gearing: Theory and Practice*, New York, John Wiley & Sons, Inc.

15. Morecki, A., Busko, Z., Gasztold, H., and Jaworek, K., 1980, "Synthesis and control of the anthropomorphic two handed manipulator," *Proc. 10th Int. symp. on Industrial Robots*, Milan, Italy, pp. 461-474.

16. Paul, R.P., 1981, "Robot Manipulators: Mathematics, Programming, and Control," Cambridge, Mass. MIT Press.

17. Stackhouse, T., 1979, "A new concept in wrist flexibility," *Proc. 9th International Symp. on Industrial Robots* (Washington, DC), pp. 589-599.

18. Thomas, M., and Tesar, D., 1982, "Dynamic modeling of serial manipulator arms," *ASME J. of Mechanisms, Transmissions, and Automation in Design*, vol. 104, pp. 218-228.

19. Thomas, M., Yuan-Chou, H. C., and Tesar, D., 1985, "Optimal actuator sizing for robotic manipulators based on local dynamic criteria,"

ASME J. of Mechanisms, Transmissions, and Automation in Design, vol. 107, pp. 163-169.

20. Tsai, L.W., 1987, "An application of the linkage characteristic polynomial to the topological synthesis of epicyclic gear trains," *ASME J. Mechanisms, Transmissions, and Automation in Design*, vol. 109, no. 3, pp. 329-336.

21. Tsai, L.W., 1988, "The kinematics of spatial robotic bevel-gear trains," *IEEE J. Robotics Automation*, vol. 4, no. 2, pp. 150-156.

22. Tsai, L.W., and Freudenstein F., 1989, "On the conceptual design of a novel class of robot configuration," *ASME J. Mechanisms, Transmissions, and Automation in Design*, vol. 111, no. 1, pp. 47-53.

23. Veitschegger, W. K., and Wu, C. H., 1986, "Robot accuracy analysis based on kinematics," *IEEE J. of Robotics and Automation*, vol. 2, no. 3, pp. 171-179.

Appendix A Interface Design

U-CHANNEL INTERFACE CIRCUITRY
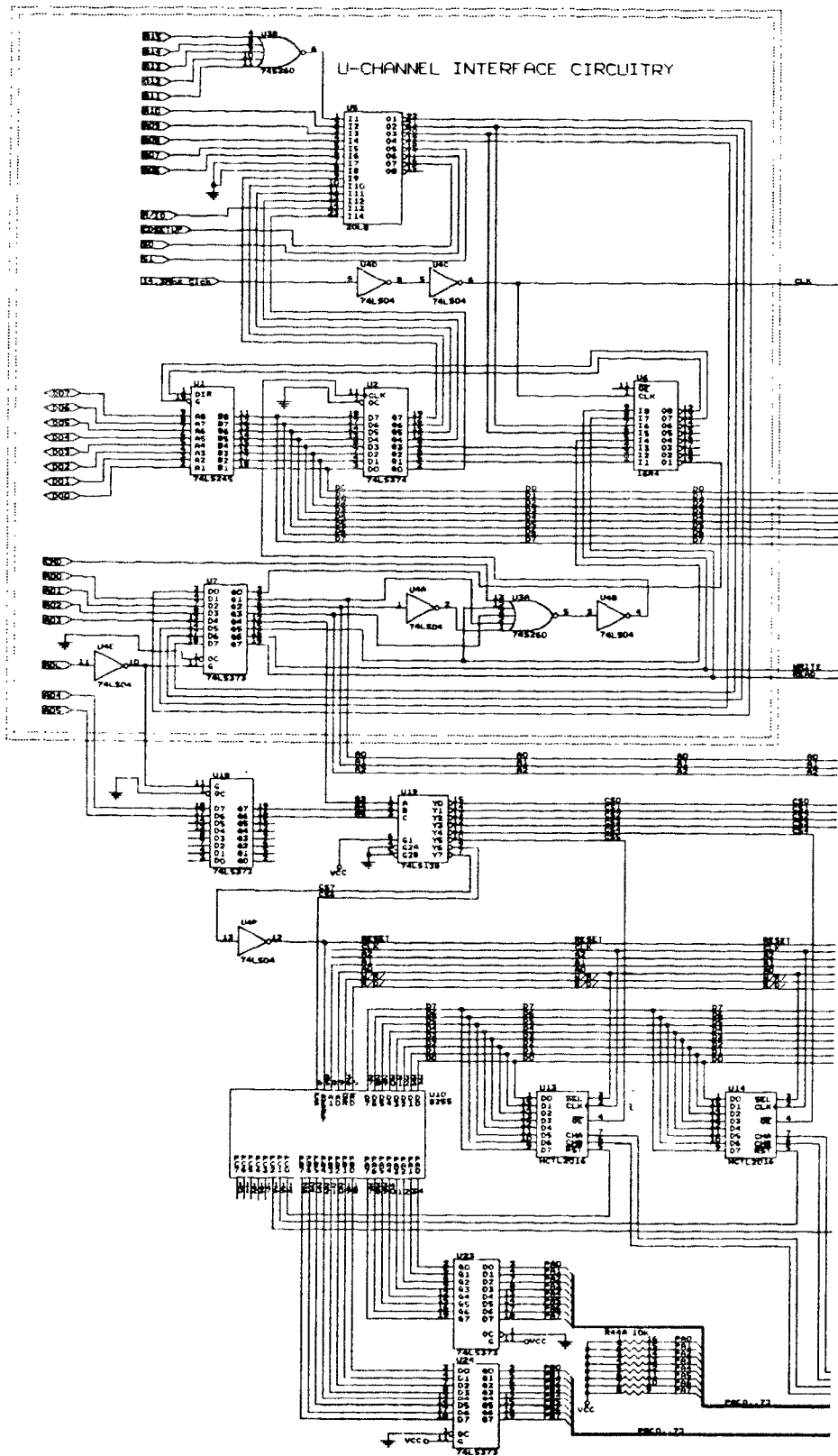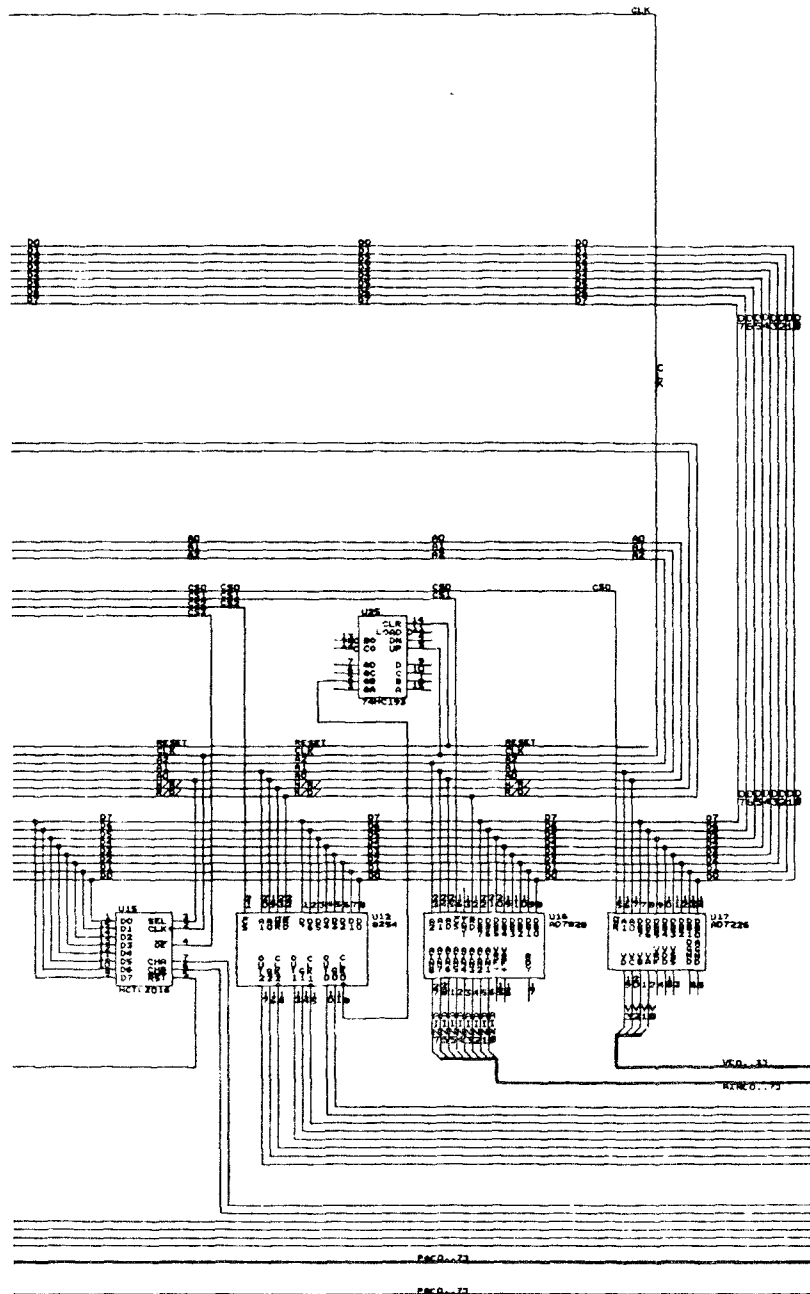
Appendix B Motion Control Program

```
#include "setup.c"
#include "path2.c"
#define mhz        1795000
/* #define gi1      0.0005  0.00005
#define gp1        0.31
#define gv1        2.2     0.8429907
#define gi2        0.002   0.0008
#define gp2        0.085   0.075
#define gv2        4.0957971  */
#define a          76.6388
#define b          1.0252285
#define c          4.5440542
#define k          2.709245
#define f1         0     /* 327.11289  */
#define f2         0     /* 40.889111  */
#define f3         0     /* 43.706842 */
#define pm1        1
#define pm2        1
#define pm3        0.5155656
#define pi         3.1415927

main(){
    unsigned int velocity1[3000],sampno1,
    velocity2[3000],sampno2;
    unsigned long int theta1[3000],theta2[3000],p2,p2p,
            target1,target2,theta10,theta20,theta1f,theta2f;
    unsigned int p11,p12,v1,count,
    p21,p22,v2,pp;
    unsigned int step1,step2,data_412,dev_code;
    int av1,av2,s,m1,m2,m3,vd1,vd2,overflow,flag;
    long int    pd1,pd2,accu1,accu2,p1,p1p;
    float   angle1,angle2,vel1,vel2,accel1,accel2,
            timeunit,raccel1,raccel2,sinbeta,cosbeta,
            f1s,f2s,f3s,ak,bk,p,q,r,av12,av1squ,
```

```
            av2squ,rac1,rac2,tor1,tor2,bit1,bit2,vbit1,
            vbit2,gi1,gp1,gv1,gi2,gp2,gv2;
   double  beta;
   div_t   n;
   char    ch;

/* theta10,theta20 : initial position in binary form
   theta1[],theta2[]: desired position in binary form
   velocity1[],velocity2[]: desired velocity in digit form
   sampno1,sampno2: no. of sample
   p11,p21: the most significant byte of position 1 and 2
   p12,p22: the least significant byte of position 1 and 2
   p1,p2 : actual position in binary form
   v1,v2 : actual velocity in digit form
   pd1,pd2: position error in binary form
   vd1,vd2: velocity error in digit form
   bit1,bit2: the coefficient betwwen degree and binary form
   vbit1,vbit2: the coefficient between degree and digit form
   tor1,tor2: torque required to apply to motor 1 and motor 3
              in digit form, motor is zero
   m1,m2,m3: torque required to apply to motors
   step1,step2: counter
   n,data_412,dev_code:timeing coefficient
   theta1f,theta2f: final position in degree
   vel1,vel2: specified velocity in degree
   accel1,accel2: preset acceleration
   timeunit: sampling period in degree
   raccel1,raccel2: preset acceleration in radian form
   beta:  position of joint 2 in radian
   sinbeta: sin(beta)
   cosbeta:cosbeta
   f2s : f2 *sgn ()
   ak : a+2*k*cos(beta)
   bk : b+k*cos(beta)
   av1,av2: actual velocity in digit form v1-128, v2-128
   av12 : av1*av2 in radian
   av1squ: av1*av1
   av2squ: av2*av2
   accu1, accu2: accumulation of position error
```

```
    */

    accel1=40.00;
    accel2=40.00;
    timeunit=0.005;
    bit1=455.11111;
    bit2=133.33333;
    vbit1=962.56;
    vbit2=653.59465;
    raccel1=accel1*pi/180.;
    raccel2=accel2*pi/180.;
    overflow=0;
    vel1=40;
    vel2=40;


    outportb(0x400,128);
    outportb(0x401,128);
    outportb(0x402,128);

    data_412=mhz*timeunit/2;
    n=div(data_412,256);
    outportb(0x413,0x56);
    outportb(0x411,2);
    p11=inportb(COUNT1_A);
    p12=inportb(COUNT1_B);
    p21=inportb(COUNT2_A);
    p22=inportb(COUNT2_B);
    pp=p11;
    p1p=0;
    p2p=0;
    target1=0;
    target2=0;

start:
    printf("\n Next step (joint angle 1, joint angle 2): \n");
    scanf("%f,%f",&angle1,&angle2);
    angle2=angle2+178.5;
    theta1f=angle1*bit1;
```

```
        theta2f=angle2*bit2;
target:

    gi1=0.0005;
    gp1=0.25;
    gv1=2.2;
    gi2=0.001;
    gp2=0.075;
    gv2=4.1;

    theta10=overflow*65536+p11*256+p12;
    theta20=p21*256+p22;
    p1=theta10;
    p2=theta20;
    pd1=0;
    pd2=0;
    path(theta10,theta1f,accel1,vel1,timeunit,&sampno1,
        bit1,theta1,velocity1,vbit1);
    path(theta20,theta2f,accel2,vel2,timeunit,&sampno2,
        bit2,theta2,velocity2,vbit2);
    printf("\n  Do you want to take this position as target \
position?(y/n)  \n");
    accu1=0;
    accu2=0;
    count=0;
    flag=0;

    step1=1;
    step2=1;
    outportb(0x413,0xb0);
    outportb(0x412,n.rem);
    outportb(0x412,n.quot);
    while(!kbhit()){
        p11=inportb(COUNT1_A);
        p12=inportb(COUNT1_B);
        p21=inportb(COUNT2_A);
        p22=inportb(COUNT2_B);
        if( pp >192 && p11 < 64){
            overflow=overflow+1;
```

```c
}
else if(p11 > 192 && pp < 64){
    overflow=overflow-1;
}
pp=p11;
p1=overflow*65536+256*p11+p12;
p2=256*p21+p22;

beta=p2*0.0001308997;
sinbeta=-sin(beta);
cosbeta=-cos(beta);
ak=a+2*k*cosbeta;
bk=b+k*cosbeta;
v1=inportb(0x408);
v1=inportb(0x408);
v2=inportb(0x409);
v2=inportb(0x409);
vd1=velocity1[step1]-v1;
vd2=velocity2[step2]-v2;
pd1=theta1[step1]-p1;
pd2=theta2[step2]-p2;
av1=v1-128;
av2=v2-128;
av12=av1*av2*0.003158165;
av1squ=av1*av1*0.001362622;
av2squ=av2*av2*0.007319717;
if (count >= max(sampno1,sampno2)){
    flag=1;
}
if (flag==0){
    if (count < sampno1){
        p1p=theta1[count+1]-theta1[count];
    }
    else{
        p1p=0;
    }
    if (count  < sampno2){
        p2p=theta2[count+1]-theta2[count];
    }
```

```
        else{
            p2p=0;
        }
    }
    else{
        f1s=f2s=f3s=0;
    }

    if(flag==0){
        if(p1p+3.41333*p2p < 0) {
            f2s=-f2;
        }
        else{
            f2s=f2;
        }
        if (p1p < 0){
            f1s=-f1;
        }
        else{
            f1s=f1;
        }
        if (p2p < 0){
            f3s=-f3;
        }
        else{
            f3s=f3;
        }
    }
    count++;
    s=velocity1[step1]-velocity1[step1-1];
    if( s != 0){
        rac1=raccel1*s/abs(s);
    }
    else{
        rac1=0;
    }
    s=velocity2[step2]-velocity2[step2-1];
    if(s != 0){
        rac2=raccel2*s/abs(s);
```

```c
}
else{
    rac2=0;
}
/*
f1s=0;
f2s=0;
f3s=0;
*/
r=(ak*c)-(bk*bk);
p=c*f1s+8*c*f2s+bk*(f2s-f3s)-k*c*sinbeta*(2*
    av12+av2squ)+av1squ*sinbeta*k*bk+
    r*(rac1+gv1*vd1+gp1*(long int)pd1+gi1*(long
    int)accu1);
q=ak*(f3s-f2s-k*sinbeta*av1squ)+bk*(k*sinbeta*
    (2*av12+av2squ)-8*f2s-f1s)+
    r*(rac2+gv2*vd2+gp2*(long int)pd2+gi2*(long
    int)accu2);
tor2=(bk*p+c*q)/(24.0*r);
tor1=(ak*p+bk*q)/(40.96*r);
tor1=tor1*1.8782505;
tor2=tor2*4.53922;
m1=128-tor1;
m2=128;
m3=128+tor2;
if (m1 < 30)
    m1=30;
if (m1 > 220)
    m1=220;
if (m3 > 220)
    m3=220;
if(m3 < 30)
    m3=30;
outportb(0x400,m1);
outportb(0x401,m2);
outportb(0x402,m3);
step1++;
step2++;
if(step1 > sampno1){
```

```c
        if(accu1*pd1 <= 0){
            accu1=pd1;
        }
        else{
            accu1=accu1+pd1;
        }
        step1--;

        gi1=0.0007;
        gp1=0.2;
        gv1=1.5;

    }
    if(step2 > sampno2){
        if(accu2*pd2 <= 0){
            accu2=pd2;
        }
        else{
            accu2=accu2+pd2;
        }
        step2--;

        gi2=0.002;
        gp2=0.09;
        gv2=4.0;
    }
    if(abs(pd1)+abs(pd2) < 3){
        accu1=0;
        accu2=0;
    }
    dev_code=inportb(0x430);
    while(!dev_code){
        dev_code=inportb(0x430);
    }
    outportb(0x412,n.rem);
    outportb(0x412,n.quot);
}
outportb(0x400,128);
outportb(0x401,128);
```

```
        outportb(0x402,128);

        p11=inportb(COUNT1_A);
        p12=inportb(COUNT1_B);
        p21=inportb(COUNT2_A);
        p22=inportb(COUNT2_B);
        if ( pp > 192 && p11 < 64){
            overflow=overflow+1;
        }
        else if(p11 > 192 && pp < 64){
            overflow=overflow-1;
        }
        pp=p11;
        p1=overflow*65536+256*p11+p12;
        p2=256*p21+p22;
        printf("%ld,%ld \n",p1-theta1[sampno1],p2-theta2[sampno2]);

repeat:
    ch=getche();
    if(ch == 'y'){
        target1=p1;
        target2=p2;
        goto start;
    }
    else if( ch == 'n'){
        printf("\n Move to target? (y/n)");
        ch=getche();
        if(ch == 'n'){
            goto start;
        }
        else {
            theta1f=target1;
            theta2f=target2;
            goto target;
        }
    }
    else{
        printf("\n Stop? (y/n)");
        ch=getche();
```

154

```
        if(ch == 'n') {
            goto repeat;
        }
    }

    outportb(0x400,128);
    outportb(0x401,128);
    outportb(0x402,128);
}
```

Appendix C: Experimental Data

Experiment 1: Conventional Control

First target position (mm):

x	y	z
486.980653	1593.003201	-24.167939

First direction:

486.738812	1592.854887	-24.181058
485.838051	1592.397990	-24.195490
486.044833	1592.500472	-24.185105
485.146270	1592.036758	-24.195382
487.198320	1593.045755	-24.184805
487.295308	1593.047007	-24.197293
487.199899	1592.979187	-24.189253
487.223137	1592.994359	-24.182124
487.348397	1593.075724	-24.178663
487.471829	1593.079152	-24.168273
487.524474	1593.082279	-24.165431
487.443514	1593.059934	-24.162886
487.388828	1593.022979	-24.167933
487.295605	1592.949973	-24.174437
487.121221	1592.949643	-24.178204

Third direction:

478.973988	1590.093955	-24.171930
479.066196	1590.104625	-24.186421
479.295591	1590.169524	-24.207587
479.113837	1590.142818	-24.186543
479.168567	1590.131972	-24.195599
478.975681	1590.091931	-24.184588
478.977769	1590.105214	-24.182506
478.983161	1590.100505	-24.189734
479.079039	1590.104338	-24.189840
479.284372	1590.160647	-24.209550
479.099676	1590.132512	-24.199380
479.038558	1590.103809	-24.200804
479.085386	1590.131046	-24.198634
479.059735	1590.110465	-24.202026
478.963231	1590.083440	-24.196291

Second direction:

482.394973	1590.692488	-24.231879
481.365708	1590.565643	-24.213858
483.728381	1591.302381	-24.212662
482.598364	1590.732747	-24.214337
482.020435	1590.644426	-24.214918
483.086993	1590.989286	-24.209940
482.074189	1590.590342	-24.210482
481.796526	1590.605994	-24.212614
481.716057	1590.540913	-24.213590
482.272578	1590.647182	-24.204713
483.690968	1591.277406	-24.199527
483.695307	1591.281220	-24.199106
481.360564	1590.538643	-24.221945
482.119978	1590.586930	-24.218017
482.250586	1590.663333	-24.211607

Fourth direction:

477.784247	1589.684795	-24.137802
477.874971	1589.725080	-24.149936
477.676042	1589.653494	-24.130010
477.654474	1589.655781	-24.145115
477.431894	1589.532454	-24.158547
477.682758	1589.669607	-24.121924
477.607742	1589.629175	-24.134598
477.587797	1589.654346	-24.133651
477.610918	1589.633140	-24.126142
477.486860	1589.562788	-24.141684
477.713161	1589.681591	-24.123722
477.782080	1589.685035	-24.132294
477.877233	1589.735625	-24.139683
477.823832	1589.690820	-24.165198
477.945457	1589.737542	-24.153426

Experiment 1: Conventional Control (Continued)

Second target position (mm):

x	y	z
373.407331	1702.452885	-21.928235

First direction:

371.527110	1701.565732	-21.953602
373.400600	1702.445918	-21.929811
373.364984	1702.412467	-21.939135
373.304812	1702.454579	-21.932559
373.376812	1702.459111	-21.914230
373.391121	1702.433981	-21.923900
373.505441	1702.499507	-21.932132
373.528758	1702.501144	-21.923496
373.492617	1702.471909	-21.941492
373.793783	1702.641533	-21.926472
373.508869	1702.466647	-21.947502
372.849237	1702.238033	-21.924129
373.070154	1702.327391	-21.942799
373.749085	1702.597497	-21.931865
373.490627	1702.485777	-21.917363

Third direction:

365.576147	1700.149492	-21.882404
365.469992	1700.168355	-21.875755
363.703866	1700.322806	-21.874740
363.734057	1700.350004	-21.874591
363.871267	1700.384462	-21.882004
363.719983	1700.362703	-21.863485
363.956048	1700.373171	-21.877462
363.836296	1700.374045	-21.864793
363.852227	1700.340910	-21.886470
363.943876	1700.346313	-21.891243
364.001453	1700.379963	-21.876918
363.852626	1700.383096	-21.883185
363.908618	1700.363715	-21.892380
363.786570	1700.342477	-21.875653
363.947695	1700.388483	-21.882685

Second direction:

368.427100	1700.147401	-21.967932
369.503144	1700.605215	-21.968700
368.847474	1700.301995	-21.969346
368.869495	1700.265254	-21.962238
368.374171	1700.139115	-21.980801
370.307402	1700.998653	-21.966713
369.105638	1700.385951	-21.986974
368.283892	1700.095224	-21.980017
368.906907	1700.297225	-21.979588
373.450311	1702.472356	-21.948219
368.388444	1700.129712	-21.980575
371.160330	1701.422714	-21.959096
368.692191	1700.222634	-21.972140
368.382163	1700.146543	-21.986086
368.716229	1700.234501	-21.965869

Fourth direction:

363.107771	1700.112481	-21.842799
363.248678	1700.175197	-21.834094
363.190541	1700.106920	-21.856582
363.283661	1700.129508	-21.836611
363.177611	1700.058937	-21.864759
363.009292	1700.029831	-21.840876
363.180006	1700.078479	-21.840207
362.802254	1699.957153	-21.846223
362.711668	1699.933896	-21.861768
362.792544	1699.930563	-21.848249
363.301520	1700.124019	-21.853455
363.025538	1700.025583	-21.838587
363.343166	1700.161586	-21.813121
362.759426	1699.932906	-21.863460
363.266794	1700.153633	-21.851252

Experiment 1: Conventional Control (Continued)

Third target position(mm):

x	y	z
339.818795	1775.535945	-20.534879

First direction:

Third direction:

340.078440	1775.550055	-20.532266	335.908962	1774.945821	-20.469909
340.117552	1775.572638	-20.536556	335.827337	1774.919175	-20.461574
340.002119	1775.578759	-20.553813	335.861522	1774.912177	-20.465578
339.997290	1775.539345	-20.531700	335.854666	1774.878377	-20.479079
340.133639	1775.591980	-20.533827	335.794997	1774.853722	-20.482269
340.144575	1775.572408	-20.526706	335.762911	1774.867743	-20.462997
340.049405	1775.588112	-20.550026	335.840166	1774.877473	-20.474260
340.177524	1775.616470	-20.530828	335.533076	1774.796054	-20.465150
339.984917	1775.517678	-20.534636	335.652643	1774.842963	-20.454959
340.133443	1775.581316	-20.539852	335.659470	1774.841306	-20.458714
340.184037	1775.613322	-20.527991	335.714042	1774.842403	-20.459964
339.955966	1775.531685	-20.541058	335.638261	1774.858437	-20.452039
340.097937	1775.560860	-20.542603	335.884194	1774.840001	-20.501691
340.131992	1775.563157	-20.546045	335.835170	1774.867409	-20.465418
340.247742	1775.629536	-20.536138	335.724686	1774.834603	-20.473010

Second direction:

Fourth direction:

337.896645	1774.649206	-20.538166	334.584140	1774.550873	-20.443823
337.936204	1774.596129	-20.549007	334.691566	1774.560599	-20.440576
337.892945	1774.602918	-20.535008	334.662489	1774.547379	-20.442918
337.867261	1774.605265	-20.532014	334.713243	1774.573527	-20.430926
337.973781	1774.611857	-20.547791	334.642911	1774.536553	-20.431410
337.870590	1774.597375	-20.546693	334.586536	1774.493718	-20.432420
337.974498	1774.616516	-20.550927	334.710200	1774.495493	-20.434158
338.010793	1774.641891	-20.544364	334.805184	1774.505994	-20.441018
337.933214	1774.597225	-20.545262	334.783504	1774.479162	-20.441809
338.024514	1774.646680	-20.544908	334.851139	1774.510392	-20.438635
338.046990	1774.642108	-20.542289	334.809458	1774.503350	-20.432760
338.099125	1774.659818	-20.533618	334.853828	1774.502593	-20.428635
337.856513	1774.588890	-20.551235	334.809135	1774.505048	-20.416504
337.980163	1774.623091	-20.543697	334.886896	1774.506297	-20.445949
337.806675	1774.596714	-20.541931	334.835942	1774.485292	-20.434425

Experiment 1: Conventional Control (Continued)

Fourth target position(mm):

x	y	z
328.142247	1853.913059	-19.109795

First direction:

328.346238	1853.864390	-19.127129
328.227969	1853.839770	-19.104928
328.324486	1853.858271	-19.112504
328.153501	1853.843063	-19.129135
328.284154	1853.829134	-19.124889
328.180031	1853.786714	-19.120950
328.131708	1853.791817	-19.128475
327.775425	1853.658111	-19.104766
328.094092	1853.760821	-19.118302
328.233569	1853.840518	-19.123218
328.086540	1853.743745	-19.143190
328.227132	1853.768804	-19.114275
328.342063	1853.785525	-19.133877
328.352574	1853.796181	-19.119806
328.268644	1853.824968	-19.140803

Third direction:

324.845019	1853.385198	-19.060818
324.912493	1853.367589	-19.076322
324.728583	1853.348955	-19.055660
324.769745	1853.389973	-19.051453
324.688278	1853.324779	-19.047501
324.778664	1853.379291	-19.047917
324.640876	1853.342296	-19.057501
324.787850	1853.364915	-19.055383
324.761733	1853.353556	-19.058669
324.769370	1853.371442	-19.048039
324.875082	1853.387978	-19.059102
324.809318	1853.380985	-19.063726
324.733781	1853.410007	-19.043730
324.740245	1853.382505	-19.046410
324.748326	1853.357181	-19.059594

Second direction:

326.529500	1853.010389	-19.113468
326.546868	1853.019970	-19.118230
326.560061	1853.030437	-19.108482
326.433106	1852.967542	-19.104500
326.590119	1853.067995	-19.112299
326.560336	1853.018063	-19.119723
326.600915	1853.061200	-19.103778
326.533696	1853.024740	-19.114487
326.532266	1853.026002	-19.109978
326.565764	1853.006024	-19.119558
326.450909	1852.984613	-19.123464
326.529494	1853.035656	-19.109178
326.542215	1852.997577	-19.125941
326.507566	1852.985807	-19.114571
326.440662	1852.949919	-19.110954

Fourth direction:

323.696563	1853.115206	-19.030691
323.744327	1853.068653	-19.013498
323.763497	1853.090700	-19.027190
323.802279	1853.083114	-19.027810
323.746166	1853.048393	-19.031332
323.488288	1852.941129	-19.035648
323.739662	1853.053201	-19.017910
323.834766	1853.070377	-19.027148
323.798846	1853.047244	-19.028900
323.738939	1853.028950	-19.045713
323.705403	1853.029776	-19.019646
323.680330	1853.012421	-19.024811
323.723746	1853.047810	-19.015964
323.930192	1853.128195	-19.045493
323.841049	1853.106577	-19.023644

Experiment 2: Redundantly driven Control

First target position (mm):

x	y	z
309.167663	1857.337207	-18.949429

First direction:

308.939450	1857.237822	-18.956039
308.854455	1857.220513	-18.972659
308.894433	1857.223181	-18.955600
309.366945	1857.374914	-18.949773
308.885230	1857.224213	-18.941603
309.321275	1857.394571	-18.947685
309.329459	1857.405601	-18.943533
309.204785	1857.354006	-18.945216
309.376551	1857.426493	-18.941085
308.926891	1857.259355	-18.952369
309.161527	1857.364255	-18.945169
308.888587	1857.202343	-18.971058
308.883715	1857.237595	-18.959370
308.959667	1857.261740	-18.954539
309.200073	1857.354639	-18.944316

Third direction:

308.973802	1857.278434	-18.942750
309.182026	1857.353594	-18.948203
309.050408	1857.331625	-18.941081
308.936756	1857.270425	-18.948422
309.348220	1857.426344	-18.946479
309.297271	1857.419267	-18.946838
309.368774	1857.445376	-18.946483
309.341007	1857.381027	-18.947004
309.063054	1857.322020	-18.937425
309.024117	1857.301832	-18.957340
309.164964	1857.348213	-18.936506
309.218276	1857.375048	-18.957849
309.349189	1857.425510	-18.949544
309.291660	1857.401842	-18.954180
309.309541	1857.391761	-18.958757

Second direction:

309.370723	1857.420249	-18.940705
309.412143	1857.429364	-18.943211
309.354632	1857.392413	-18.944870
309.422384	1857.419854	-18.922082
309.326861	1857.366102	-18.942879
309.164434	1857.349884	-18.938623
309.213349	1857.331150	-18.954877
309.309834	1857.367852	-18.939250
309.376247	1857.370224	-18.958897
309.343227	1857.410008	-18.947078
309.432581	1857.401629	-18.938312
309.293248	1857.384313	-18.948524
309.286263	1857.391899	-18.947806
309.311359	1857.381330	-18.929589
309.432830	1857.454309	-18.943020

Fourth direction:

309.113346	1857.302519	-18.959471
309.314982	1857.409959	-18.957008
309.461974	1857.479308	-18.941006
309.393019	1857.452303	-18.940714
309.454703	1857.469444	-18.941821
309.293798	1857.367790	-18.939865
309.362819	1857.409059	-18.956013
309.360920	1857.421953	-18.949473
309.230285	1857.352679	-18.973630
309.412669	1857.448828	-18.960482
309.204667	1857.362016	-18.948119
309.320702	1857.409961	-18.942086
309.353774	1857.423279	-18.951925
309.027455	1857.278173	-18.942373
309.098788	1857.283341	-18.938679

Experiment 2: Redundantly driven Control (Continued)

Second target position (mm):

x	y	z
317.316476	1778.310633	-20.356240

First direction:

317.131716	1778.265566	-20.349222
317.227551	1778.296316	-20.353519
317.319188	1778.332622	-20.344567
317.238212	1778.307750	-20.367834
317.396223	1778.368742	-20.354641
317.116669	1778.257595	-20.367382
317.272632	1778.342004	-20.348891
317.340784	1778.339698	-20.358537
317.210495	1778.280580	-20.365358
317.173016	1778.276025	-20.378524
317.389589	1778.344624	-20.346690
317.263905	1778.304327	-20.378736
317.084632	1778.249871	-20.347905
317.417028	1778.350153	-20.348400
317.270601	1778.307778	-20.366062

Third direction:

317.241010	1778.319829	-20.364145
317.321348	1778.333901	-20.353620
317.321588	1778.335445	-20.341339
317.308282	1778.322053	-20.356852
317.370343	1778.356438	-20.358785
317.350788	1778.358364	-20.355001
317.267668	1778.298985	-20.365551
317.201899	1778.272873	-20.358309
317.323632	1778.336386	-20.353637
317.352197	1778.363708	-20.357574
317.214823	1778.303687	-20.357201
317.267091	1778.303716	-20.368442
317.322492	1778.354324	-20.348799
317.348673	1778.376256	-20.341264
317.375018	1778.376391	-20.353978

Second direction:

317.394703	1778.357775	-20.353622
317.318461	1778.320459	-20.365517
317.398021	1778.342283	-20.349490
317.318304	1778.320772	-20.326561
317.291871	1778.311848	-20.366871
317.367142	1778.358789	-20.343759
317.257799	1778.294856	-20.346568
317.305152	1778.333498	-20.360472
317.262229	1778.310750	-20.349201
317.369585	1778.333941	-20.342280
317.300415	1778.334026	-20.346114
317.319441	1778.318748	-20.345229
317.341920	1778.334594	-20.337431
317.298316	1778.318879	-20.354255
317.352263	1778.341051	-20.342215

Fourth direction:

316.968630	1778.198839	-20.351127
316.952463	1778.207004	-20.352849
316.768579	1778.139782	-20.341372
317.118099	1778.262430	-20.357965
316.916985	1778.186436	-20.357524
316.898328	1778.179769	-20.345926
317.101454	1778.250902	-20.360843
316.965988	1778.203787	-20.353090
317.051578	1778.236102	-20.352753
316.927205	1778.199026	-20.348036
316.938630	1778.176166	-20.356057
316.770416	1778.102342	-20.354497
316.826403	1778.140944	-20.350703
317.092549	1778.237939	-20.354409
316.972407	1778.201962	-20.342354

Experiment 2: Redundantly driven Control (Continued)

Fourth target position(mm):

x	y	z
452.388394	1588.498864	-23.964790

First direction:

452.533412	1588.554137	-23.975102
452.314321	1588.460687	-23.956930
452.549763	1588.535194	-23.951438
452.312060	1588.465795	-23.955443
452.396650	1588.491692	-23.957147
452.481268	1588.491317	-23.954774
452.221149	1588.428173	-23.944889
452.377166	1588.491004	-23.956205
452.429973	1588.500351	-23.964534
452.320980	1588.454789	-23.960526
452.527106	1588.526333	-23.952505
452.392887	1588.492671	-23.963324
452.376911	1588.482725	-23.942707
452.473175	1588.511832	-23.958184
452.377351	1588.495018	-23.937406

Third direction:

452.526968	1588.570601	-23.965098
452.678046	1588.630533	-23.987755
452.770837	1588.652849	-23.983748
452.553672	1588.550175	-23.996887
452.603375	1588.599329	-23.998538
452.429342	1588.569778	-23.987242
452.668959	1588.652373	-23.987636
452.715494	1588.678443	-23.976109
452.601354	1588.616792	-24.002417
452.707406	1588.655689	-23.990414
452.597162	1588.621010	-23.965566
452.597599	1588.619513	-23.991113
452.519674	1588.585739	-23.982675
452.427067	1588.563421	-23.971760
452.686443	1588.648675	-23.989809

Second direction:

452.626917	1588.577498	-23.997776
452.597952	1588.555516	-23.973565
452.674624	1588.618827	-23.977738
452.719261	1588.618774	-23.977843
452.509334	1588.537117	-23.998494
452.728639	1588.628729	-23.991394
452.683789	1588.610745	-23.980458
452.566321	1588.573566	-23.985099
452.546568	1588.553466	-23.989275
452.607133	1588.582942	-23.988747
452.672474	1588.619700	-24.004121
452.553776	1588.569407	-23.985135
452.509760	1588.558211	-23.966299
452.538763	1588.559906	-23.993302
452.494808	1588.522701	-23.963408

Fourth direction:

452.301412	1588.491207	-23.955003
452.408096	1588.531594	-23.953223
452.254010	1588.467950	-23.948632
452.297984	1588.493452	-23.947231
452.375213	1588.525024	-23.962596
452.294516	1588.484145	-23.942640
452.339738	1588.495769	-23.965167
452.289718	1588.485374	-23.940818
452.359586	1588.509755	-23.928370
452.436594	1588.540342	-23.936758
452.320198	1588.495938	-23.930238
452.234306	1588.441557	-23.954470
452.320415	1588.487315	-23.952483
452.363328	1588.516646	-23.946209
452.322969	1588.499556	-23.921582

Experiment 2: Redundantly driven Control (Continued)

Third target position(mm):

x	y	z
343.082895	1702.791025	-21.702275

First direction: **Third direction:**

343.010425	1702.762893	-21.724614	343.560134	1702.942328	-21.707635
343.235832	1702.817933	-21.706340	343.410646	1702.930734	-21.690412
343.034819	1702.743307	-21.710786	343.546044	1702.950883	-21.689983
342.989985	1702.755109	-21.721358	343.525749	1702.972216	-21.730458
342.946289	1702.771135	-21.711678	343.377365	1702.926661	-21.713385
343.201527	1702.808479	-21.711634	343.488097	1702.961828	-21.697709
343.174052	1702.823314	-21.716630	343.584496	1702.974988	-21.710128
343.009986	1702.768246	-21.729460	343.564081	1702.956819	-21.698591
343.199178	1702.813170	-21.709970	343.573781	1702.974874	-21.686080
343.168254	1702.820305	-21.715082	343.610014	1702.979226	-21.708231
343.029937	1702.796934	-21.733821	343.583827	1702.996419	-21.698250
342.996453	1702.746820	-21.699653	343.553717	1702.999904	-21.724102
343.096598	1702.801879	-21.723037	343.544298	1702.995711	-21.670278
343.149920	1702.818000	-21.704617	343.357041	1702.936022	-21.693092
343.217315	1702.832924	-21.696739	343.533392	1702.980231	-21.677077

Second direction: **Fourth direction:**

343.075670	1702.832641	-21.691779	343.064604	1702.794502	-21.680624
343.184641	1702.883007	-21.703021	343.110030	1702.816904	-21.712172
343.306624	1702.937944	-21.706604	343.227569	1702.851874	-21.744620
343.161996	1702.869528	-21.725685	343.036834	1702.790655	-21.712295
342.925262	1702.785185	-21.688668	343.147292	1702.836104	-21.693379
342.980214	1702.813771	-21.692541	343.183200	1702.813860	-21.705891
343.159328	1702.866734	-21.695870	343.047926	1702.771539	-21.719797
343.002310	1702.809756	-21.696320	343.088829	1702.811468	-21.726668
343.383303	1702.953470	-21.719477	343.065813	1702.760524	-21.680835
342.938876	1702.774677	-21.702878	343.021816	1702.790263	-21.701853
343.008283	1702.797842	-21.726279	343.064846	1702.804542	-21.699503
343.109784	1702.846541	-21.708138	343.113134	1702.826480	-21.747529
343.259228	1702.905081	-21.716877	342.998666	1702.775569	-21.726346
343.075947	1702.832016	-21.711125	342.985074	1702.748194	-21.720997
343.430923	1702.970194	-21.705459	343.186092	1702.838594	-21.732981